SECONDARY STRUCTURAL AND FUNCTIONAL STUDIES OF ROTAVIRUS NSP4 AND CAVEOLIN-1 PEPTIDE-PEPTIDE INTERACTIONS

A Dissertation

by

MEGAN ELIZABETH SCHROEDER

Submitted to the Office of Graduate Studies of
Texas A&M University
in partial fulfillment of the requirements for the degree of

DOCTOR OF PHILOSOPHY

December 2009

Major Subject: Veterinary Microbiology

SECONDARY STRUCTURAL AND FUNCTIONAL STUDIES OF ROTAVIRUS NSP4 AND CAVEOLIN-1 PEPTIDE-PEPTIDE INTERACTIONS

A Dissertation

by

MEGAN ELIZABETH SCHROEDER

Submitted to the Office of Graduate Studies of
Texas A&M University
in partial fulfillment of the requirements for the degree of

DOCTOR OF PHILOSOPHY

Approved by:

Chair of Committee,	Judith M. Ball
Committee Members,	Susan Payne
	Friedhelm Schroeder
	Danna Zimmer
Head of Department,	Fuller Bazer

December 2009

Major Subject: Veterinary Microbiology

ABSTRACT

Secondary Structural and Functional Studies of Rotavirus NSP4 and Caveolin-1 Peptide-Peptide Interactions. (December 2009)

Megan Elizabeth Schroeder, B.A., Bellarmine University

Chair of Advisory Committee: Dr. Judith M. Ball

The rotavirus NSP4 protein is the first described viral enterotoxin. Abundant data from our laboratory reveals that NSP4 binds both the N- and C-termini of caveolin-1 (aa2-31 and 161-178, respectively). Yeast two-hybrid and peptide binding analysis mapped the caveolin-1 binding site to three hydrophobic residues within the amphipathic α-helix, enterotoxic peptide domain (aa114-135). The research studies herein utilized peptides to investigate the interaction between NSP4 and caveolin-1. Peptides were synthesized corresponding to the amphipathic α-helix and caveolin-1 binding domain of NSP4 (aa112-140) and to the N- (aa2-20 and 19-40) and C- (161-178) termini of caveolin-1, and were utilized in structural and functional studies. Fluorescence binding assays revealed that NSP4 (aa112-140) binds to the N-terminus (aa19-40) of caveolin-1 with a stronger affinity than the C-terminus (aa161-178). In addition, this assay further delineated the NSP4 binding domain on caveolin-1 to aa19-40. Secondary structural changes following NSP4-caveolin-1 peptide-peptide interactions were investigated by circular dichroism analysis. Changes in α-helix formation were observed only upon

interaction of the $NSP4_{112-140}$ peptide with the C-terminal caveolin-1 peptide ($C\text{-}Cav_{161-178}$).

The $NSP4_{112-140}$ peptide contains a potential cholesterol recognition amino acid consensus (CRAC) sequence. Therefore this peptide was examined for cholesterol binding. Results of the binding assay revealed NSP4 binds cholesterol with a K_d of 7.67 ± 1.49nM and this interaction occurs via aa112-140. Mutation of amino acid residues within the CRAC motif resulted in weaker binding affinities between each of the corresponding mutant peptides and cholesterol.

NSP4 peptides containing mutations within the hydrophobic and charged faces of the amphipathic α-helix, enterotoxic peptide and caveolin-1 binding domain of NSP4 were examined for changes in secondary structure as well as diarrhea induction in mouse pups. Circular dichroism analysis revealed that mutation of hydrophobic residues resulted in a decrease in α-helix formation, whereas mutation of acidic and basic charged residues caused little to no change in α-helical content. When tested for diarrhea induction in mouse pups, the peptides containing mutations of either the hydrophobic or basic charged residues did not cause diarrhea. Taken together, the results of this research suggest a complex interplay between NSP4 secondary structure, caveolin-1 and cholesterol binding and diarrheagenic function.

DEDICATION

To my parents, Rod and Kathy Schroeder, who have always supported and encouraged me in my educational endeavors. Thank you for always believing in me.

ACKNOWLEDGEMENTS

I would like to thank my committee chair, Dr. Judith Ball, and my committee members, Dr. Susan Payne, Dr. Friedhelm Schroeder and Dr. Danna Zimmer for their guidance, support and expert advice throughout the course of this research.

Thanks also go to the faculty and staff of the Department of Veterinary Pathobiology for making my time at Texas A&M University a wonderful experience. I want to thank everyone in Dr. Ball's Laboratory: Dr. Rebecca Parr, Dr. DeAnne Moore-Smith, Dr. Stephen Storey, Major Thomas F. Gibbons, Ph.D. (USAF), Dr. Cecelia V. Williams, Kiran Mir, Pam Miller and Krystle Yakshe, for the guidance, support and camaraderie. I also want to thank Dr. Heather Hostetler, Dr. Huan Huang, Dr. Avery McIntosh and Dr. Greg Martin for their immense knowledge and expert advice.

I am grateful for the support, encouragement and listening ears of the numerous friends I have met during my graduate school experience. Thank you especially to Cecelia Williams, Gina Lungu and Lina Covaleda for your friendship—you are truly amazing women and I am honored to be your friend. I am also most appreciative of the individuals who have provided me with numerous experiences and stories which are sure to offer endless entertainment and laughter for years to come. Furthermore, I would like to thank Gold's Gym and Skydive Aggieland for providing stress relief and "therapy" during these last few years.

Finally, thanks to my family and friends—Rod, Kathy and Laura Schroeder, Patricia and Eric Hacker, Kimberly Thompson, Traci and Michael Jackson and family,

Pam and Joe Hickl and Tricia and Maurice Warren—for your continual encouragement and shoulders on which to cry during the last several years. Words cannot express my deep gratitude to each and every one of you.

NOMENCLATURE

aa	Amino Acid
AAH	Amphipathic α-helix
$A_{660/795}$	Absorbance
$[Ca^{2+}]_i$	Intracellular Calcium
cav-1	Caveolin-1
CCD	Coiled Coil Domain
CD	Circular Dichroism
Cl^-	Chloride
C-MAD	C-Terminal Membrane Attachment Domain
CRAC	Cholesterol Recognition/Interaction Consensus Sequence
CSD	Caveolin Scaffolding Domain
DIPCIDI	N,N'-diisopropylcarbodiimide
DIPEA	N,N-diisopropylethylamine
DLP	Double Layered Particle
DOPS	1,2-dioleoyl-*sn*-glycero-3-[phosphor-L-serine]
dsRNA	Double-Stranded RNA
eIF4G	Eukaryotic Initiation Factor 4G
ELISA	Enzyme-Linked Immunosorbent Assay
ER	Endoplasmic Reticulum
EU	Endotoxin Units

F_{max}	Maximum Fluorescence
Fmoc	Fluorenylmethoxycarbonyl
FRET	Fluorescence Resonance Energy Transfer
H_2SO_4	Sulfuric Acid
HBTU	O-Benzotriazole-N,N,N',N'-tetramethyluronium-hexafluoro-phosphate
HCl	Hydrochloric Acid
HOBt	1-hydroxy-benzotriazole
HPLC	High Performance Liquid Chromatography
kDa	Kilodalton
K_d	Dissociation Constant
LAL	*Limulus* Amebocyte Lysate
LS	Light Scattering
$Mg(NO_3)_2$	Magnesium Nitrate
MALDI	Matrix-Assisted Laser Desorption/Ionization
MOPS	3-morpholinopropanesulfonic Acid
mt	Mutant
N_2	Nitrogen
nM	Nanomolar
N-MAD	N-Terminal Membrane Attachment Domain
NMR	Nuclear Magnetic Resonance
NSP	Non-Structural Protein
NTP	Nucleotide Triphosphate

OD	Oligomerization Domain
PABP	Poly(A) Binding Protein
PBS	Phosphate Buffered Saline
PLC-IP_3	Phospholipase C-inositol 1,4,5-triphosphate
POPC	1-palmitoyl-2-oleoyl-*sn*-glycero-3-phosphocholine
PM	Plasma Membrane
RV	Rotavirus
SEC	Size Exclusion Chromatography
SPPS	Solid Phase Peptide Synthesis
ssRNA	Single-Stranded RNA
SUV	Small Unilamellar Vesicles
TFA	Trifluoroacetic Acid
TFE	Trifluoroethanol
TLC	Thin Layer Chromatography
TLP	Triple Layered Particle
TMD	Transmembrane Domain
VP	Viral Protein
wt	Wild Type
Y131	Tyrosine 131

TABLE OF CONTENTS

CHAPTER Page

CHAPTER Page

LIST OF FIGURES

FIGURE Page

LIST OF TABLES

CHAPTER I

INTRODUCTION: ROTAVIRUS, NON-STRUCTURAL PROTEIN 4 (NSP4), CAVEOLIN-1 AND THEIR INTERACTION

Rotavirus

As the major cause of severe gastrointestinal disease in children under the age of five, rotavirus (RV) infection is responsible for approximately 440,000 childhood deaths worldwide every year (*1*). While most of these deaths occur in developing countries, primarily due to the lack of adequate medical care, the disease continues to be a problem in developed countries as well. In the United States alone, RV infections result in 400,000 doctor visits, 55,000-70,000 hospitalizations and 20-60 deaths each year (*2*). While infection occurs in all mammals and generally affects the young (< 5yrs) (*3, 4*), some studies have reported that RV infections occur in young adults, immunocompromised individuals and the elderly as well (*5, 6*). The severe diarrhea that occurs in infected individuals is a result of fluid imbalance in the small intestine, which can lead to dehydration and eventually death without proper care (*7*). Several reports indicate that rotavirus does not remain solely within the intestine, but can escape the gastrointestinal tract and be found in various organs (i.e. stomach, liver, lungs, kidneys, heart, pancreas and bladder), indicating that antigenemia and viremia occur during infection (*8, 9, 10, 11*).

This dissertation follows the style of *Biochemistry.*

RV is a nonenveloped RNA virus that belongs to the *Reoviridae* family of viruses. The viral genome is composed of eleven segments of double stranded RNA (dsRNA) which encode six structural proteins (VP1, VP2, VP3, VP4, VP6, VP7) and six non-structural proteins (NSP1, NSP2, NSP3, NSP4, NSP5, NSP6). Each protein is encoded by a single segment of RNA with the exceptions of NSP5 and NSP6, which are encoded by overlapping reading frames of a single genome segment (*12*). Surrounding the segmented genome is a triple layered icosahedral capsid that is composed of three concentric protein coats. The VP1, VP2 and VP3 structural proteins make up the inner core that contains the viral dsRNA. The intermediate capsid surrounds the inner core and is composed solely of the VP6 structural protein. The outer capsid is formed from the VP7 and VP4 structural proteins, the latter of which forms spikes on the surface of the virion (*12, 13*). Figure 1A depicts the structure of the rotavirus virion and the proteins involved in each capsid layer. Figure 1B is a western blot of each viral protein and their corresponding RNA segment. Table 1 lists each viral protein and their function(s).

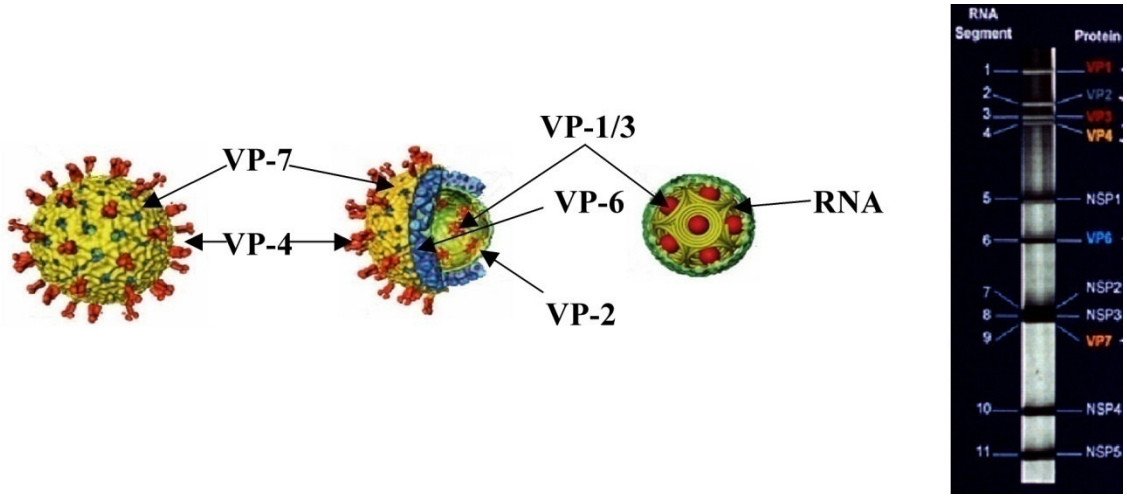

Figure 1: A. Cryo-EM Reconstruction of the Rotavirus Triple-Layer Particle Depicting the Structural Proteins. The outer capsid is composed of VP-7 (yellow) and VP-4 (orange). The middle capsid is composed of VP-6 (blue). The inner capsid is composed of VP-2 (green). VP1 and VP3 (red) are transcriptional enzymes located within the inner core. Surrounding the transcriptional enzymes are the genome segments (RNA) which are shown as inverted conical spirals (*14*). **B. Rotavirus Western Blot**. Western blot of a simian rotavirus depicting the structural and nonstructural proteins and their corresponding RNA transcripts (*14*).

Table 1: Rotavirus Proteins and Their Functions (*4, 12*)

Genome Segment:	Rotavirus Protein:	Description / Function / Location:
1	VP1	Core capsid protein; RNA-dependent RNA polymerase; located in the inner core
2	VP2	Core capsid protein; RNA binding; required for replicase activity of VP1; located in the inner core
3	VP3	Core capsid protein; Guanylytransferase and methyltransferase activity; RNA binding; located in the inner core
4	VP4 (following cleavage: VP5 and VP8)	Outer capsid spike protein; cellular attachment and infectivity
5	NSP1	RNA binding; nonstructural
6	VP6	Inner capsid protein
7	NSP3	Binds 3' end of viral mRNAs; inhibits host cell translation by competing with cellular PABP for binding to eIF-4G; nonstructural
8	NSP2	RNA binding; involved in viroplasm formation; helicase activity; nonstructural
9	VP7	Outer capsid protein
10	NSP4	ER receptor for DLPs; acts as an enterotoxin by mobilizing $[Ca^{2+}]_i$ and causing Cl^- secretion; regulates viral transcription; recruits VP6 to viroplasms; nonstructural
11	NSP5	RNA binding; involved in viroplasm formation; nonstructural
	NSP6	Interacts with NSP5, in viroplasms; nonstructural

Rotavirus Replication

Rotavirus primarily infects mature villus enterocytes of the small intestine (*7*). Cellular entry of the RV virion requires cleavage of the VP4 spike protein, into VP5 and

VP8, which remain associated with the virion (*15*). The VP8 cleavage fragment of VP4 in some rotavirus strains has been shown to bind N-acetylneuraminic acid (sialic acid) on the cell surface, while the VP5 fragment is involved in the permeabilization of the cellular membrane (*14, 16*). In addition to sialic acid, several integrin molecules (α2β1, αxβ2, αvβ3 and α4β1), as well as the heat shock cognate protein hsc70, have been implicated in binding and entry of RV virions (*16*). Furthermore, entry appears to require lipid rafts, as cholesterol sequestration from the plasma membrane prevents RV infectivity (*16, 17*).

Following entry, the outer capsid, containing the VP4 and VP7 viral proteins, is lost from the virion, due to the low $[Ca^{2+}]_i$ environment of the cytosol, producing a transcriptionally active double-layered particle (DLP) (*18*). Transcription of viral mRNAs occurs within the DLP. Viral mRNA transcripts are synthesized by VP1, the viral RNA-dependent RNA polymerase, and capped at the 5' end by VP3, the viral methyltransferase and guanylyltransferase (*19*). Unlike eukaryotic mRNA, however, the mRNA transcripts do not contain a poly(A) tail. Once synthesized, the transcripts are extruded through the vertices of the DLP for translation within the cytoplasm. Translation of viral mRNAs involves the viral NSP3 protein, which functions similar to the cellular poly(A) binding protein (PABP) (*20*). NSP3 binds to the 3'-end of the viral mRNA transcripts to allow interaction with the eIF4G protein of the cellular translational complex. This interaction enables circularization of the viral mRNA, thus promoting translation of viral proteins.

Replication of the viral genome occurs within electron dense areas known as viroplasms. Several studies have demonstrated the involvement of the NSP2 and NSP5

RV proteins in not only viroplasm formation, but genome replication and packaging as well (*21, 22, 23, 24, 25, 26, 27*). Since NSP2 has RNA-binding and NTPase (nucleotide triphosphatase) activities, it is believed to function as a molecular motor that uses energy from NTP hydrolysis to assist in packaging the RV genome (*28*). NSP5 has been shown to interact with VP2, as well as ssRNA and dsRNA, suggesting that the protein is involved in both genome replication and virion core assembly (*29, 30*).

Packaging of the RV genome into newly formed DLPs occurs within the viroplasm. Each virion contains one copy of each of the 11 segments of dsRNA. Exactly how the 11 segments are packaged such that each newly assembled virion contains only one copy of each segment is still unknown. Following formation, the DLPs bud into the lumen of the ER through an interaction with the viral NSP4 protein, which is located within the ER membrane and acts as a receptor for the subviral particles. It is within the lumen of the ER that the DLPs acquire the outer capsid protein, VP7, as well as a transient envelope. Prior to release from the host cell, the spike protein, VP4, is added to the virion, thus forming a mature TLP. While is was previously thought that VP4 was added within the lumen of the ER, some studies have suggested that VP4 may be added to the TLP at the plasma membrane (*31, 32*). Once fully assembled, the infectious TLPs are released from the host cell. Traditionally thought to be released by cell lysis, recent research indicates RV viral particles are also released via a nonlytic vesicular transport pathway which bypasses the Golgi (*33, 34, 35*).

NSP4

The multifunctional viral protein NSP4 has been shown to be involved in a number of events in the RV life cycle including morphogenesis, pathogenesis and

intracellular signaling processes (*4, 12*). NSP4 was identified as the first viral enterotoxin when it was discovered that intraperitoneal delivery of the full-length protein or a short peptide (aa114-135) of the protein exhibited toxin-like activity in mice (*3*). The full-length protein is 175 residues and has an approximate molecular weight of 28kD (Figure 2) (*36*). Three hydrophobic domains (H1, H2 and H3) and two N-linked high mannose glycosylation sites (aa8 and aa18) are located near the N-terminus. A single transmembrane domain (aa24-44), which overlaps the second hydrophobic domain (H2), serves to insert the viral protein into the lipid bilayer of the endoplasmic reticulum (ER) (*37*). This insertion into the ER membrane anchors NSP4 such that a short N-terminus (aa1-24) remains within the lumen of the ER while a long C-terminus (aa45-175) extends into the cytoplasm. The extended cytoplasmic tail of NSP4 contains an amphipathic α-helix, coiled coil domain (aa95-137) (*38, 39*), VP4 and VP6 binding domains (aa112-148 and aa161-175, respectively) (*40, 41, 42*), an enterotoxic domain (aa114-135) (*3*), a tubulin binding domain (aa120-175) (*43*), an integrin receptor binding domain (aa114-130) and an interspecies variable domain (aa135-142) (*44*).

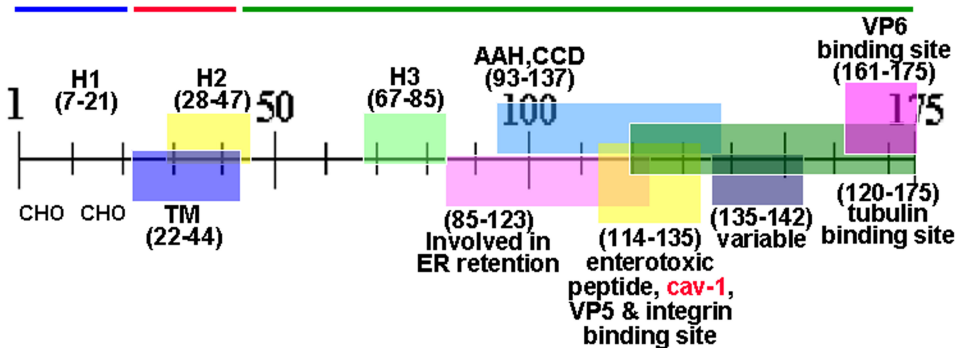

Figure 2: **Linear Schematic of Structural and Functional Domains of Rotavirus NSP4**. NSP4 is 175 amino acids long and contains three N-terminal hydrophobic domains (H1, H2 and H3), the second of which overlaps the transmembrane domain (TM). The N-terminus also contains two glycosylation sites (CHO). The C-terminus contains an amphipathic α-helix, coiled-coil, oligomerization domain, a VP4 binding domain, a caveolin-1 (cav-1) binding domain, an enterotoxic peptide domain, an integrin binding domain, a variable domain, a tubulin binding domain and a VP6 binding domain. Numbers correspond to amino acid positions. (*45*).

Structure of NSP4

Crystallographic analysis of NSP4 has proven to be a difficult task hence structural data on the full-length protein is currently lacking. However, a few studies on a segment of the C-terminus have provided structural details on the biologically relevant portion of the protein. Cross-linking experiments suggest that the C-terminus forms homotetrameric structures in solution (*38*). Circular dichroism (CD) spectroscopy confirmed this finding, while revealing the presence of an extended α-helical secondary structure and predicting that oligomerization occurred via a coiled-coil motif. This prediction was verified four years later when the crystal structure of aa95-137 was determined (*39*). Crystallographic analysis revealed aa95-137 oligomerizes into a homotetrameric coiled-coil with a parallel packing arrangement. At the core of the tetrameric structure is a cation binding site. Modeling analysis based on the crystallographic data predicted that residues E120 and Q123 coordinate the binding of a Ca^{2+} ion which presumably stabilizes the homotetramer. An additional crystallographic

study on aa95-146 found slight variations in organization of the homotetrameric structure of separate NSP4 genotypes and suggested that these structural differences may account for differences in virulence properties between NSP4 genotypes (*46*).

Role of NSP4 in Morphogenesis

As an ER-localized glycoprotein, NSP4 functions as a receptor for DLPs by binding to VP6 to facilitate the translocation of the DLPs across the ER membrane (*41, 42*). The mechanism for ER retention currently remains unknown, as NSP4 does not contain a traditional ER retention signal. However, one study suggests that aa85-123 in the cytoplasmic tail of NSP4 are involved in ER retention, possibly as a result of structural motifs which help stabilize the protein's interaction with the ER membrane (*47*). The acquisition of the outer coat (VP7) and spike protein (VP4) to become mature infectious TLPs is likely facilitated by NSP4, as NSP4 contains a VP4 binding domain (aa112-148) and forms a complex with both VP7 and VP4 (*40, 48*).

Role of NSP4 in Viral Replication

Through silencing RNA (siRNA) studies, NSP4 was shown to play a role in RV replication (*49, 50, 51, 52*). Surprisingly, when NSP4 expression was silenced in RV infected cells, researchers observed an increase in plus-strand RNA synthesis, an increase in empty virions as well as a decrease in virion assembly and the presence of immature, underdeveloped viroplasms. Together, these results suggest that NSP4 is a regulator of viral transcription.

Confocal microscopy studies show NSP4 colocalizing with LC3, an autophagosomal marker (*53*). This association with autophagosomes is calcium dependent and is hypothesized to enhance viral replication, thus providing further

evidence for NSP4's role in regulating viral replication. This study also suggests that there is a distinct NSP4 pool, separate from that found in the ER that is associated with the autophagosomal pathway.

Role of NSP4 in Pathogenesis

The profuse diarrhea that occurs in RV-infected individuals is a result of several factors, including malabsorption due to the destruction of intestinal enterocytes, fluid mobilization as a result of chloride (Cl^-) secretion in crypt cells, villus ischemia and activation of the enteric nervous system (ENS) (*7, 18, 54*). While the host's response to infection may account for some of the cellular responses that lead to diarrhea, the effects of NSP4 expression likely result in several disruptions within the small intestine that cause fluid loss in the infected host. NSP4 induced diarrhea is a result of a signaling cascade that alters intracellular calcium ($[Ca^{2+}]_i$) (*7, 55, 56, 57*). When added exogenously, NSP4 mobilizes $[Ca^{2+}]_i$ from ER stores through a phospholipase C-inositol 1,4,5-triphosphate (PLC-IP_3) pathway (*55*). This disruption in $[Ca^{2+}]_i$ causes malabsorption in villus enterocytes of the intestine (*7*). When added to polarized epithelial cells, NSP4 has been shown to disrupt tight junctions thus affecting paracellular permeability and further contributing to malabsorption (*58*). Rotavirus induced diarrhea is also a result of chloride (Cl^-) secretion from intestinal crypt cells (*3, 7*). Several recently published studies show the release of NSP4 from RV infected cells and hypothesize that the enterotoxin exogenously acts on neighboring uninfected cells, disrupting $[Ca^{2+}]_i$ and promoting Cl^- secretion (*59, 60, 61*). Similar to exogenous addition, endogenous expression of NSP4 also results in disruption of $[Ca^{2+}]_i$, however,

the mechanism by which this occurs is through a PLC-independent signaling pathway (*57, 62*).

Yeast two-hybrid, coimmunoprecipitation and colocalization assays identified the extracellular matrix proteins laminin-β3 and fibronectin as NSP4 binding partners (*59*). NSP4 was found to be localized at the basement membrane (BM) of RV infected cells, suggesting a basolateral release mechanism for the enterotoxin. Release from the BM of infected enterocytes was proposed as a means by which NSP4 can travel to the crypt region of the intestinal villus and induce Cl^- secretion, thus contributing to the secretory component of diarrhea.

A recent study found that the integrins α1β1 and α2β1 act as cellular receptors for NSP4 (*60*). Two distinct domains of NSP4 (aa114-130 and aa131-140) were reported to be involved in integrin I binding and signaling. Amino acids 114-130 of NSP4 were shown to bind to the metal ion-dependent adhesion site (MIDAS) motif on the α1 and α2 I domain, while aa131-140 appeared to initiate integrin signaling through interaction with another domain of α2β1. Binding to the MIDAS motif is possibly mediated by residue E120, which, along with residue Q123, has been revealed by crystallographic analysis to coordinate with a divalent cation (probably Ca^{2+}, Mg^{2+} or Mn^{2+}) (*39, 60*). Since integrins are localized to the basolateral surface of intestinal enterocytes (*63*), this finding further supports the hypothesis that NSP4 initiates signaling processes in uninfected cells, following basolateral release from infected cells, which contributes to diarrhea in an RV infected host.

NSP4-induced changes in $[Ca^{2+}]_i$ also result in actin remodeling, particularly at the basolateral surface of RV infected cells (*64*). These changes appear to be mediated

by endogenously expressed NSP4. Upon mobilization of intracellular Ca^{2+}, actin polymerization increases through alteration of the activity of cofilin, an actin dynamics-regulating protein. Previous research demonstrates VP4-induced actin remodeling occurs along the apical membrane of VP4-transfected cells which result in destabilization of the apical membrane (*65*). Based on these data, it has been hypothesized that remodeling of the cellular cytoskeleton in RV infected cells contributes to RV pathogenesis by directing newly formed virions away from the actin stabilized basolateral membrane and towards the actin destabilized apical membrane for release into the intestinal lumen.

Locations of NSP4

Numerous studies provide evidence for multiple pools of NSP4 within RV infected cells (*43, 53, 66, 67*). The first pool of NSP4 is localized within the ER membrane where it serves as a receptor for DLPs that are budding into the lumen of the ER for maturation into TLPs (*41, 42*). The second pool is found in association with microtubules, radiating from the ERGIC compartment (*43*). The third pool is associated with autophagosomes and viroplasms and is believed to help regulate viral replication (*53*). The fourth pool of NSP4 is found in caveolae localized to the plasma membrane (PM) (*67*).

Several studies in our laboratory have demonstrated that full-length NSP4 colocalizes with caveolin-1, a structural protein of caveolae, and can be found in caveolae isolated from the plasma membrane (PM) of RV infected cells (*45, 67*). Additional research revealed that not only is the C-terminus of NSP4 exposed on the exofacial leaflet of both RV-infected and NSP4-transfected cells, but the full-length, fully-glycosylated protein is released from infected cells prior to the release of virus (*61*). This finding

correlates with a study in which a cleavage fragment of NSP4 (aa112-175) was isolated from the media of cultured mammalian cells infected with RV (*68*).

Caveolae and Caveolin-1

Caveolae, traditionally defined as flask-shaped invaginations in the cellular PM, are a subset of lipid rafts that can assume a variety of shapes (*69, 70, 71*). They can either be open at the cell surface or can close off to form cytoplasmic caveolae vesicles. These membrane microdomains are rich in not only the protein caveolin-1, but also in glycosphingolipids, sphingomyelin, cholesterol and PTRF-Cavin (*72, 73, 74*). Caveolins and cavin are predicted to act as a coat protein to help stabilize the membrane structure of caveolae (*73*).

The main protein constituent of caveolae is caveolin-1 (cav-1). Caveolin-1 is a 21kD protein that forms a hairpin-like structure within membranes such that both the N- and C-termini are found in the cytoplasm (Figure 3). The N-terminal domain (aa1-101) contains an oligomerization domain (OD, aa61-101) such that 14-16 cav-1 molecules interact to form high molecular mass oligomers (*75, 76*). Contained within the OD is a caveolin scaffolding domain (CSD, aa82-101) which serves as an interaction domain for other proteins as well as cholesterol (*77*). The transmembrane domain (TMD, aa102-134) forms a hairpin-like loop within membranes and is bordered on either side by the N-terminal membrane attachment domain (N-MAD, aa82-101) and the C-terminal membrane attachment domain (C-MAD, aa135-150), both of which serve to anchor the protein to the membrane (*70*). The C-terminal domain (aa135-178) contains three palmitoylated cysteine residues (aa133, 143, 156) which also anchor the C-terminus to the membrane (*78*). Palmitoylation of these residues appears to be important for

regulating the interaction of cav-1 with signaling molecules and is also required for the binding and transport of cholesterol (*79, 80*).

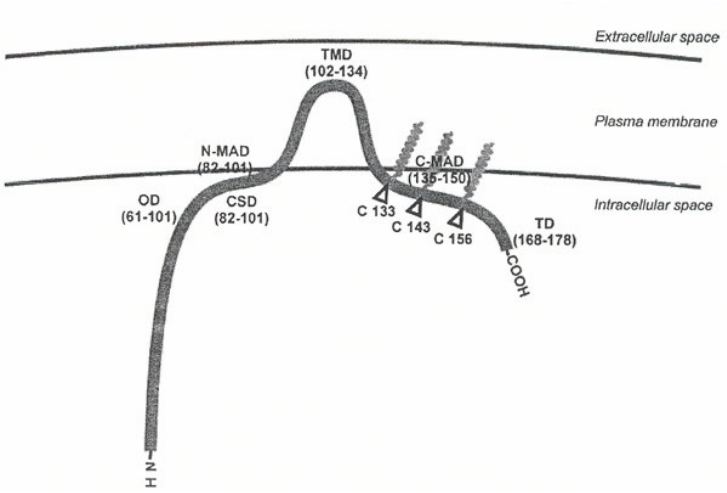

Figure 3: Caveolin-1 Schematic Depicting Membrane Topology and Functional Domains. Caveolin-1 is arranged within the membrane such that the N- and C-termini are oriented towards the cytoplasm. OD-oligomerization domain; CSD-caveolin scaffolding domain; N-MAD and C-MAD-N- and C-terminal membrane attachment domains; TMD-transmembrane domain; TD-terminal domain; C133, C143, C156-palmitoylation sites. Numbers correspond to amino acid positions (*70*).

Formation of caveolae commences following the synthesis of cav-1 in the ER and its subsequent entry into the secretory pathway (*81, 82, 83, 84*). During transport to the PM, cav-1 monomers begin to assemble into high molecular weight oligomers, which associate with cholesterol, to form mature caveolar vesicles (*81, 82*). Oligomerization of cav-1 monomers occurs in a side by side fashion, such that the monomers interact N-terminus to N-terminus and C-terminus to C-terminus (*75, 85*). One study did suggest, however, that the C-terminal domains can also bind the N-termini of adjacent monomers, within the oligomerization domain, to provide further stabilization of the oligomers (*85*).

Caveolin-1 Structure

Studies have yet to elucidate the complete structure of cav-1. To date, the only insights into cav-1 structure consist of limited secondary structural data on the N-terminal portion of the protein (*75*). This study utilized CD to determine the secondary structure of a peptide that contained a majority of the N-terminus (aa1-101) (*75*). While the peptide was determined to be ~20% α-helix, additional structural analysis of deletion peptides determined that aa79-96 constituted the α-helical portion of the peptide, while the first 78 residues appear to lack appreciable secondary structure. The authors predict that these initial residues of the cav-1 protein wrap around the α-helical portion and assist in the stabilization of oligomers (*75*).

A second study utilized a bioinformatics approach to gain structural insights into cav-1 (*76*). Using protein structural prediction programs, their study confirmed the above mentioned CD results in that they found that the N-terminus of cav-1 is relatively unstructured. In addition to verifying that aa81-101 have significant secondary structure, Spisni *et al*. were able to further determine that aa95-101 are involved in α-helix formation, while aa84-94 form two β-strands arranged in an anti-parallel fashion. Consensus secondary structure prediction analysis revealed that aa134-167 of the C-terminus of cav-1 form an α-helix (*76*). The reminder of the C-terminus (aa168-178) is predicted to be unstructured.

Caveolin-1 and Cholesterol

Contained within the CSD of cav-1 is a cholesterol recognition/association consensus (CRAC) sequence: -L/V-$(X)_{1-5}$-Y-$(X)_{1-5}$-R/K-, where $(X)_{1-5}$ represents one to five residues of any amino acid (*76, 86*). This CRAC sequence serves as a cholesterol

binding motif and is located at cav-1 aa94-101. Experiments have shown that cav-1 and cholesterol bind at a 1:1 ratio and the interaction between the two molecules is critical in the formation of caveolae and the transport of cholesterol throughout the cell (*80*). Caveolae formation is dependent on cholesterol. Experiments in which cholesterol was depleted from the cell using various drugs show a decrease or disappearance of caveolae (*87, 88*).

Caveolae, Caveolin-1 and Signaling

Caveolae also participate in a number of cellular signaling events (*89, 90*). Numerous signaling molecules such as receptor tyrosine kinases, G-protein coupled receptors and eNOS localize to caveolae where they bind cav-1 and either activate or inhibit signaling processes (*70, 84*). Also localized in caveolae are the plasma membrane calcium pump (*91*), and an inositol 1,4,5-trisphosphate receptor-like protein (*92*). Signaling is regulated through the interaction of these signaling proteins with the scaffolding domain of cav-1 (aa61-101). Because of the involvement of caveolae in cellular signaling and cholesterol transport, studies focusing on the pathway(s) of NSP4 transport from the ER to the PM of RV infected cells have been directed towards understanding the NSP4-caveolae/caveolin-1 interaction.

NSP4-Caveolin-1 Interaction

Extensive research in our laboratory has demonstrated that NSP4 interacts with cav-1 and caveolae. Circular dichroism (CD) data reveals that full-length NSP4 and the enterotoxic peptide, $NSP4_{114-135}$, preferentially interact with a model membrane lipid domain that is highly curved, rich in anionic phospholipids and highly enriched in cholesterol, similar to caveolae (*93, 94*). Furthermore, interaction with these caveolae-

like model membranes induces an increase in the α-helical secondary structure of NSP4 and the enterotoxic peptide. Confocal microscopy shows that NSP4 colocalizes with cav-1 and caveolae in both NSP4 transfected and RV-infected cells (*45, 67*). While confocal analysis resolves this interaction between NSP4 and cav-1 to within 200nm, fluorescence resonance energy transfer (FRET) analysis narrows the distance to approximately 10nm (*67*). Yeast two-hybrid and coimmunoprecipitation assays subsequently verified this protein-protein interaction. When caveolae was isolated from the PM of RV-infected cells, full-length, fully glycosylated NSP4 was found to be present in these microdomains (*67*). Additional yeast two-hybrid assays, as well as peptide binding assays, revealed that cav-1 binds NSP4 between aa114-135, which is equivalent to the enterotoxic domain (aa114-135) and is located within the amphipathic α-helix, coiled coil domain (aa95-137) (*45*). Interestingly, when the assays were repeated to determine the NSP4 binding domain on cav-1, NSP4 was found to bind both the N- and C- termini (aa2-22 and 161-178, respectively) (*45, 95*).

To further characterize the interaction between NSP4 and cav-1, two NSP4 mutants ($NSP4_{HydroMut}$ and $NSP4_{Ala6}$) were generated using site-directed mutagenesis. Figure 4 shows a linear schematic of the full-length NSP4 mutant proteins. The $NSP4_{HydroMut}$ mutant contains three mutations (aa113, aa124 and aa131) within the hydrophobic face of the amphipathic α-helix, while the $NSP4_{Ala6}$ mutant contains six mutations (aa114, aa115, aa119, aa125, aa132, aa133) within the charged face of the amphipathic α-helix (Figure 5). The hydrophobic residues on the hydrophobic face were mutated to charged residues, while the residues on the charged face were mutated to neutral alanine residues.

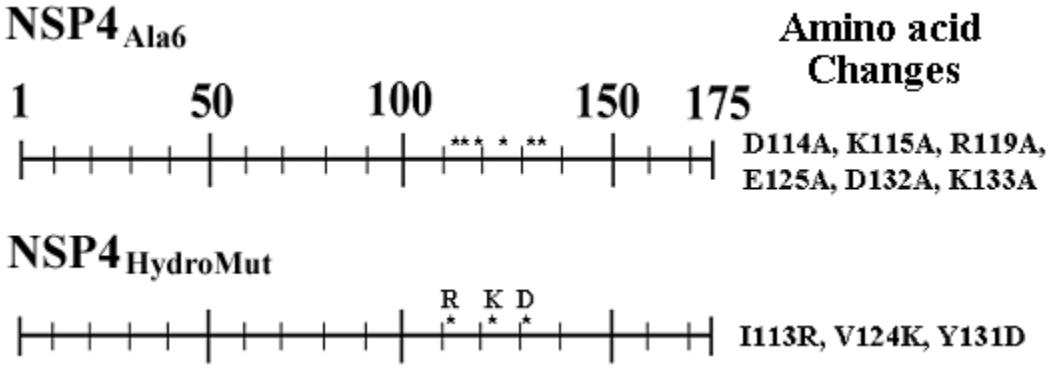

Figure 4: **Linear Schematics of Mutant NSP4 (NSP4$_{Ala}$ and NSP4$_{HydroMut}$) Proteins**. Asterisks denote mutations present in each protein. To the right of each schematic are the amino acid mutations (*45*).

Yeast-two hybrid analyses indicated that the mutations in the hydrophobic face of the amphipathic α-helix inhibit the viral protein from interacting with and binding to cav-1 (*45*). The alanine mutations in the charged face of the amphipathic α-helix, however, do not appear to affect the binding of NSP4 to cav-1. Therefore, the binding between NSP4 and cav-1 was revealed to occur through a hydrophobic interaction. Further mutational analyses delineated the cav-1 binding site on NSP4 to a clustering of three hydrophobic residues within the amphipathic α-helix (*96*).

To summarize, cav-1 binds NSP4 within the hydrophobic face of the amphipathic α-helix, enterotoxic peptide domain (aa114-135). NSP4 in turn binds both the N- and C-termini of cav-1. This interaction between NSP4 and cav-1 and caveolae is hypothesized to facilitate transport of NSP4 from the ER to the PM of RV infected cells. What currently remains unknown, however, is what role, if any, secondary structure plays in the NSP4-cav-1 interaction.

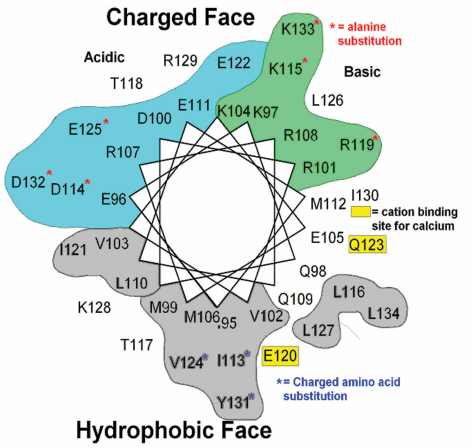

Figure 5: **Helical Wheel of the Amphipathic α-helix Domain of NSP4 (aa95-134)**. The amphipathic α-helix domain of NSP4 contains a hydrophobic face and a charged face. The charged face is further separated into an acidic face and a basic faces (*96*).

Role of Amphipathic Helices in the NSP4-Caveolin-1 Interaction

Amphipathic α-helixes are secondary structural motifs found in proteins and peptides and consist of an α-helical domain that contains both a polar face and a nonpolar/hydrophobic face (*97*). Amphipathic α-helixes generally associate with lipids and are involved in membrane fusion or lysis, and signal transduction processes. They also play a role in DNA replication as they are found in transcription factors that directly bind to DNA (*98*).

There are seven classes of amphipathic α-helixes (A, H, L, G, K, C and M), which are grouped based on their physical-chemical (i.e. hydrophobic moment, hydrophobicity and charged residue density) and structural properties (*97*). Class A, H, L and M amphipathic α-helixes associate with lipids, while classes G, K and C are involved in protein-protein interactions (*97*). Examples of each α-helix class are as follows: class A are apolipoproteins, class H are polypeptide hormones, class L are lytic polypeptides, class G are globular α-helical proteins, class K are calmodulin-binding domains of

calmodulin-regulated protein kinases, class C are coiled-coil proteins and class M are complex transmembrane proteins (*97*).

The RV NSP4 amphipathic α-helix appears to be most similar to the class A helixes. These helixes are characterized by their ability to associate with lipids, with apolipoproteins being the most notable α-helixes in this group. Structurally, class A helixes display a clustering of positively charged residues at the polar-nonpolar interface and a clustering of negatively charged residues at the center of the polar face. It is through these charged residues that the helix associates with lipids (*99, 100, 101, 102, 103*). Due to the tendency of amphipathic α-helices to associate with both proteins and lipids, it is reasonable to assume that the amphipathic α-helix of NSP4 not only binds cav-1, but associates with lipids as well.

Specific Aims of Dissertation Research

- Aim 1: Determine the binding affinities of wild-type (wt-) $NSP4_{112-140}$ with cav-1 synthetic peptides corresponding to the N-and C-termini of cav-1.
- Aim 2: Ascertain the extent of secondary structural changes in the wt- and mutant (mt-) $NSP4_{112-140}$ peptides when in the absence or presence of cav-1 specific peptides or model membranes (small unilamellar vesicles, i.e. SUV).
- Aim 3: Resolve the binding affinity of cholesterol with wt- and mt-$NSP4_{112-140}$ peptides.
- Aim 4. Examine the biological significance of the specific mutations within the amphipathic α-helix of NSP4.

The studies involved herein focused on evaluating the secondary structural and functional effects of the mutated residues in the enterotoxic peptide/cav-1 binding

domain of NSP4. Structural and functional studies utilized NSP4 wt- and mt- peptides. These peptides encompassed the majority of the amphipathic α-helix (AAH, aa112-140). Rather than using the original $NSP4_{Ala6}$ mutant, which contained six mutations within the charged face, we separated the mutations into those that were in the acidic face from those that were in the basic face and synthesized the corresponding peptides. Three mt-NSP4 peptides were synthesized which contained the following mutations: (1) $NSP4_{112-140Hydro}$-hydrophobic residues mutated to charged residues (I113R, V124K, Y131D); (2) $NSP4_{AlaAcidic112-140}$-acidic amino acids were mutated to alanines (D114A, E125A, D132A); and (3) $NSP4_{AlaBasic112-140}$-basic wherein the basic residues were mutated to alanines (K115A, R119A, K133A). The cav-1 synthetic peptides utilized to the N- or C-termini of the protein (aa2-20, aa19-40 and aa161-178, respectively).

Many caveolae-localized signaling molecules interact with cav-1 through the caveolin scaffolding domain (aa82-101) (*104, 105, 106, 107*). Previous NSP4-cav-1 binding studies, however, revealed that unlike most proteins, NSP4 does not bind cav-1 within the scaffolding domain (*95*). Consequently, a synthetic peptide corresponding to a portion of the scaffolding domain (aa68-80) of cav-1 was used as a negative control. Conversely, cav-1 does not bind the extreme C-terminus of NSP4 (aa150-175) (*45*). Therefore a synthetic peptide of this region of NSP4 was also used as a peptide-binding control.

Rational for Utilizing Peptides to Analyze the NSP4-Caveolin-1 Interaction

The study of protein-protein interactions is important for understanding various cellular processes and has been particularly useful in the area of drug design. The use of peptides, which contain the relevant binding domains of two interacting proteins, has

aided in the investigation of these interactions. Several recently published articles demonstrate the use of peptides for investigating peptide-peptide structural interactions that reflect what is seen in the full length proteins (*108, 109, 110, 111*). One study used synthetic peptides corresponding to separate regions of the HIV-1_{LAI} gp41 protein to investigate peptide-peptide interactions utilizing both circular dichroism and sedimentation equilibrium analyses techniques (*108*). The findings of this study provide insight into the structural changes that occur in gp41 during membrane fusion and predict a mechanism for HIV-1 fusion with cellular membranes. In another peptide-peptide interaction study, a peptide corresponding to the E2 envelope protein of the hepatitis G virus (GBV-C/HGV) was found to modify the conformational structure of the fusion peptide (FP) of the HIV-1 gp41 protein (*111*). The authors speculated that the use of this GBV-C/HGV peptide in inducing a conformational change in HIV-1 gp41 may potentially be used as an antiviral therapeutic agent as the structural change prevents cellular fusion of HIV-1 and thus prevents entry of the virus. These studies highlight the use of peptides for studying structural changes following interactions with other peptides. Furthermore, they demonstrate how the study of peptide-peptide interactions provides a means by which protein-protein interactions can be dissected and the mechanisms of these interactions further defined.

Techniques Employed to Accomplish the Specific Aims

A solution fluorescence binding assay was utilized to examine the binding affinity of the wtNSP$4_{112-140}$ peptide with N-and C-terminal cav-1 peptides. Secondary structural changes in the wt- and mt-NSP4-specific peptides, both in the absence and presence of cav-1 peptides and model membranes (small unilamellar vesicles, i.e. SUV), were

evaluated by circular dichroism (CD) analyses. Since NSP4 has a potential CRAC sequence ((L)LKRIYDK) located between aa126/127-133, each of the NSP4-specific wt- and mt-peptides were also evaluated for cholesterol binding. The biological importance of these mutations and their effect on secondary structure in disease induction was evaluated by diarrhea studies in mouse pups.

Peptide Synthesis, Purification, and Characterization

Many peptide chemists employ the Fluorenylmethoxycarbonyl solid-phase peptide synthesis (Fmoc SPPS) chemistry (*112*) technique for peptide synthesis. This technique uses the base-labile *N*-Fmoc group for the protection of the α-amino group of coupling amino acids, while acid-labile groups protect the amino acid side-chains. Removal of these protecting groups occurs by different chemical mechanisms and therefore can be performed under relatively mild chemical conditions.

Synthesis begins when the first amino acid is coupled to an insoluble resin support via its carboxyl group (*112*). Side-chain groups of the amino acid are protected with protecting groups that are not affected by the chemical conditions utilized during assembly of the peptide chain. The Fmoc-protecting group that shields the α-amino group of the first coupled amino acid is removed under basic conditions. The carboxy group of the second amino acid is activated for amide bond formation and the amino acid is then coupled to the amino group of the first amino acid. Excess reagents are removed by washing, the N-terminal Fmoc-protecting group of the second amino acid is removed and the third amino acid is then added. Following synthesis of the complete sequence, the peptide is cleaved from the resin support and the side-chain protecting groups are removed. Following ether extraction of the synthesized peptide, organic contaminants

and incomplete peptide fragments are removed by gel filtration and high-performance liquid chromatography (HPLC) purification. Peptides are then characterized by mass spectroscopy to assure that they are the correct mass and contain the proper sequence.

Circular Dichroism

Circular dichroism (CD) is a spectroscopic technique that is used to study peptide and protein conformations (*113, 114, 115, 116, 117*). The technique measures the difference in absorbance between left and right circularly polarized light of chiral molecules. The CD spectrum of a peptide or protein is due to the peptide amide chromophore which absorbs in the far-UV (below 250nm). Data collected generally consists of a combination of secondary structure, including α-helix, β-sheet, turns and random coils. There are several programs available which can calculate the percentage of each secondary structure in a sample by utilizing reference sets of proteins of known structure (*118, 119*).

CD has many advantages as a spectroscopic technique for peptide and protein structural analysis. It is relatively fast and easy, requires low sample concentrations and allows researchers to study the structure of peptides or proteins in solution. CD is particularly useful for monitoring changes in secondary structure that occur as a result of changes in the surrounding environment (i.e. pH, solvent or concentration) and interaction with other peptides/proteins/ligands. It can also be used to detect changes in secondary structure due to the mutation of amino acid residues within a peptide or protein.

Fluorescence Binding Assays

A fluorescence binding assay is a technique used to monitor the binding of two molecules (*120, 121*). The method generally relies on the intrinsic fluorescence of a molecule that comes from the aromatic side-chains of tyrosine or tryptophan. However, in the cases where intrinsic fluorescence is lacking, the molecule can be labeled with an extrinsic fluorophore. The assay monitors the environment around the fluorophore in response to ligand binding. When the fluorophore is in a hydrophilic environment and exposed to the surrounding solvent, its fluorescence is quenched. If upon ligand binding the fluorophore is placed in a hydrophobic environment where it is shielded from the solvent, its fluorescence will be dequenched.

CHAPTER II

PEPTIDE-PEPTIDE STUDIES OF THE NSP4-CAVEOLIN-1 INTERACTION

Overview

Recent yeast two-hybrid and peptide binding data from our laboratory show that the rotavirus (RV) enterotoxic protein NSP4 binds both the N- and C-termini of caveolin-1. Here, we utilize synthetic peptides to further investigate this interaction between NSP4 and caveolin-1. Peptides were synthesized that corresponded to the amphipathic α-helix and caveolin-1 binding domain of NSP4 (aa112-140) as well as to the N- (aa2-20 and 19-40) and C- (161-178) termini of caveolin-1. Direct fluorescence binding assays were used to determine the binding affinities between the NSP4 and caveolin-1 peptides. Secondary structural changes following peptide-peptide interactions were discerned by circular dichroism analysis. Results indicated that $NSP4_{112-140}$ binds to the N-terminus of caveolin-1 (aa19-40) with a significantly higher affinity than the C-terminus, indicating preferential binding to caveolin-1 residues 19-40. These data further delineated the NSP4 binding domain on caveolin-1 to aa19-40. Secondary structural analysis of NSP4-caveolin-1 peptide-peptide interactions revealed that conformational changes only occur upon interaction of NSP4 with the C-terminus of caveolin-1. These findings are hypothesized to have implications in NSP4 function(s) at the plasma membrane.

Introduction

As the leading cause of gastroenteritis in young children under the age of five, rotavirus (RV) infections are responsible for approximately 440,000 deaths worldwide annually (*1*). During infection, the RV nonstructural protein 4 (NSP4) functions as a viral enterotoxin by activating a signal transduction pathway which increases intracellular

calcium $[Ca^{2+}]_i$ levels through the release of ER calcium stores (*3, 57*). This increase in intracellular Ca^{2+} induces secretory chloride currents which result in diarrhea due to intestinal fluid imbalance (*3*).

Traditionally defined as an ER glycoprotein, NSP4 contains a single transmembrane domain which serves to anchor the protein into the ER membrane, such that a short N-terminus (aa1-24) remains within the lumen of the ER while a longer C-terminus (aa45-175) extends into the cytoplasm (*37*). Interactions with numerous viral and cellular proteins occur within the extended C-terminal tail of NSP4 (*40, 41, 42, 43, 59, 60*). Also contained within the C-terminal cytoplasmic tail is an amphipathic α-helix (AAH), coiled-coil domain (aa95-137) (*38, 39*). Cross-linking and crystallographic experiments reveal that this region of NSP4 oligomerizes into dimers and tetramers and contains a cation-binding site (*38, 39, 48*). Residing within the amphipathic α-helix, coiled-coil domain is the enterotoxic peptide region (aa114-135) as well as the caveolin-1 (cav-1) binding domain (*3, 45*).

There is compelling evidence that NSP4 and the enterotoxic peptide ($NSP4_{114-135}$) interact with cav-1. *In vivo* laser scanning confocal microscopy (LSCM) colocalizations, fluorescent energy transfer (FRET) analyses, and co-immunoprecipitation data from our laboratory show that NSP4 binds cav-1, the main constituent protein of caveolae (*45, 96*). Yeast two-hybrid and *in vitro* binding assays confirm an interaction between NSP4 and cav-1 and map the cav-1 binding domain to $NSP4_{114-135}$ (*45*). Using deletion and site-directed mutagenesis, the binding site was delineated to three hydrophobic residues in the enterotoxic region indicating NSP4 and cav-1 associate via a hydrophobic interaction

(*96*). Additional studies reveal that the cav-1 binding site for NSP4 maps to both the N- and C-termini of cav-1, residues 2-31 and 161-178, respectively (*95*).

Cav-1 is an intracellular 21kD protein bound by the inner leaflet of the plasma membrane (PM). Cav-1 interaction with membranes is distinct in that a hairpin-like structure is formed in the membrane resulting in both the N- and C-termini oriented towards the cytoplasm (*70, 122*). Numerous signaling molecules, such as those involved in calcium signaling, are localized to caveolae and their function appears to be dependent on interaction with cav-1 (*89, 123, 124*). Cav-1 also binds cholesterol (*79*), which has been shown to be vital to caveolae biogenesis and the transport of cholesterol throughout the cell (*83, 87, 89*).

Full-length NSP4 and the $NSP4_{114-135}$ peptide interact with caveolae-like model membranes, i.e., those that have a high radius of curvature and are rich in anionic phospholipids and cholesterol (*93, 94*). Upon interaction with model membranes, both the protein and the peptide undergo a change in secondary structure characterized by an increase in α-helix formation. Additional secondary structural studies of other NSP4 peptides that encompass the enterotoxic peptide and cav-1 binding domain confirm that this region is important for membrane interactions. Transport of NSP4 to the plasma membrane (PM) is believed to occur through this interaction with cav-1 and caveolae. When caveolae microdomains are isolated from enriched PM fractions of RV-infected MDCK cells, the full-length, fully-glycosylated, endoglycosidase-H sensitive NSP4 is present in the isolated caveolae fractions verifying transport of NSP4 to the PM and caveolae (*67*). Additional studies reveal the exposure of the NSP4 C-terminus and enterotoxic region, but not the N-terminus, on the outer PM leaflet and subsequent

release into culture media at a time when the membrane is intact as verified by a lack of exposure of cav-1 and other intracellular markers (*61, 68*).

In this report, we have extended these studies using synthetic peptides to address the following questions: (**i**) Does NSP4 interact with both termini of cav-1 with equal affinity? (**ii**) Can the binding domain be further delineated using synthetic peptides and determining binding constants (K_d)? (**iii**) Do the two termini of cav-1 interact with one another? (**iv**) Is there a structural change when NSP4 and cav-1 peptides interact? To answer these questions we employed peptide-peptide fluorescence binding assays and circular dichroism techniques. Direct fluorescence binding assays were utilized to determine the binding affinity (K_d) of the NSP4-cav-1 peptide-peptide interaction. Circular dichroism (CD) was used to investigate secondary structural changes upon interaction of the peptides in the absence or presence of membranes.

Materials and Methods

Materials

Phospholipids DOPS (1,2-dioleoyl-*sn*-glycero-3-[phosphor-L-serine]) and POPC (1-palmitoyl-2-oleoyl-*sn*-glycero-3-phosphocholine) were purchased from Avanti Polar Lipids (Alabaster, AL). Cholesterol, Sephadex G-25 and trifluoroethanol (TFE) were purchased from Sigma (St. Louis, MO). Trifluoroacetic acid (TFA), 1-hydroxy-benzotriazole (HOBt) and O-Benzotriazole-N,N,N',N'-tetramethyluronium-hexafluoro-phosphate (HBTU) were purchased from American Bioanalytical (Natick, MA). N,N-diisopropylethylamine (DIPEA) and N,N'-diisopropylcarbodiimide (DIPCIDI) were purchased from CreoSalus (Louisville, KY). Thioanisole, ethanedithiol and anisole were purchased from EMD chemicals (Gibbstown, NJ).

Synthesis and Purification of NSP4 and Caveolin-1 Peptides

All peptides were synthesized by fluorenylmethoxycarbonyl (Fmoc) solid-phase chemistry with either 1-hydroxy-benzotriazole (HOBt), O-Benzotriazole-N,N,N',N'-tetramethyluronium-hexafluoro-phosphate (HBTU) and N,N-diisopropylethylamine (DIPEA), or HOBt and N,N'-diisopropylcarbodiimide (DIPCIDI) activation using the Model 90 Peptide Synthesizer (Advanced Chemtech; Louisville, KY). Following synthesis, the peptides were cleaved from the solid resin support and all side-chain protecting groups removed by the addition of Reagent R (90% trifluoroacetic acid (TFA), 5% thioanisole, 3% ethanedithiol and 2% anisole). The peptide/Reagent R cleavage mixture was incubated at RT for a maximum of 2 hours with gentle mixing.

To separate the peptides from the solid support, the mixture was filtered through a sintered glass filter into a 50mL conical tube containing cold diethyl ether in a dry ice/ethanol bath. Following 2-3 rinses of the filter with TFA, the ether solution containing the precipitated peptide was centrifuged at ~300*g* for 4 minutes. The supernatant was removed and additional cold diethyl ether was added to the peptide pellet. The mixture was allowed to cool in the dry ice/ethanol bath for several minutes before repelleting. The supernatant was removed, more ether added and this step was repeated an additional two times. The crude peptide precipitate was dried under N_2, resolubilized in 10% acetic acid and lyophilized.

The lyophilized crude peptide was resuspended in 5-10% acetic acid and purified from organic contaminants and incomplete peptide fragments by gravimetric gel filtration chromatography (Sephadex G25 medium). The eluted peptide was lyophilized and further purified by reverse-phase HPLC using a reverse phase C4 Delta Pak column

(Waters Chromatography Division, Milford, MA) or a reverse phase C18 column (Beckman-Coulter, Fullerton, CA), depending on the hydrophobicity of the peptide. Eluted peaks were lyophilized and characterized by matrix-assisted laser desorption/ionization (MALDI) mass spectrometry (Laboratory for Biological Mass Spectrometry, Department of Chemistry, Texas A&M University, College Station, TX).

Circular Dichroism (CD) and Secondary Structure Estimation

The secondary structures of the NSP4 and caveolin-1 specific peptides were determined by circular dichroism following a previously published protocol (*93, 94*). Briefly, each peptide (15-35μM) was suspended in 10mM potassium phosphate buffer, pH 7.4, or 50% trifluoroethanol (TFE), to promote a hydrophobic environment and correct folding of the peptide, in the presence or absence of lipid vesicles (1mM). Samples containing buffer or lipid vesicles without peptide were used for background correction. Peptide concentrations were determined by amino acid analysis (Protein Chemistry Laboratory, Department of Biochemistry, Texas A&M University, College Station, TX). CD spectra were obtained in a 1mm circular quartz cell at room temperature using a Model J-710 JASCO spectropolarimeter (JASCO, Easton, MD) or in a 1mm rectangular quartz cell in a Model 202 Aviv spectrometer (Aviv Biomedical, Lakewood, NJ). The spectra for each of the peptides were recorded from 185nm to 260nm, with a step resolution of 1nm, speed of 50nm/min, response of 1sec, bandwidth of 2.0nm and sensitivity of 10mdeg. Data were averaged from 5 scans, background subtracted, smoothed and converted into mean residue molar ellipticity [θ] (deg cm^2/dmol).

To determine the percent α-helix for each of the NSP4 and cavolin-1 specific peptides, the following equation was used: $\theta_{222} = (f_h - \text{í}\kappa/N)[\theta_{h\ 222\infty}]$ (*93, 94, 125*). In this equation, θ_{222} is the mean residue molar ellipticity at 222nm, f_h is the fraction in α-helical form, í is the number of helices, κ is a wavelength-specific constant with a value of 2.6 at 222nm, *N* is the number of residues in the peptide and $\theta_{h\ 222\infty}$ is the molar ellipticity for a helix of infinite length at 222nm (i.e. -39,500 deg cm^2/dmol).

Direct Fluorescence Binding Assays

A fluorescence binding assay was utilized to demonstrate direct binding of the $wtNSP4_{112\text{-}140}$ peptide with each of the cav-1 peptides (N-$Cav_{2\text{-}20}$, $Cav_{19\text{-}40}$, and C-Cav) (*45, 126*). All of the cav-1 peptides (N-$Cav_{2\text{-}20}$, $Cav_{19\text{-}40}$, and C-Cav) were directly labeled with a Cy3 fluorescent dye, using the Cy3 Mono-reactive dye pack from Amersham Biosciences (Piscataway, NJ), according to the manufacturer's protocol.

To demonstrate a direct peptide-peptide interaction between the $wtNSP4_{112\text{-}140}$ peptide and each of the caveolin-1 peptides, increasing quantities of $wtNSP4_{112\text{-}140}$ peptide (10-500nM) were added to 25-100nM of the Cy3-labeled caveolin-1 peptides in 2mL of phosphate buffered saline (pH 7.4). Excitation of the Cy3 fluorophore was carried out at 550nm, and emission spectra was scanned from 560-700nm. Fluorescence emission spectra were obtained at 25ºC with a PC1 photon-counting spectrofluorometer (ISS, Inc., Champaign, IL), with excitation and emission slit widths of 1.0. Spectra were corrected for background and maximal fluorescence intensities were measured. The dissociation constant (K_d) was obtained by a reciprocal plot of $1/(1\text{-}F/F_{max})$ and $C_L/F/F_{max}$ according to the following equation: $y = bx + y_o$, where F is the fluorescence intensity at

a given concentration of ligand, F_{max} is the maximal fluorescence obtained and C_L is the ligand concentration. The slope of the line (b) is equal to $1/K_d$.

Preparation of Small Unilamellar Vesicles (SUV)

SUV composed of the neutral lipid POPC, cholesterol and the anionic phospholipid DOPS in the molar ratio 55:35:30 were prepared following a previously published protocol (*93*). This membrane composition was chosen as it has previously been shown to promote an interaction with NSP4-specific peptides as observed by an increase in peptide α-helix formation (*93, 94*). Stock solutions of the lipids dissolved in chloroform were mixed together in the proper ratio in an amber glass vial. The solvents were removed under N_2 with constant rotation so that the dried lipids formed a thin film on the wall of the glass vial. The vial containing the dried lipids was further dried under vacuum for a minimum of 4 hrs. The dried lipids were resuspended in 10mM MOPS buffer, pH 7.4 (prefiltered through a 0.45μm filter; Millipore, Bedford, MA), vortexed and bath sonicated. The resulting multilamellar membrane suspension was sonicated with a microprobe under N_2 at 4ºC at 2 min. intervals, followed by 1 min. pauses to prevent overheating of the lipid solution. The sonicated lipid solution was then centrifuged at 110,000*g* for 4 hrs to remove any multilamellar vesicles and titanium debris from the sonicator probe. The lipid concentration of the SUV solution was determined by a previously described standard phosphate assay (*127*). Briefly, the SUV solutions were mixed with 14 drops of a 10% magnesium nitrate ($Mg(NO_3)_2$) solution (in 95% ethanol) and heated for 30 min. in a 120ºC dry bath. Each sample was then ashed by heating in a flame. Next, 600μL of 0.5N HCl was added to each sample and the samples were heated in boiling water for 15 min. Each of the samples were then mixed

with 1400µL of a 10% ascorbic acid solution that contained 6 parts of a 0.42% ammonium molybdate solution in 1N sulfuric acid (H_2SO_4). The samples were incubated for 20 min. at 45ºC before reading the absorbance at 660nm (A_{660}). Lipid concentrations of the SUV were determined by comparison to a standard curve of 0-200nmol phosphate.

Results

Synthesis of Peptides

Sequences from the SA11 rotavirus simian strain of NSP4 and human caveolin-1 were used to generate the peptides listed in Table 2. A portion of the AAH of NSP4 that encompassed both the enterotoxic peptide and caveolin-1 binding domain (aa112-140) was chosen for synthesis and used in this study. A C-terminal NSP4 peptide ($NSP4_{150\text{-}175\Delta Ala}$) was also synthesized for use as a negative control.

Caveolin-1 peptides that corresponded to various segments of the N-terminus (aa2-20, aa19-40) and to the extreme C-terminus (aa161-178) similarly were synthesized. Additionally, a peptide corresponding to the central region of cav-1 (aa68-80) was synthesized for use as a negative control, as this region is known to not be involved in binding NSP4 (*95*).

Table 2: Sequences of NSP4 and Caveolin-1 Peptides

Peptide Name:	Peptide Sequence (N→C):
$NSP4_{112\text{-}140}$ (aa112-140)	MIDKLTTREIEQVELLKRIYDKLTVQTTG
$NSP4_{150\text{-}175\Delta Ala}$	QKNVRTLEEWESGKNPYEPREVTAM
N-$Cav_{2\text{-}20}$ (aa2-20)	SGGKYVDSEGHLYTVPIRE
$Cav_{19\text{-}40}$ (aa19-40)	REQGNIYKPNNKAMADELSEKQ
$Cav_{68\text{-}80}$ (aa68-80)	FEDVIAEPEGTHS
C-$Cav_{161\text{-}178}$ (aa161-178)	EAVGKIFSNVRINLQKEI

Direct Fluorescence Binding Assays

wtNSP4$_{112-140}$ binds the N-terminus of Caveolin-1 (Cav$_{19-40}$) with greater affinity than the C-terminus

Previously published data from our laboratory demonstrate that NSP4 (aa114-135) interacts with both the N- and C-termini of caveolin-1 (*95*). To further investigate this interaction and determine the binding affinity of the NSP4-cav-1 interaction in the absence of other cellular components, the wtNSP4$_{112-140}$ peptide and various cav-1 peptides (N-Cav$_{2-20}$, Cav$_{19-40}$ and C-Cav$_{161-178}$) were utilized in a direct fluorescence binding assay. Each of the cav-1 peptides was labeled with a Cy3-fluorophore and then titrated with the wtNSP4$_{112-140}$ peptide.

Upon titration with increasing concentrations of wtNSP4$_{112-140}$, each of the cav-1 peptides showed an increase in fluorescence intensity at 565nm. Plots of wtNSP4$_{112-140}$ peptide concentrations versus maximum fluorescent intensities demonstrated saturable binding curves for each of the cav-1 peptides (Figure 6). Linear reciprocal plots were used to calculate the binding affinities (K_d) for each peptide-peptide pair (Table 3). The calculated K_d values for the NSP4-cav-1 peptide-peptide interactions indicated that wtNSP4$_{112-140}$ bound the Cav$_{19-40}$ peptide with the strongest affinity (39.55 ± 10.19nM), while it bound the C-Cav$_{161-178}$ peptide with the weakest affinity (216.64 ± 35.16). The N-Cav$_{2-20}$ peptide bound with intermediate affinity (84.60 ± 6.09nM). None of the cav-1 peptides bound to the control peptide corresponding to the C-terminus of NSP4 (NSP4$_{150-175\Delta Ala}$), which is known to not bind cav-1 (*45*). These results compliment previous findings (*95*) and further delineate the NSP4 binding domain on the N-terminus of cav-1 to aa19-40.

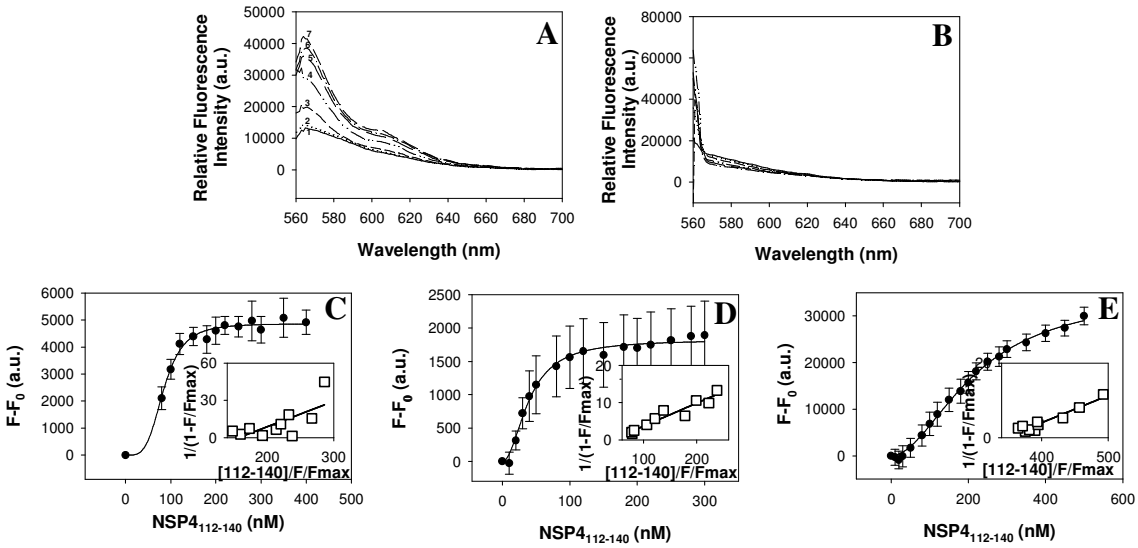

Figure 6: Direct Fluorescence Binding Assays-wtNSP4$_{112-140}$ Peptide with Caveolin-1 Peptides. *A*-fluorescence spectra of Cy3-C-Cav$_{161-178}$ titrated with increasing concentrations of wtNSP4$_{112-140}$. *Spectrum 1*-100nM Cy3-C-Cav$_{161-178}$ in buffer only. *Spectra 2-11*, 100nM Cy3-C-Cav$_{161-178}$ in the presence of 10, 100, 150, 200, 250, 300, 350, 400, 450 and 500nM of NSP4$_{112-140}$, respectively. *B*-fluorescence spectra of Cy3-Cav$_{19-40}$ titrated with increasing concentrations of NSP4$_{150-175}$ (negative control) *C-E*-plots of maximal fluorescence emission (measured at 565nm upon excitation at 550nm) for wtNSP4$_{112-140}$ in the presence of 25nM Cy3-N-Cav$_{2-20}$ (*C*), 25nM Cy3-Cav$_{19-40}$ (*D*) and 25nM Cy3-C-Cav$_{161-178}$ (*E*). *Insets*, linear plots of the binding curve of wtNSP4$_{112-140}$.

Table 3: Binding Affinities (K_d) for wtNSP4$_{112-140}$ + Caveolin-1 Peptides[a].

Sample:	K_d (nM):
Cy3-N-Cav$_{2-20}$ + wtNSP4$_{112-140}$	84.60 ± 6.09
Cy3-Cav$_{19-40}$ + wtNSP4$_{112-140}$	39.55 ± 10.19
Cy3-C-Cav$_{161-178}$ + wtNSP4$_{112-140}$	216.64 ± 35.16

[a]Peptides were synthesized as mentioned in Materials and Methods. The K_d values were calculated as outlined in Materials and Methods and are presented as means ± SD, n = 4.

The cav-1 N-terminal peptides (aa2-20 and 19-40) do not bind the cav-1 C-terminal peptide (aa161-178) in the absence of NSP4

Our laboratory has reported that NSP4 binds to both termini of cav-1 based on yeast two-hybrid and peptide binding assays (*95*). We verified this finding with fluorescence binding assays and further delineated the NSP4 binding site to aa19-40 on the N-terminus of cav-1. Next, we questioned whether both termini of cav-1 bound one another and mediated the interaction with NSP4. We utilized the fluorescence binding assay to investigate binding between the N- and C-terminal peptides of cav-1 in an effort to explain how NSP4 binds both termini. The C-terminal C-$Cav_{161-178}$ peptide was labeled with a Cy3-fluorophore and titrated with either the N-Cav_{2-20} or Cav_{19-40} peptide. Titration of C-$Cav_{161-178}$ with increasing concentrations of either N-Cav_{2-20} or Cav_{19-40} resulted in no change in fluorescence intensity at 565nm, indicative of a lack of binding between the two peptides (Figure 7). Therefore, the interaction between NSP4 and cav-1 does not appear to be a result of initial binding between the N- and C-termini of cav-1, followed by subsequent binding to NSP4.

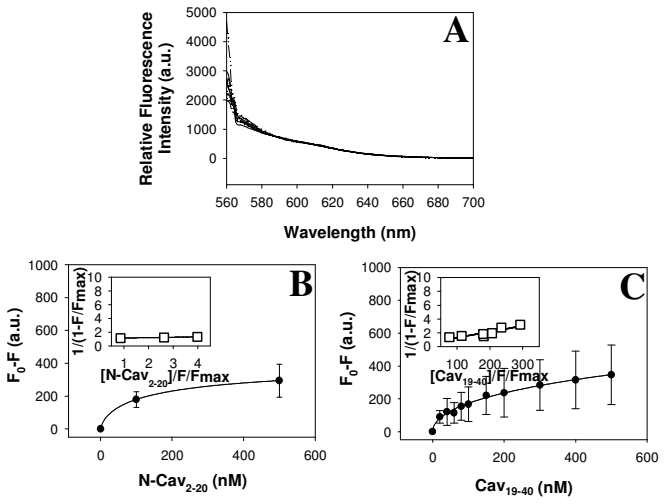

Figure 7: Direct Fluorescence Binding Assays-N-Cav_{2-20} or Cav_{19-40} Peptide with C-$Cav_{161-178}$ Peptide. *A*-fluorescence spectra of Cy3-C-$Cav_{161-178}$ titrated with increasing concentrations of Cav_{19-40} (0-500nM). *B-C*-plots of maximal fluorescence emission (measured at 565nm upon excitation at 550nm) for N-Cav_{2-20} (*B*) and Cav_{19-40} (*C*) in the presence of 100nM Cy3-C-$Cav_{161-178}$. *Insets*, linear plots of the binding curve of N-Cav_{2-20} (*B*) and Cav_{19-40} (*C*).

We were then interested in investigating the structural interaction between the $wtNSP4_{112-140}$ and N- and C-terminal cav-1 peptides. While binding assays revealed the affinity of each of the peptide-peptide interactions, circular dichroism analysis was utilized to analyze the secondary structure of the peptides, individually and following peptide-peptide interaction.

Circular Dichroism Analysis

Secondary Structure of $wtNSP4_{112-140}$

The structure of the wild-type (wt)-$NSP4_{112-140}$ peptide was first determined in aqueous buffer, (10mM potassium phosphate buffer, pH = 7.4) (Figure 8, dark circles). The CD spectrum showed double minima at 208 and 222nm and a single maximum peak at 190nm, indicative of α-helical secondary structure. Using the molar ellipticity value at

222nm the α-helical content of the wtNSP4$_{112-140}$ peptide was calculated to be 30.6 ± 2.4% (Table 4) (*125*).

Trifluoroethanol (TFE) is a hydrophobic solvent that promotes intramolecular hydrogen bonding and thus secondary structure formation in peptides. Therefore, the secondary structure of wtNSP4$_{112-140}$ in 50% TFE was determined by CD (Figure 8, open circles). The CD spectrum showed a dramatic increase in α-helix formation of the peptide, as evidenced by an increase in both the negative molar ellipticity at 208 and 222nm and the positive molar ellipticity at 190nm. The α-helical content was calculated using the molar ellipticity value at 222nm and determined to be 79.6 ± 4.6%.

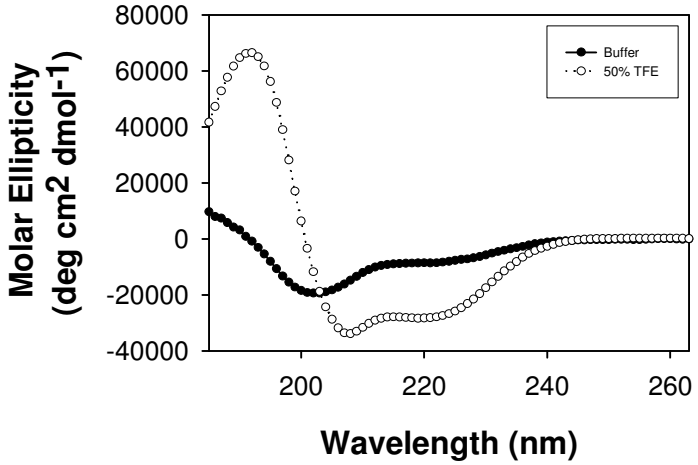

Figure 8: CD spectra of wtNSP4$_{112-140}$ in Aqueous Buffer (●) and 50% TFE (○).

Previous CD experiments with the enterotoxic NSP4 peptide (NSP4$_{114-135}$) demonstrate that the α-helical content of the peptide increases in the presence of small unilamellar vesicles (SUV) containing POPC (a neutral lipid), cholesterol and DOPS (a negatively charged lipid) at a 55:35:10 molar ratio (*93, 94*). To determine the secondary

structural changes that occur in the presence of membranes, the wtNSP4$_{112-140}$ peptide was mixed with SUV model membranes and changes in α-helical content were noted by CD.

The CD spectrum of the wtNSP4$_{112-140}$ peptide in the presence of 1mM SUV showed a 2-fold increase in α-helix formation over that in aqueous buffer, as evidenced by the increase in both the negative molar ellipticity as 208 and 222nm and the positive molar ellipticity at 190nm (Figure 9). The α-helical content was calculated using the molar ellipticity value at 222nm and determined to be 57.9 ± 1.6% (Table 4).

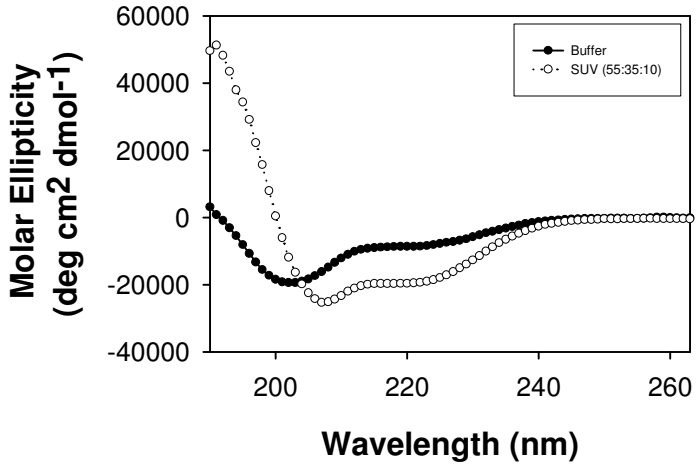

Figure 9: CD Spectra of wtNSP4$_{112-140}$ in Aqueous Buffer (●) and in the Presence of 1mM SUV Model Membranes (55:35:10, POPC/cholesterol/DOPS) (○).

Table 4: Percent α-helix[a] of wtNSP4$_{112-140}$ and Caveolin-1 Peptides in Aqueous Buffer, 50% TFE and in the Presence of 1mM SUV.

Peptide:	Aqueous Buffer:	50% TFE:	1mM SUVs:
NSP4$_{112-140}$	30.6 ± 2.4%	79.6 ± 4.6%	57.9 ± 1.6%
N-Cav$_{2-20}$	18.9 ± 2.8%	16.5 ± 0.9%	18.5 ± 1.9%
Cav$_{19-40}$	20.7 ± 0.6%	33.4 ± 0.5%	20.5 ± 2.7%
Cav$_{68-80}$	23.4 ± 0.9%	24.4 ± 0.8%	21.4 ± 2.0%
C-Cav$_{161-178}$	43.4 ± 3.8%	57.4 ± 4.4%	42.5 ± 10.6%

[a]Percent α-helix for each peptide was calculated as described in Materials and Methods. Data is presented as mean ± SD, n= 4.

Secondary Structure of Caveolin-1 Peptides

The secondary structures of caveolin-1 peptides corresponding to the N- (N-Cav$_{2-20}$ and Cav$_{19-40}$) and C-termini (C-Cav$_{161-178}$), as well as to a central region (Cav$_{68-80}$) of the protein, were determined by CD (Table 4). In aqueous buffer, the α-helical content of N-Cav$_{2-20}$, Cav$_{19-40}$ and Cav$_{68-80}$ was quite similar, at 18.9%, 20.7% and 23.4% respectively (Figure 10, dark circles). The α-helical content of the C-terminal peptide (C-Cav$_{161-178}$) was approximately twice (43.4%) that of the N-terminal peptides. When placed in 50% TFE, the α-helical content of N-Cav$_{2-20}$, Cav$_{19-40}$ and Cav$_{68-80}$ and C-Cav$_{161-178}$ peptides was calculated to be 16.5%, 33.4%, 23.1% and 67.1% respectively (Figure 10, open circles). Only Cav$_{19-40}$ and C-Cav$_{161-178}$ showed an increase in α-helix formation in the presence of 50% TFE.

When mixed with SUV model membranes, none of the cav-1 peptides demonstrated a change in α-helix formation over that seen in aqueous buffer (Figure 10,

dark triangles; Table 4). This result was anticipated as none of these peptides corresponded to a membrane interacting domain within cav-1.

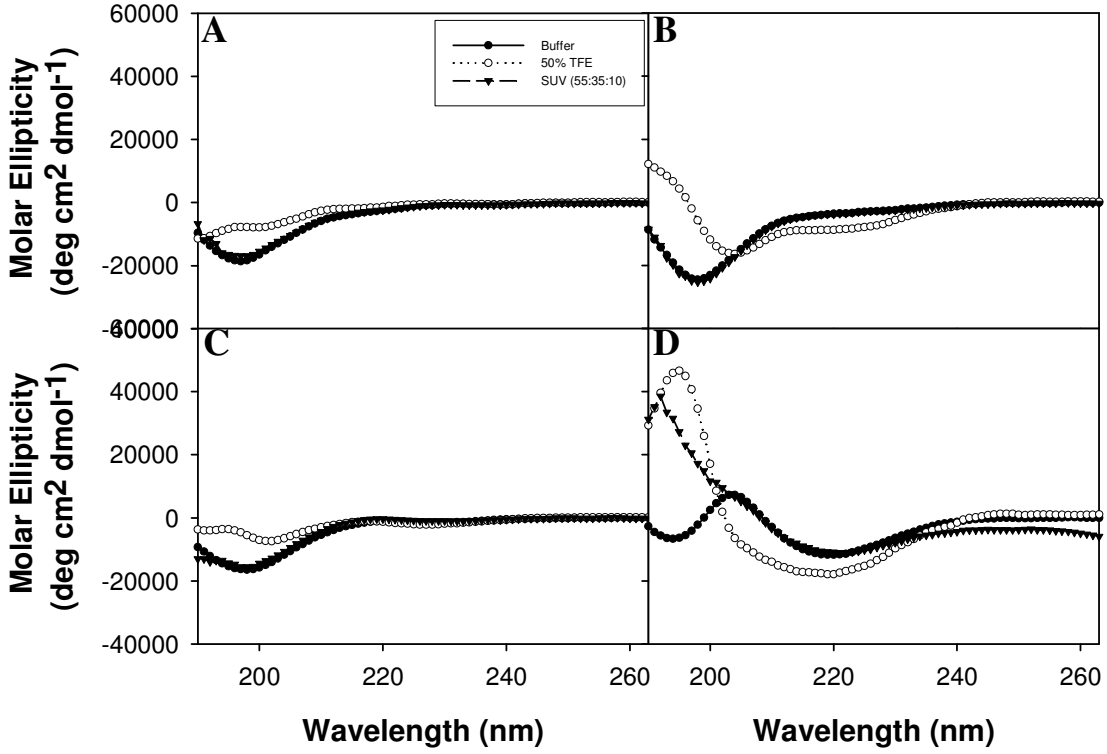

Figure 10: CD Spectra of Caveolin-1 Peptides in Aqueous Buffer (●), 50% TFE (○) and in the Presence of 1mM SUV (55:35:10, POPC/cholesterol/DOPS) (▼). (A) N-Cav_{2-20}; (B) Cav_{19-40}; (C) Cav_{68-80}; (D) C-$Cav_{161-178}$.

Secondary structural changes are observed when wtNSP4$_{112-140}$ is mixed with C-Cav$_{161-178}$

Since previous yeast two-hybrid and binding assay data from our laboratory demonstrate binding of NSP4 (aa114-135) to both termini of cav-1 (*95*) and further analyses by direct fluorescence binding assays revealed that the N-terminus binds with a stronger affinity than the C-terminus, we investigated whether structural changes occur upon the interaction between NSP4 and cav-1 peptides. Each of the cav-1 peptides (N-Cav_{2-20}, Cav_{19-40} and C-$Cav_{161-178}$) was mixed with the wtNSP4$_{112-140}$ peptide and potential

secondary structural changes were analyzed by CD. A peptide corresponding to the middle portion of cav-1 (aa68-80) was used as a negative control peptide, as previous studies have shown that NSP4 does not interact with this region of cav-1 (*45, 95*). Analysis of the mixing experiments was performed by comparing the spectrum of each peptide-peptide mixture (observed) with the sum of the individual spectra of each peptide (theoretical). The α-helical content was calculated and statistically significant differences (student's t-test, $p<0.05$) between the observed and theoretical values indicated a change in secondary structure upon mixing of the wtNSP4$_{112-140}$ and cav-1 peptides. This change in secondary structure was indicative of binding between the two peptides. A lack of secondary structural alterations upon mixture of the peptides, however, did not negate binding between the wtNSP4$_{112-140}$ and cav-1 peptides. While the direct fluorescence binding assays demonstrated that the peptides do in fact interact, the CD experiments revealed the extent to which this interaction caused a change in the secondary structure.

When each of the caveolin-1 peptides was mixed with wtNSP4$_{112-140}$ in aqueous buffer, only the wtNSP4$_{112-140}$-C-Cav$_{161-178}$ mixture showed a significant difference between the observed and theoretical values (25.0 ± 1.7% vs. 35.3 ± 1.6%) (Figure 11D; Table 4). No change in secondary structure was observed for the wtNSP4$_{112-140}$-N-Cav$_{2-20}$ (21.7 ± 0.8% vs. 23.6 ± 2.6%), the wtNSP4$_{112-140}$-Cav$_{19-40}$ (23.8 ± 1.2% vs. 24.4 ± 0.6%) or the wtNSP4$_{112-140}$-Cav$_{68-80}$ negative control (24.2 ± 0.3% vs. 23.9 ± 0.7%) mixtures (Figures 11A-C; Table 5). Similarly, when each peptide-peptide pair was placed in 50% TFE, only the wtNSP4$_{112-140}$-C-Cav$_{161-178}$ mixture showed a significant change in secondary structure (44.2 ± 10.6% vs. 67.8 ± 3.2%) (Table 5).

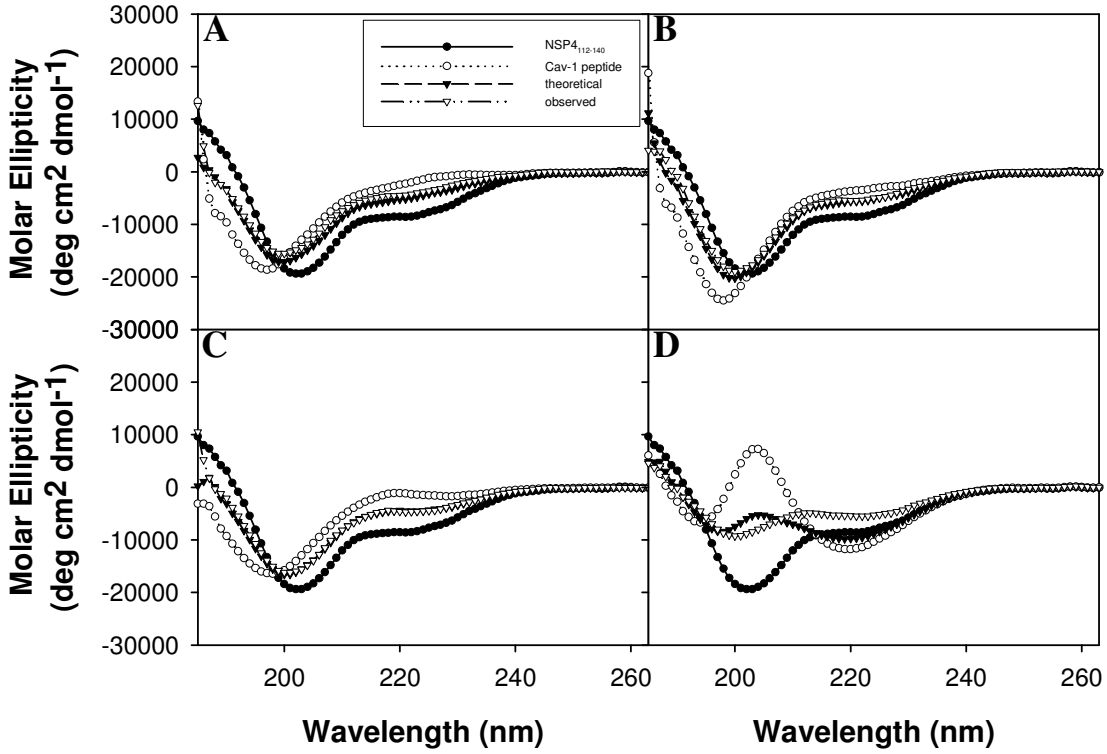

Figure 11: CD Spectra of wtNSP4$_{112-140}$-Caveolin-1 Peptide-Peptide Interactions in Aqueous Buffer. (A) wtNSP4$_{112-140}$ + N-Cav$_{2-20}$; (B) wtNSP4$_{112-140}$ + Cav$_{19-40}$; (C) wtNSP4$_{112-140}$ + Cav$_{68-80}$; (D) wtNSP4$_{112-140}$ + C-Cav$_{161-178}$. (●)-wtNSP4$_{112-140}$ spectra; (○)-Cav-1 peptide spectra; (▼)-Theoretical spectra; (Δ)-Observed spectra.

Table 5: Wild-type (wt)NSP4$_{112-140}$-Caveolin-1 Peptide-Peptide Interactions

	N-Cav$_{2-20}$		Cav$_{19-40}$		Cav$_{68-80}$		C-Cav$_{161-178}$	
	Observed	**Theoretical**	**Observed**	**Theoretical**	**Observed**	**Theoretical**	**Observed**	**Theoretical**
Aqueous Buffer	21.7 ± 0.8	23.6 ± 2.6	23.8 ± 1.2	24.4 ± 0.6	24.2 ± 0.3	23.9 ± 0.7	25.0 ± 1.7*	35.3 ± 1.6
50% TFE	46.3 ± 7.2	47.6 ± 1.8	58.7 ± 7.7	56.3 ± 2.3	45.9 ± 2.8	49.8 ± 1.8	44.2 ± 10.6*	67.8 ± 3.2
1mM SUV	34.7 ± 6.0	37.7 ± 1.9	37.7 ± 3.6	39.0 ± 2.3	31.3 ± 0.2*	37.5 ± 1.9	51.9 ± 2.4	49.5 ± 6.2

Percent α-helical content of wtNSP4$_{112-140}$ peptide + Caveolin-1 peptides, in aqueous buffer (10mM potassium phosphate buffer), 50% trifluoroethanol (TFE) and in the presence of 1mM SUV (55:35:10, POPC/cholesterol/DOPS). Observed values were compared with theoretical values, and those that were statistically significant by a student's t-test ($p<0.05$; denoted by an asterisk) were considered structurally altered, indicative of an interaction. Results are presented as means ± S.D. (n= 3 or 4).

Effect of SUV model membranes on the wtNSP4$_{112-140}$-Caveolin-1 peptide-peptide interactions

Since cav-1 is a membrane bound protein, and NSP4 and the NSP4$_{114-135}$ peptide interact with membranes (*93*), we were interested in whether the presence of membranes would result in secondary structural alterations of the NSP4-cav-1 peptide-peptide interaction. To investigate potential secondary structural changes, each wtNSP4$_{112-140}$-cav-1 peptide-peptide combination was mixed with lipid vesicles (SUV), and changes in structure were observed by CD.

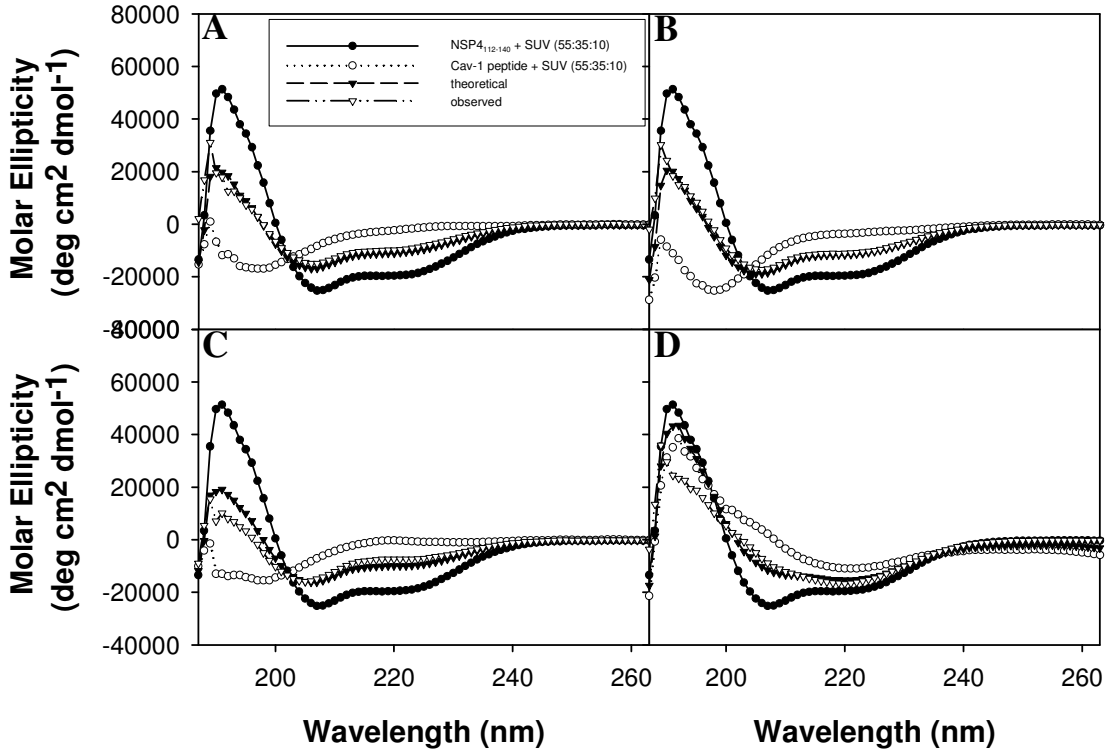

Figure 12: CD Spectra of wtNSP4$_{112-140}$-Caveolin-1 Peptide-Peptide Interactions in the Presence of 1mM SUV (55:35:10, POPC/cholesterol/DOPS) in Aqueous Buffer. (A) wtNSP4$_{112-140}$ + N-Cav$_{2-20}$; (B) wtNSP4$_{112-140}$ + Cav$_{19-40}$; (C) wtNSP4$_{112-140}$ + Cav$_{68-80}$; (D) wtNSP4$_{112-140}$ + C-Cav$_{161-178}$. (●)-wtNSP4$_{112-140}$ spectra; (○)-Cav-1 peptide spectra; (▼)-Theoretical spectra; (Δ)-Observed spectra.

For each NSP4-caveolin-1 peptide-peptide mixture, only the $wtNSP4_{112-140}$ peptide mixed with the Cav_{68-80} peptide (negative control) showed a change in α-helical content in the presence of SUV (31.3 ± 0.2% vs. 37.5 ± 1.9%) (Figure 12C; Table 5). Upon investigation of cav-1 topology, it was noted that aa68-80 are located near the membrane interacting domain and therefore may account for the observed structural changes when combined with NSP4. While the $wtNSP4_{112-140}$-C-$Cav_{161-178}$ peptide pair showed the most change in α-helical content in aqueous buffer and 50% TFE, the presence of SUV model membranes did not result in a significant conformational change (observed vs. theoretical values, Table 5). This observation suggests that the structural interaction between $wtNSP4_{112-140}$ and C-$Cav_{161-178}$ is not enhanced by the presence of model membranes.

Taken together with the results from the direct fluorescence binding assays, $wtNSP4_{112-140}$ binds Cav_{19-40} with the strongest affinity, yet this interaction causes no significant change in secondary structure conformation. The observed α-helical content did not vary from the expected theoretical value, regardless of whether the peptide mixture was in aqueous buffer, 50% TFE or mixed with SUV model membranes. These results suggest that the strong binding between $wtNSP4_{112-140}$ and Cav_{19-40} requires neither a change in structure, nor the presence of lipids, for this peptide-peptide interaction to occur.

In contrast, $NSP4_{112-140}$ binds C-$Cav_{161-178}$ with the weakest affinity, yet this interaction results in a significant change in α-helix formation. A change in structure was noted when the peptide-peptide mixture was in aqueous buffer or 50% TFE.

However, the addition of SUV model membranes had no affect on the structural interaction between the two peptides.

Discussion

Data from our laboratory show an interaction between NSP4 and the cellular protein caveolin-1 (*45, 67, 95*). Initial studies delineated the cav-1 binding domain to NSP4 residues 114-135 and more recently to three hydrophobic amino acid residues within this domain (*45, 96*). Additional in vivo yeast two-hybrid analyses and in vitro peptide binding assays reveal that NSP4 interacts with cav-1 via both the N- and C-termini of cav-1 (aa2-31 and 161-178, respectively) (*95*). Herein, we confirmed the interaction between NSP4 and the N- and C-termini of cav-1 and further delineated the NSP4 binding domain within cav-1 through the use of direct fluorescence binding assays. Utilizing an NSP4 peptide ($NSP4_{112-140}$) which encompasses the amphipathic α-helix and cav-1 binding domain, as well as cav-1 peptides corresponding to the N- (N-Cav_{2-20} and Cav_{19-40}) and C- (C-$Cav_{161-178}$) termini, we ascertained NSP4-cav-1 peptide-peptide binding affinities. Results of the peptide-peptide fluorescence binding assays showed that the N-terminus of cav-1 has a stronger affinity for NSP4 than the C-terminus. Calculation of binding constants (K_d) gave values of 39.55 ± 10.19nM for the $NSP4_{112-140}$-Cav_{19-40} interaction, 84.60 ± 6.09nM for $NSP4_{112-140}$-N-Cav_{2-20} and 216.64 ± 35.16nM for $NSP4_{112-140}$-C-$Cav_{161-178.}$ Through the use of peptides corresponding to separate regions of the N-terminus of cav-1, we were able to further define the NSP4 binding domain within cav-1. While previous research mapped the NSP4 binding site to

aa2-31 of cav-1, the results of our peptide-peptide fluorescence binding assays further narrowed this domain to aa19-40.

Following conformation of an interaction between NSP4 and both termini of cav-1, we were interested in analyzing potential secondary structural changes upon peptide-peptide interaction. Circular dichroism analysis was utilized to first reveal the structures of the peptides in aqueous buffer. Previous secondary structure analysis of an NSP4 peptide corresponding to aa114-135 ($NSP4_{114-135}$) gave an estimation of 37% α-helix for the peptide (*93, 94*). When the secondary structure of the full-length NSP4 protein was analyzed, it was found to consist of ~26% α-helix (*93*). Secondary structure analysis of our NSP4 peptide ($NSP4_{112-140}$) revealed that the peptide contained 30% α-helix, which is within the range calculated for the enterotoxic peptide and the full-length protein. When placed in the presence of SUV model membranes, which mimics a more biologically relevant environment, $NSP4_{112-140}$ demonstrated an increase in α-helical content. This increase in α-helix formation indicated that the peptide interacts with membranes in a similar manner as the $NSP4_{114-135}$ peptide.

To date the crystallographic structure of cav-1 has not been resolved; however limited secondary structural studies and bioinformatics analyses have provided insight into its structure (*75, 76*). CD analysis of aa1-101 reveals that the N-terminus contains 20% α-helix, with aa79-96 constituting the α-helix portion, while aa1-78 likely lacks significant secondary structure. An additional study, which used a bioinformatics approach, found that aa95-101 contains α-helix structure, while aa84-94 form two β-strands. The data presented herein expands on the currently known structural

information. Using peptides corresponding to the extreme N-terminus of cav-1, we show that aa2-20 and aa19-40 contain roughly 20% α-helix. Unexpectedly, the extreme C-terminus of cav-1 was determined to contain 43% α-helix, twice that of the N-terminus. This was surprising, as the bioinformatics study predicted that the C-terminus contains primarily random secondary structure.

Circular dichroism analysis of NSP4-cav-1 peptide-peptide interactions revealed that there is no significant change in α-helix formation upon binding between $NSP4_{112-140}$ and the N-terminal cav-1 peptides ($N\text{-}Cav_{2-20}$ and Cav_{19-40}). However, a structural change was noted upon interaction of $NSP4_{112-140}$ with $C\text{-}Cav_{161-178}$. Taken together with the binding assays, these results reveal that while the interaction between $NSP4_{112-140}$ and the N-terminal cav-1 peptides occurs with a strong affinity, binding does not require a conformational change in secondary structure. However, the structural change observed upon mixture of the $NSP4_{112-140}$ and $C\text{-}Cav_{161-178}$ peptides likely occurs in order to allow the two peptides to weakly interact.

The addition of SUV model membranes had no effect on the $NSP4_{112-140}$-cav-1 peptide-peptide structural interaction with the N- or C-terminal cav-1 peptides. Hence, the secondary structural interaction is not enhanced in the presence of membranes. A statistically significant conformational change was observed, however, for the $NSP4_{112-140}$-Cav_{68-80} mixture when combined with model membranes. Since aa68-80 are located near the N-terminal membrane attachment domain (N-MAD; aa82-101), as well as the transmembrane domain (aa102-134) of cav-1, it was postulated that the observed conformational change was due to the interaction of Cav_{68-80} with the membranes.

However, when Cav_{68-80} was mixed with model membranes, in the absence of $NSP4_{112-140}$, no change in secondary structure was observed. Further analysis is needed to determine the reason for this conformational change.

The interaction of NSP4 with both termini of cav-1 is unique, as most cav-1 binding proteins interact with the cav-1 scaffolding domain (CSD, aa82-101) (*128, 129, 130*). Since NSP4 (aa112-140) interacts with the N-terminus of cav-1 more strongly than the C-terminus, it is possible that the interaction with the C-terminus is transitory. NSP4 activates signaling pathways that mobilize Ca^{2+}_{i}, requiring the protein to interact with membrane-associated signaling molecules (*57*). The weak binding between NSP4 and the C-terminus of cav-1 may serve to present and/or orient the viral protein for lipid interactions. After NSP4 is properly presented to molecules within the membrane, the C-terminus of cav-1 may then quickly disassociate thus allowing NSP4 to carry out its biological function(s). Since the C-terminus of the cav-1 protein is closely associated with membranes and does not extend into the cytoplasm to the same extent as the N-terminus, it likely has less flexibility and/or accessibility for interactions with other proteins. This lack of freedom is another potential explanation for the weak binding observed between NSP4 and the C-terminus of cav-1.

It has been hypothesized that NSP4 is released from RV-infected cells. Several reports support this hypothesis by either showing the release of full-length NSP4 or a C-terminal fragment (aa112-175) (*61, 68*) or by demonstrating interactions with extracellular proteins (*59, 60*). The differential binding of NSP4 to the N- and C-termini

of cav-1 therefore may also potentially function in the presentation and transport of NSP4 across the cellular membrane.

What currently remains unknown is how both termini of cav-1 bind to the same domain within NSP4. Results of the fluorescence binding assay show that the N- and C-termini of cav-1 do not interact. Therefore, it doesn't appear that binding of both termini to NSP4 is a result of an initial interaction between the N- and C-termini, followed by binding to NSP4. Crystallographic and cross-linking data on NSP4 reveal that aa95-137 of the enterotoxic protein oligomerizes into a homotetrameric coiled-coil (*38, 39, 48*). Hence, it is likely that the two termini of cav-1 are binding two different molecules of NSP4.

Several reports highlight the use of peptides and the study of peptide-peptide interactions as a means of investigating the interactions that occur between full length proteins (*108, 109, 110, 111*). This study similarly demonstrates the utility of peptides for investigating the interaction(s) between two proteins. Through the use of peptides we further delineated the NSP4 binding domain on cav-1, demonstrated differential binding of NSP4 to each of the cav-1 termini and revealed that conformational changes in secondary structure are not necessary for the interaction between the NSP4 and cav-1 binding domains. These data provide additional insight into the relationship between NSP4 and cav-1.

CHAPTER III

THE ENTEROTOXIC PEPTIDE AND CAVEOLIN-1 BINDING DOMAINS OF THE ROTAVIRUS NON-STRUCTURAL PROTEIN 4 (NSP4) BINDS CHOLESTEROL

Overview

Rotavirus non-structural protein 4 (NSP4), the first described viral enterotoxin, is a multi-functional protein with roles in viral morphogenesis, replication and pathogenesis. Our studies reveal NSP4 and the enterotoxic peptide ($NSP4_{114-135}$) interact with model membranes similar in composition and curvature to caveolae and binds the N- and C- termini of caveolin-1. We now report that a $NSP4_{112-140}$ peptide, which encompasses both the previously reported enterotoxic and caveolin-1 binding domains, directly interacted with cholesterol. Mutations within the cholesterol recognition amino acid consensus (CRAC) domain were generated and tested for cholesterol binding. Binding results suggest the importance of the NSP4 CRAC sequence in cholesterol binding.

Introduction, Results and Discussion

The Rotavirus (RV) NSP4 protein was the first described viral enterotoxin (*3*). Several studies highlight its role in diarrhea induction in the absence of other viral proteins or replication (*3, 7, 18, 54, 55, 56, 57, 58*). Exogenous addition of NSP4 causes an increase in $[Ca^{2+}]_i$ through a phospholipase C-inositol 1,4,5-triphosphate (PLC-IP_3) mediated pathway (*55*). When expressed endogenously, NSP4 mobilizes $Ca^{2+}{}_i$, through

a PLC-independent pathway (*57, 62*). It has been hypothesized that NSP4 is released from RV infected cells whereupon it binds to neighboring uninfected cells to initiate signaling pathways resulting in diarrhea (*59, 60*).

We have shown that full-length NSP4 and its enterotoxic peptide, $NSP4_{114-135}$, preferentially interacts with model membranes that are highly curved and rich in anionic phospholipids and cholesterol (*93, 94*). These membranes closely resemble caveolae, which are highly-curved, sphingomyelin- and cholesterol-rich membrane microdomains that also contain glycosphingolipids. Caveolae primarily are identified by the presence of caveolin-1, although other proteins such as PTRF-Cavin are present (*72, 73*). Additional studies report that NSP4 colocalizes with caveolin-1 in RV-infected cells and full-length, fully glycosylated NSP4 has been found in enriched caveolae fractions isolated from the plasma membrane (*45, 67*). The enterotoxic peptide of NSP4 (aa114-135) specifically binds to both the N- and C-termini of caveolin-1 (aa2-31 and 161-178, respectively) (*45, 95*). Since caveolin-1 and caveolae participate in cholesterol transport, and NSP4 binds caveolin-1 and traffics to caveolae, we evaluated whether NSP4 directly interacts with cholesterol.

Many cholesterol binding proteins contain a cholesterol recognition amino acid consensus (CRAC) domain, which is characterized by the sequence –L/V-$(X)_{(1-5)}$-Y-$(X)_{(1-5)}$-R/K-, where $(X)_{(1-5)}$ represents between one and five unspecified residues (*86*). This sequence was first characterized in the peripheral-type benzodiazepine receptor molecule (*86*). Numerous proteins involved in cholesterol transport contain this sequence, including caveolin-1 (*79*) However, the presence of such a sequence does not

necessarily indicate an interaction with cholesterol, as this sequence allows for variability and likely is not the only requirement for cholesterol binding (*131*).

A number of viral proteins have been shown to bind cholesterol. These include the HIV-1 gp41 transmembrane glycoprotein, the influenza M2 protein and the E1 fusion protein of Semliki Forest virus (*132, 133, 134*). Upon analysis of the amino acid sequence of RV NSP4, a CRAC motif was noted between amino acids 126/127-133, which localized within the amphipathic α-helix, enterotoxic peptide and caveolin-1 binding domain (*3, 38, 39, 45*). To determine the extent to which NSP4 binds cholesterol and whether the binding occurs within this domain, a panel of synthetic peptides overlapping this region (aa112-140) were labeled with a Cy5-fluorophore and titrated with cholesterol in a direct fluorescence binding assay. $NSP4_{112\text{-}140}$ peptides containing mutations within the hydrophobic and charged faces of the amphipathic α-helix, and overlapping the hypothesized CRAC domain of NSP4, were synthesized, characterized and utilized to assess the importance of specific residues within the CRAC domain. Mutations were introduced into the hydrophobic face ($NSP4_{Hydro112\text{-}140}$) and the charged face ($NSP4_{AlaAcidic112\text{-}140}$ and $NSP4_{AlaBasic112\text{-}140}$) of the amphipathic α-helix of NSP4 as indicated in Table 6 (see Supporting Information).

We hypothesized that the amphipathic α-helix of NSP4 contributes to cholesterol interaction. By disrupting the amphipathicity of the CRAC sequence, we directly addressed this question. We also determined the K_d of the interaction to acquire relative binding affinities to cholesterol (*45, 126*).

Wt- and mtNSP4$_{112\text{-}140}$ peptides were labeled with a Cy5 fluorescent dye, using the Cy5 Mono-reactive dye pack from Amersham Biosciences (Piscataway, NJ), according to the manufacturer's protocol. To analyze a binding interaction between each of the peptides and cholesterol, an increasing quantity of cholesterol (5-35nM) was added to 10-20nM of the Cy5-labeled wt- or mtNSP4$_{112\text{-}140}$ peptides in 2mL of phosphate buffered saline (pH 7.4). The Cy5 fluorophore was excited at 649nm and the emission spectra were scanned from 655-720nm (see Supporting Information). Measurements of fluorescent intensities (at 665nm) of the Cy5-NSP4-specific peptides in the presence of increasing concentrations of cholesterol were corrected for background (Cy5-NSP4-specific peptides in buffer alone) and plotted as a function of cholesterol concentration. In the absence of cholesterol, the Cy5-NSP4$_{112\text{-}140}$ peptide showed maximum fluorescence at 665nm (Figure 13). Upon titration with cholesterol (5-35nM), Cy5-NSP4$_{112\text{-}140}$ showed a decrease in fluorescence intensity, indicative of an interaction (Figure 13B). A linear reciprocal plot was generated to determine the binding affinity (K_d) of cholesterol for NSP4$_{112\text{-}140}$, which was calculated as 7.67 ± 1.49nM. A control peptide (NSP4$_{150\text{-}175\Delta Ala}$), corresponding to the C-terminus of NSP4 and lacking the CRAC motif, did not demonstrate a change in fluorescence intensity in the presence of cholesterol, and therefore lacked binding (Figures 13C and 13D).

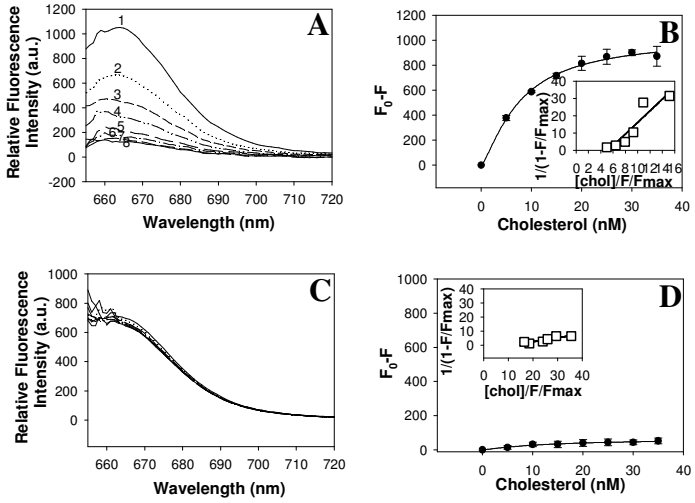

Figure 13: Cholesterol Directly Binds the NSP4$_{112\text{-}140}$ Peptide. (*A*)-Fluorescence spectra of Cy5-NSP4$_{112\text{-}140}$ titrated with increasing concentrations of cholesterol. *Spectrum 1*, 10nM Cy5-NSP4$_{112\text{-}140}$ in buffer only. *Spectra 2-8*, 10nM Cy5-NSP4$_{112\text{-}140}$ in the presence of 5, 10, 15, 20, 25, 20 and 35nM of cholesterol, respectively. (*B*)-Plot of maximal fluorescence emission (measured at 665nm upon excitation at 649nm) for cholesterol in the presence of 10nM Cy5-NSP4$_{112\text{-}140}$. *Inset*, linear plot of the binding curve of cholesterol. (*C*)-Fluorescence spectra of Cy5-NSP4$_{150\text{-}175}$ (negative control) titrated with increasing concentrations of cholesterol. (*D*)-Plot of maximal fluorescence emission (measured at 665nm upon excitation at 649nm) for cholesterol in the presence of 10nM Cy5-NSP4$_{150\text{-}175}$. *Inset*, linear plot of the binding curve of cholesterol.

Synthetic peptides containing mutations within the amphipathic α-helix/CRAC motif similarly were examined for cholesterol binding. Each of the mutant peptides was labeled with a Cy5-fluorophore and evaluated for cholesterol binding by the direct fluorescence binding assay as before. When titrated with increasing concentrations of cholesterol (5-35nM), the Cy5-NSP4$_{AlaBasic112\text{-}140}$ peptide demonstrated a decrease in fluorescent intensity, similar to that seen with wt-NSP4$_{112\text{-}140}$ (Figure 14A). This change in fluorescence was indicative of cholesterol binding and the K_d for this interaction was calculated to be 11.49 ± 2.53nM. The Cy5-NSP4$_{AlaAcidic112\text{-}140}$ peptide also demonstrated a change in fluorescence intensity in the presence of cholesterol, although the observed change was less than that seen with the NSP4$_{112\text{-}140}$ and NSP4$_{AlaBasic112\text{-}140}$ peptides. The

calculated K_d value for the $NSP4_{AlaAcidic112-140}$ interaction was highly variable, suggesting that the interaction with cholesterol was weak.

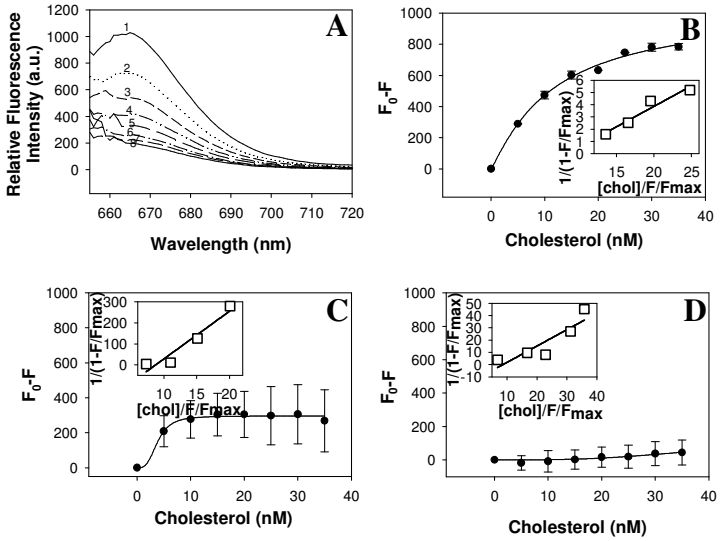

Figure 14: Cholesterol Directly Binds to $NSP4_{AlaBasic112-140}$ and $NSP4_{AlaAcidic112-140}$, but not $NSP4_{Hydro112-140}$. (*A-B*): Fluorescence spectra of Cy5-$NSP4_{AlaBasic112-140}$ (*A)* titrated with increasing concentrations of cholesterol. Spectrum 1, 10nM Cy5-$NSP4_{AlaBasic112-140}$ in buffer only. Spectra 2-8, 10nM Cy5-$NSP4_{AlaBasic112-140}$ in the presence of 5, 10, 15, 20, 25, 20 and 35nM of cholesterol, respectively. (*B-D*): Plot of maximal fluorescence emission (measured at 665nm upon excitation at 649nm) for cholesterol in the presence of 10nM Cy5-$NSP4_{AlaBasic112-140}$ (*B*), 20nM Cy5-$NSP4_{AlaAcidic112-140}$ (*C*) and 10nM Cy5-$NSP4_{Hydro112-140}$ (*D*). Insets, linear plots of the binding curve of cholesterol.

Distinct from the $NSP4_{AlaBasic112-140}$ and $NSP4_{AlaAcidic112-140}$ mutants, the Cy5-$NSP4_{Hydro112-140}$ peptide showed no significant change in fluorescent intensity upon titration with cholesterol, indicative of a lack of binding (Figure 14D). The binding affinity (K_d) could not be calculated within the tested cholesterol concentration range. These assays were then repeated using unlabeled wt- and mt$NSP4_{112-140}$ peptides and fluorescent NBD-cholesterol. The results from these experiments verified the results from the Cy5-labeled peptide experiments (data not shown).

Taken together, we demonstrated for the first time that a RV NSP4 peptide directly interacted with cholesterol and this interaction overlapped the amphipathic α-helix, enterotoxic peptide and caveolin-1 binding domains (aa112-140). This interaction between cholesterol and the NSP4 CRAC sequence has implications for the trafficking of NSP4 in RV infected cells. Abundant data from our laboratory reveal that NSP4 interacts with caveolin-1 and caveolae (*45, 67, 93, 94, 95, unpublished experiments*). Given that caveolae are involved in de novo cholesterol transport from the ER to the PM (*76, 80, 87, 135*) and caveolin-1 assists in cholesterol transport, contains a CRAC motif and binds cholesterol in a 1:1 ratio (*79, 88*), it is reasonable that caveolin-1 and cholesterol function in NSP4 intracellular transport. NSP4 interacts with caveolin-1, encodes a CRAC motif, traffics to the cell surface via an unconventional pathway and as we now show, interacts with cholesterol, with a K_d of 7.67 ± 1.49nM. We also showed that the cholesterol-NSP4 interaction was specific to aa112-140. Based on these results, we reasoned that NSP4 also traffics with cholesterol and caveolin-1 from the ER to the plasma membrane by an unconventional transport pathway.

To further evaluate the role of the CRAC sequence in more detail, $NSP4_{112\text{-}140}$ peptides containing mutations within the CRAC domain, were assessed for cholesterol binding. The $NSP4_{AlaBasic112\text{-}140}$ peptide contains a lysine to alanine mutation within the CRAC motif. Mutation of the lysine 133 residue failed to abolish cholesterol binding, as the peptide bound cholesterol with a K_d of 11.49 ± 2.53nM. However, when compared with the wt-$NSP4_{112\text{-}140}$ peptide, the K_d for the $NSP4_{AlaBasic112\text{-}140}$-cholesterol interaction is 1.5-fold higher, indicative of a weaker binding affinity. The

$NSP4_{AlaAcidic112\text{-}140}$ peptide contains an aspartic acid to alanine mutation within the CRAC domain and demonstrated an even weaker binding affinity to cholesterol with a highly variable K_d value. The observance of a weaker binding affinity for cholesterol indicates the importance of the aspartic acid 132 residue. However, this residue is located within a variable position within the CRAC motif and therefore may not be required for cholesterol binding.

Lack of cholesterol binding to the $NSP4_{Hydro112\text{-}140}$ peptide suggests the tyrosine 131 residue within the amphipathic α-helix is important for the NSP4-cholesterol interaction. Another cholesterol binding study on peptides of the CRAC motif of the peripheral-type benzodiazepine receptor suggests that the aromatic ring of tyrosine may stack with the A ring of cholesterol (*136*). Since the $NSP4_{Hydro112\text{-}140}$ peptide contains a tyrosine mutation and completely lacks cholesterol binding activity, it is possible that the tyrosine residue of NSP4 likewise is important for binding to cholesterol. Additional studies are needed to confirm this hypothesis.

Together, these results demonstrate that NSP4 binds cholesterol within the amphipathic α-helix/enterotoxic peptide/caveolin-1 binding domain and implies that the tyrosine 131 residue is important for binding. In addition, the interaction between NSP4 and cholesterol supports the hypothesis that NSP4 traffics via a cholesterol transport pathway in RV infected cells. This interaction may also be important for enterotoxic function as a previous study utilizing a peptide containing a tyrosine mutation demonstrated a lack of diarrheagenic function in mouse pups (*94*). The interaction of

NSP4 with cholesterol adds to the multitude of unique features of NSP4 and helps to explain its novel unconventional transport to the plasma membrane and caveolae.

Supporting Information-Materials and Methods

Materials

Cholesterol, Sephadex G-25 and trifluoroethanol (TFE) were purchased from Sigma (St. Louis, MO). Trifluoroacetic acid (TFA), 1-hydroxy-benzotriazole (HOBt) and O-Benzotriazole-N,N,N',N'-tetramethyluronium-hexafluoro-phosphate (HBTU) were purchased from American Bioanalytical (Natick, MA). N,N-diisopropylethylamine (DIPEA) and N,N'-diisopropylcarbodiimide (DIPCIDI) were purchased from CreoSalus (Louisville, KY). Thioanisole, ethanedithiol and anisole were purchased from EMD chemicals (Gibbstown, NJ).

Synthesis and Purification of NSP4 Peptides

All NSP4 peptides were synthesized by fluorenylmethoxycarbonyl (Fmoc) solid-phase chemistry with either 1-hydroxy-benzotriazole (HOBt), O-Benzotriazole-N,N,N',N'-tetramethyluronium-hexafluoro-phosphate (HBTU) and N,N-diisopropylethylamine (DIPEA), or HOBt and N,N'-diisopropylcarbodiimide (DIPCIDI) activation using the Model 90 Peptide Synthesizer (Advanced Chemtech; Louisville, KY). Following synthesis, the peptides were cleaved from the solid resin support and all side-chain protecting groups removed by addition of Reagent R (90% trifluoroacetic acid (TFA), 5% thioanisole, 3% ethanedithiol and 2% anisole). The peptide/Reagent R cleavage mixture was incubated at RT for a maximum of 2 hours with gentle mixing.

To separate the peptides from the solid support, the mixture was filtered through a sintered glass filter into a 50mL conical tube containing cold diethyl ether in a dry ice/ethanol bath. Following 2-3 rinses of the filter with TFA, the peptide precipitate was pelleted by centrifugation at ~300*g* for 4 minutes. The supernatant was removed and additional cold diethyl ether was added to the peptide pellet. The mixture was allowed to cool in the dry ice/ethanol bath for several minutes before repelleting. The supernatant was removed, more ether added and the step was repeated an additional two times. The crude peptide precipitate was dried under N_2, resolubilized in 10% acetic acid and lyophilized.

Each lyophilized crude peptide was resuspended in 5-10% acetic acid and purified from organic contaminants and incomplete peptide fragments by gravimetric gel filtration chromatography (Sephadex G25 medium). The eluted peptide was collected by void volume (~190mL), lyophilized and further purified by reverse-phase HPLC using a reverse phase C4 Delta Pak column (Waters Chromatography Division, Milford, MA) or a reverse phase C18 column (Beckman-Coulter, Fullerton, CA). Peptides were purified using a linear gradient of water to acetonitrile over 30-45 minutes. Eluted peaks were lyophilized and characterized by matrix-assisted laser desorption/ionization (MALDI) mass spectrometry (Laboratory for Biological Mass Spectrometry, Department of Chemistry, Texas A&M University, College Station, TX). Mass chromatograms revealed if the full-length peptide was present, the mass of the peptide and the extent of contaminates in the eluted fraction. Only peptides of ~95% purity were used in this study.

Direct Peptide-Cholesterol Interactions

A previously established direct fluorescent binding assay was utilized to determine the binding of wt- and mtNSP4$_{112\text{-}140}$ peptides with cholesterol (*45, 126*). The wt- and mtNSP4$_{112\text{-}140}$ peptides were labeled with a Cy5 fluorescent dye, using the Cy5 Mono-reactive dye pack from Amersham Biosciences (Piscataway, NJ). Cy5 labeling of the peptide followed the manufacturer's protocol.

To analyze a binding interaction between the wt- and mtNSP4$_{112\text{-}140}$ peptides and cholesterol, an increasing quantity of cholesterol (5-35nM) was added to 10-20nM of the Cy5-labeled wt- or mtNSP4$_{112\text{-}140}$ peptides in 2mL of phosphate buffered saline (pH 7.4). Excitation of the Cy5 fluorophore was carried out at 649nm, and the emission spectra was scanned from 655-720nm. Fluorescence emission spectra were obtained at 25ºC with a PC1 photon-counting spectrofluorometer (ISS, Inc., Champaign, IL) with excitation and emission slit widths of 1.0. Spectra were corrected for background and maximal fluorescence intensities were measured. Calculation of the dissociation constant (K_d) was performed from the titration curves plotted as quenching in peptide fluorescence intensity (F_0-F, where F_0 and F represented the Cy5-NSP4$_{112\text{-}140}$ fluorescence intensities in the absence and presence of cholesterol, respectively, at each titration point) as a function of cholesterol concentration. A reciprocal plot of $1/(1-F/F_{max})$ *vs.* $C_L/F/F_{max}$ was used to calculate the K_d value according to the following equation: $y = bx + y_o$, where F is the fluorescence intensity at a given concentration of ligand, F_{max} is the maximal fluorescence obtained and C_L is the ligand concentration. The slope of the line (b) is equal to $1/K_d$. The sigmoidal curves were also fit to a Hill

plot, according to the following equation: $y = ax^b/(c^b + x^b)$, where y and x correspond to (F_0-F) and the ligand concentration at each point, while a, b and c represent the maximum binding (B_{max}), the number of binding sites (n) and the K_d value, respectively.

Table 6: NSP4 Peptides and Cholesterol Binding

Peptide:	Sequence:	CRAC Sequence (aa126/127-133)	Cholesterol Binding:	K_d (nM):
$NSP4_{112-140}$	MIDKLTTREIEQVELLKRIYDKLTVQTTG	(L)LKRIYDK	Yes	7.67 ± 1.49nM
$NSP4_{Hydro112-140}$	M**R**DKLTTREIEQ**K**ELLKRI**D**DKLTVQTTG	(L)LKRI**D**DK	No	N/A
$NSP4_{AlaAcidic112-140}$	MI**A**KLTTREIEQV**A**LLKRIY**A**KLTVQTTG	(L)LKRIY**A**K	No	N/A
$NSP4_{AlaBasic112-140}$	MID**A**LTT**A**EIEQVELLKRIYD**A**LTVQTTG	(L)LKRIYD**A**	Yes	11.49 ± 2.53nM
$NSP4_{150-175\Delta Ala}$	QKNVRTLEEWESGKNPYEPREVTAM	N/A	No	N/A

Mutated amino acids are shown in red.

CHAPTER IV

ADDITIONAL DATA, CONCLUSIONS AND FUTURE RESEARCH

Additional Data

Secondary Structure of mtNSP4$_{112\text{-}140}$ Peptides

The amphipathic α-helix (AAH) of NSP4 contains a hydrophobic face and a charged face with both acidic and basic charged regions. Mutational analysis of the AAH of NSP4 recently revealed that binding to cav-1 occurs via a hydrophobic interaction (*96*). However, the extent to which the mutations alter the secondary structure and thus affect binding to cav-1 was unknown. Therefore circular dichroism was utilized to investigate changes in the secondary structure as a result of the mutations in the AAH. Three peptides encompassing aa112-140 of NSP4 were synthesized that contained mutated residues in the hydrophobic (NSP4$_{Hydro112\text{-}140}$), acidic (NSP4$_{AlaAcidic112\text{-}140}$) or basic (NSP4$_{AlaBasic112\text{-}140}$) face of the AAH. The sequences of each of the NSP4 peptides are given in Table 7. NSP4$_{Hydro112\text{-}140}$ contains three charged amino acids (aa113, 124, 131) that were mutated from the original hydrophobic residues. NSP4$_{AlaAcidic112\text{-}140}$ and NSP4$_{AlaBasic112\text{-}140}$ each contain three alanine residues substituted for negatively charged (aa114, 125, 132) and positively charged (aa115, 119, 133) residues, respectively.

Table 7: Sequences of wt- and mtNSP4$_{112\text{-}140}$ Peptides[a]

Peptide Name:	Peptide Sequence (N→C):
NSP4$_{112\text{-}140}$ (aa112-140)	MIDKLTTREIEQVELLKRIYDKLTVQTTG
NSP4$_{Hydro112\text{-}140}$ (aa112-140)	M**R**DKLTTREIEQ**K**ELLKRI**D**DKLTVQTTG
NSP4$_{Ala\ Acidic112\text{-}140}$ (aa112-140)	MI**A**KLTTREIEQV**A**LLKRIY**A**KLTVQTTG
NSP4$_{Ala\ Basic112\text{-}140}$ (aa112-140)	MID**A**LTT**A**EIEQVELLKRIYD**A**LTVQTTG

[a]Amino acid residues that have been mutated are highlighted in red.

Mutations within the hydrophobic face of the amphipathic α-helix of NSP4 alter the secondary structure

As shown in Figure 15, the CD spectra of the mutant NSP4 (mtNSP4) peptides in aqueous buffer differed from that of the wild-type peptide (Figure 15B-D, dark circles). The α-helical content was calculated based on the molar ellipticity values at 222nm. The NSP4$_{Hydro112\text{-}140}$ peptide seemed to be most affected by the mutations made in the AAH, as the α-helical content was determined to be 19.4 ± 2.2% (Table 8). The mutations made in each of the charged faces of the AAH had less of an affect on α-helix formation within the corresponding peptides. The α-helical content for the NSP4$_{AlaAcidic112\text{-}140}$ and NSP4$_{AlaBasic112\text{-}140}$ peptides was determined to be 23.7 ± 0.6% and 26.2 ± 2.9%, respectively.

In the presence of 50% TFE, the α-helical secondary structure of each of the mutant NSP4 peptides increased 2.5-3 times over that observed in aqueous buffer (Figure 15B-D, open circles). As in aqueous buffer, the NSP4$_{Hydro112\text{-}140}$ peptide exhibited less α-helical formation (57.8 ± 0.6%) than the NSP4$_{AlaAcidic112\text{-}140}$ and NSP4$_{AlaBasic112\text{-}140}$ peptides (73.1 ± 7.3% and 75.3 ± 2.8%, respectively) (Table 8). Therefore, mutation of

hydrophobic residues within the amphipathic α-helix/cav-1 binding domain of NSP4 most negatively affected the α-helix forming ability of the peptide. Mutation of charged residues, however, only had a slight affect ($NSP4_{AlaAcidic112-140)}$ or no affect ($NSP4_{AlaBasic112-140}$) on the α-helix forming ability of the peptides.

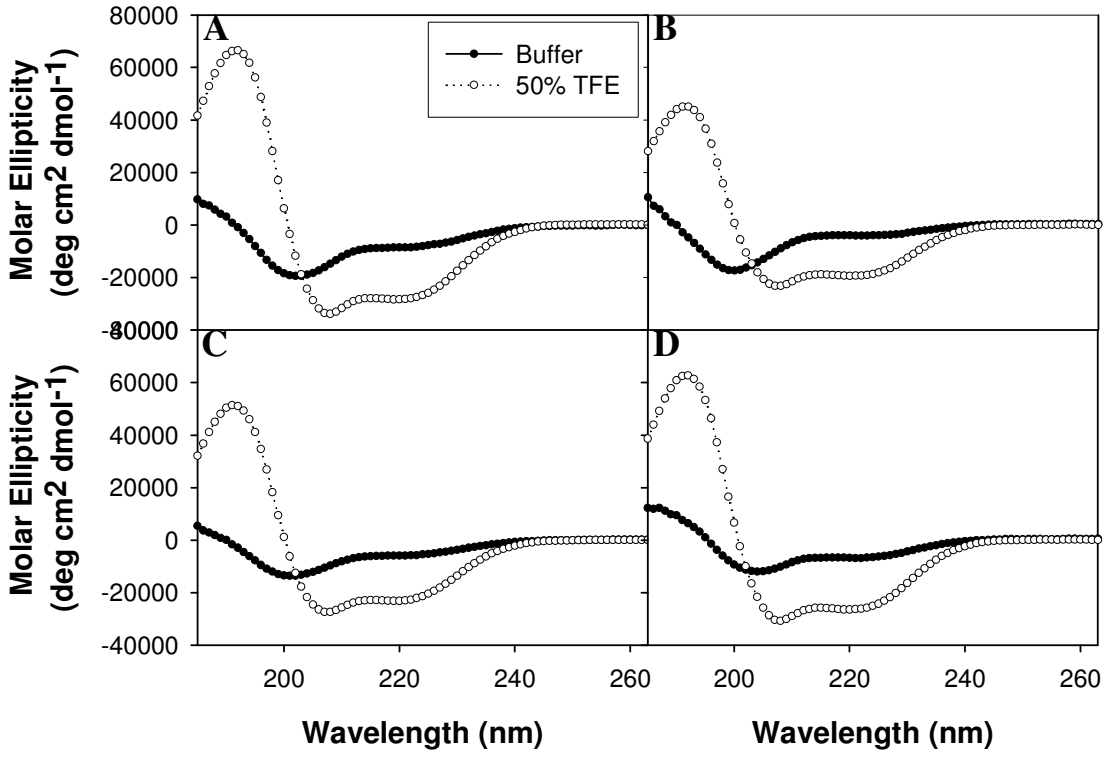

Figure 15: CD Spectra of wt- and mt$NSP4_{112-140}$ Peptides in Aqueous Buffer (●) and 50% TFE (○). (A) wt$NSP4_{112-140}$; (B) $NSP4_{Hydro112-140}$; (C) $NSP4_{AlaAcidic112-140}$; (D) $NSP4_{AlaBasic112-140}$.

Table 8: Percent α-helix[a] of wt- and mtNSP4$_{112-140}$ Peptides in Aqueous Buffer, 50% TFE and in the Presence of 1mM SUV (55:35:10, POPC/cholesterol/DOPS).

Peptide:	Aqueous Buffer:	50% TFE:	1mM SUV:
NSP4$_{112-140}$	30.6 ± 2.4%	79.6 ± 4.6%	57.9 ± 1.6%
NSP4$_{Hydro112-140}$	19.4 ± 2.2%	57.8 ± 0.6%	30.9 ± 0.7%
NSP4$_{AlaAcidic112-140}$	23.7 ± 0.6%	73.1 ± 7.3%	36.9 ± 0.7%
NSP4$_{AlaBasic112-140}$	26.2 ± 2.9%	75.3 ± 2.8%	49.2 ± 0.5%

[a]Data is presented as mean ± SD, n= 4.

To determine how the mutations within the AAH affect membrane interactions, each of the mtNSP4$_{112-140}$ peptides was mixed with SUV model membranes (55:35:10, POPC/cholesterol/DOPS) and changes in α-helical content were noted by CD.

The CD spectrum of the mtNSP4$_{112-140}$ peptides showed a 1.5-2-fold increase in α-helix formation from that in aqueous buffer (Figure 16). While α-helix formation of the mutant peptides increased in the presence of SUV, the calculated content was less than that observed with the wtNSP4$_{112-140}$ peptide in the presence of SUV. The NSP4$_{AlaBasic112-140}$ peptide demonstrated a 2-fold increase in α-helix formation in the presence of membranes (49.2 ± 0.5%). The α-helical content of the NSP4$_{Hydro112-140}$ and NSP4$_{AlaAcidic112-140}$ peptides was significantly less than that of wtNSP4$_{112-140}$, however, and was determined to be 30.9 ± 0.7% and 36.9 ± 0.7%, respectively (Table 8). Thus, mutation of residues within the AAH of NSP4 results in decreased α-helix formation and thus interaction with lipids.

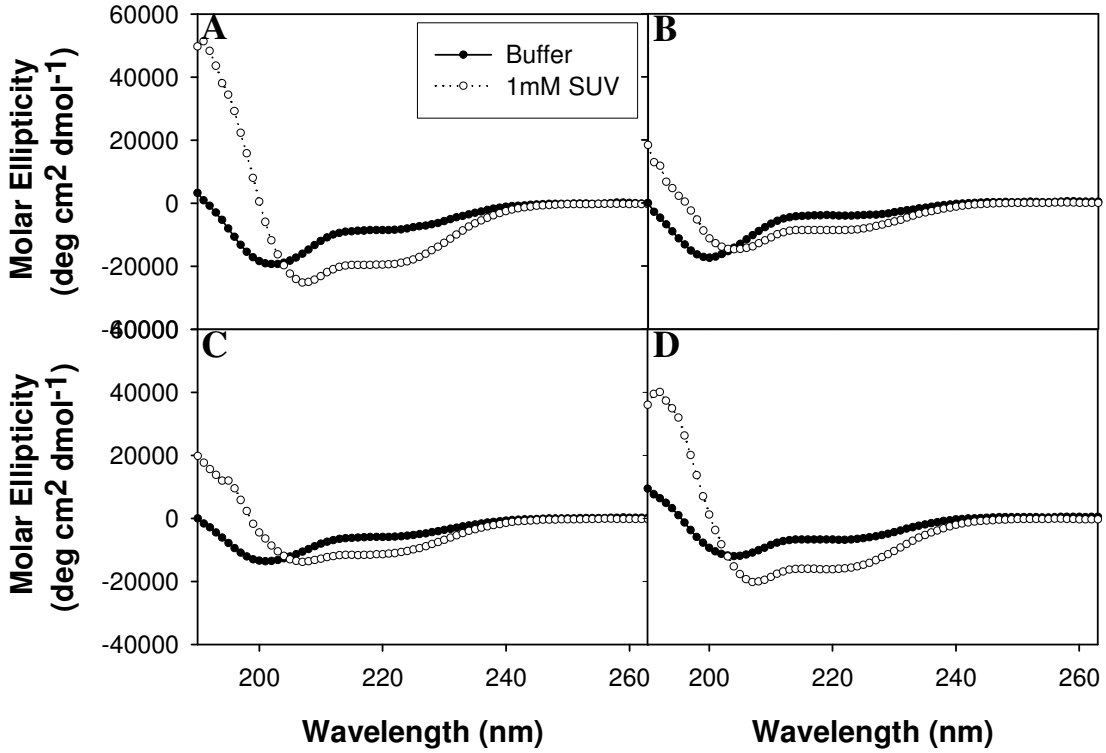

Figure 16: CD Spectra of wt- and mtNSP4$_{112\text{-}140}$ Peptides in Aqueous Buffer (●) and in the Presence of 1mM SUV (55:35:10, POPC/cholesterol/DOPS) (○). (A) wtNSP4$_{112\text{-}140}$; (B) NSP4$_{Hydro112\text{-}140}$; (C) NSP4$_{AlaAcidic112\text{-}140}$; (D) NSP4$_{AlaBasic112\text{-}140}$.

Taken together with previous yeast two-hybrid and peptide-binding assay data, these peptide secondary structural studies suggest that the structural conformation of NSP4 may play a role in cav-1 binding. Mutation of the hydrophobic face of the AAH of NSP4 abolishes binding to cav-1 (*96*), and results in secondary structural changes in the corresponding peptide (NSP4$_{Hydro112\text{-}140}$). Circular dichroism analysis revealed a significant decrease in α-helix formation from that of the wtNSP4$_{112\text{-}140}$ peptide. Conversely, mutation of the charged face of the AAH resulted in minimal, if any, change in the secondary structure of the corresponding peptides (NSP4$_{AlaAcidic112\text{-}140}$ and NSP4$_{AlaBasic112\text{-}140}$). Additional studies that abolish cav-1 binding while maintaining the secondary structure are needed to verify the role of conformation in cav-1 binding.

Mutagenesis of the AAH also had an affect on the structural interactions of the mutant peptides with model membranes. When in the presence of model membranes, each of the mutant peptides demonstrated an increase in α-helix formation, indicative of an interaction. While the α-helical content was shown to increase, it was still less than that observed for the wtNSP4$_{112\text{-}140}$ peptide following lipid interaction. This alteration in structure may have potential implications for NSP4 function.

Diarrhea Induction in Mouse Pups

To examine the biological relevance (enterotoxic activity) of the mutations made in the amphipathic α-helix/enterotoxic peptide/caveolin-1 binding domain of NSP4, each of the NSP4-specific peptides was tested for diarrhea induction in mouse pups as previously described (*3, 68*). Briefly, each of the NSP4-specific peptides (200-400nmol) was administered by intraperitoneal delivery to 6-10 day old mouse pups. Prior to injection, all purified peptide samples were tested for endotoxin by the *Limulus* Amebocyte Lysate (LAL) test (Associates of Cape Cod, Inc.) according to the manufacturer's protocol, to ensure that samples were endotoxin free. A value of 0.5 EU/mL or less was considered acceptable for use in the diarrhea studies. Mouse pups injected with endotoxin free PBS served as a control. Mouse pups were monitored for diarrhea every 2 hours for 12 hours and then at 24 hours post injection. The severity of the diarrhea was scored on a scale of 1 to 4.

Mutations within the hydrophobic and basic charged faces of the amphipathic α-helix of NSP4 abolish diarrheagenic activity in mouse pups

Following injection, both the wt-NSP4$_{112\text{-}140}$ and NSP4$_{\text{AlaAcidic}112\text{-}140}$ peptides were found to cause diarrhea in 50% and 67% of the mouse pups tested, respectively (Table 9).

The $NSP4_{Hydro112-140}$ and $NSP4_{AlaBasic112-140}$ peptides, however, did not induce diarrhea in any of the mouse pups tested. While this study merits repeating, these preliminary results suggest that residues within both the hydrophobic face and the basic face of the amphipathic α-helix of NSP4 are important for enterotoxic activity.

Table 9: Diarrheagenic Activity of wt- and mt$NSP4_{112-140}$ Peptides in Mouse Pups.

Peptides	% Diarrhea
$NSP4_{112-140}$	50% (3/6)
$NSP4_{Hydro112-140}$	0% (0/6)
$NSP4_{AlaAcidic112-140}$	67% (4/6)
$NSP4_{AlaBasic112-140}$	0% (0/6)
PBS (negative control)	0% (0/4)

A previous study highlighted the importance of the tyrosine residue in the hydrophobic face of the amphipathic α-helix (*94*). A synthetic peptide in which the tyrosine residue was mutated to a lysine was found to lack diarrhea inducing function. The current study supports those results and further suggests that the positively charged face of the amphipathic α-helix may also be important for diarrhea function, possibly through a lipid interaction.

A recent study revealed that the α1β1 and α2β1 integrins are receptors for NSP4 (*60*). Binding to these receptors initiates cellular signaling processes (particularly PLC-mediated signaling) which result in diarrhea in RV infected individuals. This agrees with previous data demonstrating that exogenous addition of NSP4 mobilizes $[Ca^{2+}]_i$ from ER stores through a phospholipase C-inositol 1,4,5-triphosphate (PLC-IP_3) pathway (*55*). While integrin receptor binding was shown to occur via aa114-130, signaling was shown

to occur via an interaction between aa131-140 and a separate integrin domain. Given that integrin signaling occurs via aa131-140, and $NSP4_{AlaBasic112-140}$ has a mutation at aa133 which abolishes enterotoxic function, it is possible that the lack of diarrhea induction seen with this peptide is a result of an inability to initiate signaling through the integrin receptor. Similarly, $NSP4_{Hydro112-140}$ contains a mutation at aa131, which is within the integrin signaling domain, and does not cause diarrhea. Lack of enterotoxic function with this mutant peptide may also be a result of its inability to initiate integrin mediated signaling.

Conclusions and Significance

The purpose of this research was to examine and analyze the secondary structural and functional interactions between NSP4 and caveolin-1. Peptides corresponding to the amphipathic α-helix, enterotoxic peptide and caveolin-1 binding domain of NSP4 (aa112-140), as well as the N- (aa2-20 and 19-40) and C- (aa161-178) termini of cav-1, were synthesized and characterized for the studies involved herein. Fluorescence binding assays demonstrated differential binding of the N- and C-termini of cav-1 to the $NSP4_{112-140}$ peptide and were used determined the relative binding affinities (K_d) of these interactions. Utilization of two peptides corresponding to different regions of the N-terminus of cav-1 allowed for further delineation of the binding domain of NSP4 to aa19-40 of cav-1. Subsequent circular dichroism analysis of the NSP4-cav-1 peptide-peptide interactions revealed that conformational changes in the secondary structure only occur following interaction of $NSP4_{112-140}$ with $C\text{-}Cav_{161-178}$. Additionally, NSP4 peptides were examined for cholesterol binding utilizing the fluorescence binding assay. NSP4 was shown to bind cholesterol and this interaction occurs via aa112-140.

Mutant peptides were synthesized containing mutations within the hydrophobic and charged faces of the amphipathic α-helix (AAH). Secondary structural analysis of the mutant peptides revealed the extent to which the mutations affected the secondary structure of the peptides. Cholesterol binding and diarrhea induction studies using the mutant peptides suggested the importance of hydrophobic and basic amino acid residues within the AAH in mediating these functions.

$NSP4_{112-140}$ binds the N-terminus of cav-1 with a stronger affinity than the C-terminus

While previous research reveals that NSP4 (aa114-135) binds both termini of cav-1 (*45, 95*), this study demonstrated differential binding of the cav-1 termini to NSP4. NSP4- and cav-1-specific peptides were utilized in a fluorescence binding assay to analyze binding between NSP4 and the N- and C-termini of cav-1. In addition, relative binding affinities were determined for these interactions. Results of the binding assays revealed that the $NSP4_{112-140}$ peptide binds the N-terminus (K_d (aa2-20) = 84.60 ± 6.09nM; K_d (aa19-40) = 39.55 ± 10.19nM) of cav-1 with a stronger affinity than the C-terminus (K_d (aa161-178) = 216.64 ± 35.16nM). Moreover, the NSP4 binding domain was further delineated to aa19-40 within the N-terminus of cav-1.

Secondary structural changes are observed only for the $NSP4_{112-140}$-C-$Cav_{161-178}$ peptide-peptide interaction

The $NSP4_{112-140}$ peptide was mixed with each of the cav-1 peptides and secondary structural changes were investigated by circular dichroism. No significant change in secondary structure was observed upon interaction of $NSP4_{112-140}$ with N-Cav_{2-20}, Cav_{19-40} or the control peptide, Cav_{68-80}. However, mixture of $NSP4_{112-140}$ with C-$Cav_{161-178}$

resulted in a significant change in secondary structure. Taken together with the results of the binding assay, the relatively strong interaction between $NSP4_{112-140}$ and the N-terminal cav-1 peptides occurs with no change in secondary structure. Conversely, the relatively weak binding between the $NSP4_{112-140}$ and $C\text{-}Cav_{161-178}$ peptides results in a conformational change in secondary structure.

NSP4 binds cholesterol within the amphipathic α-helix, enterotoxic peptide and caveolin-1 binding domains

Analysis of the NSP4 sequence revealed a potential cholesterol recognition amino acid consensus (CRAC) motif between aa126/127-133, which is located within the amphipathic α-helix, enterotoxic peptide and cav-1 binding domain. Therefore, NSP4-specific peptides were utilized to examine a potential NSP4-cholesterol interaction through a direct fluorescence binding assay. The $wtNSP4_{112-140}$ peptide bound cholesterol with a K_d of 7.67 ± 1.49nM. A control peptide ($NSP4_{150-175\Delta Ala}$) corresponding to the extreme C-terminus of NSP4 and lacking a CRAC motif, did not bind cholesterol. Hence, the cholesterol binding domain of NSP4 was determined to be between aa112-140.

Mutant NSP4 peptides ($NSP4_{Hydro112-140}$, $NSP4_{AlaAcidic112-140}$ and $NSP4_{AlaBasic112-140}$), each containing a mutation with the putative CRAC domain, were used to analyze the importance of specific residues within the cholesterol binding domain. The $NSP4_{AlaBasic112-140}$ peptide, containing a lysine to alanine mutation at residue 133, bound cholesterol with a K_d of 11.49 ± 2.53nM. While this mutation resulted in a slight decrease in cholesterol binding, the lysine residue within the CRAC domain does not appear to be important for cholesterol binding. Similarly, the $NSP4_{AlaAcidic112-140}$ peptide,

containing an aspartic acid to alanine mutation at residue 132, also bound cholesterol with a highly variable K_d value. The affinity of this interaction was weaker than that observed with both the $wtNSP4_{112-140}$ and $NSP4_{AlaBasic112-140}$ peptides. The $NSP4_{Hydro112-140}$ peptide, however, demonstrated no interaction with cholesterol. Since this peptide contained a tyrosine to aspartic acid mutation at residue 131, the lack of binding suggests the importance of the tyrosine 131 residue in cholesterol binding.

Mutation of hydrophobic residues within the amphipathic α-helix disrupt the secondary structure

Peptides containing mutated residues within either the hydrophobic ($NSP4_{Hydro112-140}$) or charged face ($NSP4_{AlaAcidic112-140}$ or $NSP4_{AlaBasic112-140}$) of the amphipathic α-helix of NSP4 were examined for secondary structural changes by circular dichroism analysis. Mutation of hydrophobic residues within the AAH resulted in the most significant alterations in the overall structure. The α-helical content for the $NSP4_{Hydro112-140}$ peptide was calculated to be 19.4 ± 2.2%, which is significantly less than that of the $wtNSP4_{112-140}$ peptide (30.6 ± 2.4%). Conversely, mutation of either acidic ($NSP4_{AlaAcidic112-140}$) or basic ($NSP4_{AlaBasic112-140}$) residues within the AAH had very little or no affect on the secondary structure (23.7 ± 0.6% and 26.2 ± 2.9% for $NSP4_{AlaAcidic112-140}$ and $NSP4_{AlaBasic112-140}$, respectively). Since previous data reveals that mutation of residues within the hydrophobic face abolishes cav-1 binding (*96*), these results suggest that conformation plays a role in the interaction between NSP4 and cav-1.

The addition of model membranes resulted in a 1.5-2-fold increase in α-helix formation for each of the mutant peptides. However, the total α-helical content was less than that observed following interaction of the $wtNSP4_{112-140}$ peptide with membranes.

Therefore, mutations within the AAH affect α-helix formation, and thus interaction, with membranes.

Hydrophobic and basic amino acid residues within the amphipathic α-helix, enterotoxic peptide and caveolin-1 binding domains contribute to diarrheagenic function

Each of the wt- and mtNSP4$_{112\text{-}140}$ peptides was tested for diarrheagenic function in mouse pups. The wtNSP4$_{112\text{-}140}$ peptide caused diarrhea in 50% of the mouse pups tested, which agreed with previously published reports (*3, 94*). Similarly, the NSP4$_{AlaAcidic112\text{-}140}$ peptide caused diarrhea in 67% of the mouse pups tested, indicating that acidic residues within the AAH of NSP4 are not important for diarrheagenic function. Both the NSP4$_{Hydro112\text{-}140}$ and NSP4$_{AlaBasic112\text{-}140}$ peptides, however, failed to induce diarrhea in mouse pups. These results suggested that both hydrophobic and basic residues within the AAH of NSP4 are involved in diarrhea induction.

Secondary Structure, caveolin-1, cholesterol and enterotoxic function

The results of this research provide insight into the relationship among NSP4 secondary structure, cav-1 binding, cholesterol and diarrheagenic function. Table 10 illustrates the relationship between secondary structure and function. While synthetic peptides were used in these studies to further investigate and dissect the various functions of NSP4, these findings are postulated to be relevant to the full length protein.

Table 10: Relationship Between Secondary Structure and Function, Including Caveolin-1 and Cholesterol Binding and Diarrhea Induction, of the wt- and mtNSP4$_{112\text{-}140}$ Peptides.

Peptide:	Sequence:	% α-helix: Buffer	% α-helix: 1mM SUV (55:35:10)	Caveolin -1 Binding*	Cholesterol Binding	Diarrhea Induction
NSP4$_{112\text{-}140}$	MIDKLTTREIEQVELLKRIYDKLTVQTTG	30.6%	57.9%	yes	yes	yes
NSP4$_{Hydro112\text{-}140}$	M**R**DKLTTREIEQ**K**ELLKRI**D**DKLTVQTTG	19.4%	30.9%	no	no	no
NSP4$_{AlaAcidic112\text{-}140}$	MI**A**KLTTREIEQV**A**LLKRIY**A**KLTVQTTG	23.7%	36.9%	yes	yes	yes
NSP4$_{AlaBasic112\text{-}140}$	MID**A**LTT**A**EIEQVELLKRIYD**A**LTVQTTG	26.2%	49.2%	yes	yes	no

(*tested by yeast two-hybrid (*96*))

These data indicate that the hydrophobic face of the amphipathic α-helix of NSP4 plays an essential role in binding to cav-1 and inducing diarrhea, as mutation of hydrophobic residues abolished both of these functions (*96; Chapter IV, this work*). In addition, the hydrophobic face, in particular the tyrosine 131 residue, appears to not only be important for enterotoxic activity (*94*) but for cholesterol binding as well. Secondary structural analysis suggests that conformation may also contribute to each of these functions. However, the extent to which the structure influences the function is debatable, as mutagenesis affected both the structure and the function. Additional studies in which hydrophobic residues are replaced with residues that maintain the structural conformation are needed to provide clarification on this relationship.

Results from the cholesterol binding and diarrhea induction assays revealed that both the wtNSP4$_{112\text{-}140}$ and NSP4$_{AlaAcidic112\text{-}140}$ peptides bind cholesterol and induce diarrhea in mouse pups, while the NSP4$_{Hydro112\text{-}140}$ peptide neither binds cholesterol nor induces diarrhea. Since previous yeast two-hybrid data shows that cav-1 binding occurs via three hydrophobic residues within the amphipathic α-helix of NSP4 (*96*), these studies seem to suggest that both cav-1 and cholesterol binding contribute to diarrheagenic function (Table 10). However, it appears that cav-1 and cholesterol binding are not the only requirements. Circular dichroism analysis of the NSP4$_{AlaBasic112\text{-}140}$ peptide revealed that mutation of basic residues within the AAH of NSP4 caused no significant change in secondary structure over that of the wtNSP4$_{112\text{-}140}$ peptide, nor did they affect cholesterol binding. However, mutation of the basic residues did eliminate diarrheagenic function. Together, these results suggest that enterotoxic function may be dependant on the interaction of NSP4 with a molecule other than cav-1 or cholesterol.

The integrins α1β1 and α2β1 were recently shown to be receptors for NSP4 (*60*). The interaction between NSP4 and the integrin receptors initiates PLC-mediated signaling which mobilizes $Ca^{2+}{}_i$ and induces diarrhea in mouse pups (*60*). Two separate domains of NSP4 are involved in binding to the integrins. The first domain (aa114-130) binds the α1β1 integrin receptor, while the second domain (aa131-140) initiates signaling through the α2β1 domain. Examination of the $NSP4_{AlaBasic112-140}$ peptide sequence reveals a lysine to alanine mutation at residue 133, which is within the integrin-mediated signaling domain (*60*). Since this peptide is structurally similar to the $wtNSP4_{112-140}$ peptide and similarly bound cholesterol, yet did not induce diarrhea in mouse pups, it is likely that diarrheagenic function is associated with integrin receptor interaction more so than secondary structure conformation, cav-1 binding or cholesterol interaction. Additionally, secondary structural analysis of the $NSP4_{AlaBasic112-140}$ peptide in the presence of model membranes revealed a decrease in α-helix formation. It is possible that the modified structural conformation prevents the interaction of certain amino acid residues of NSP4 with the signaling domain of the integrin receptor located within the membrane.

Previous reports suggest that NSP4 traffics from the ER to the PM of RV infected cells through an association with cav-1 (*45, 61, 67*). Since cav-1 binds and transports cholesterol from the ER to the PM (*76, 79, 80, 87, 135*), and NSP4 has been shown to bind cholesterol (*Chapter III, this work*), it is postulated that the NSP4-cav-1-cholesterol interaction is for NSP4 trafficking more so than for enterotoxic function. Figures 17 and 18 depict two potential models for the intracellular interaction of NSP4 with cav-1 and cholesterol. In the first model (Figure 17), both the N- and C-termini of cav-1, as well as

cholesterol, are postulated to interact with three separate hydrophobic amino acid residues within the AAH of a single NSP4 monomer. Yeast two-hybrid data indicates that cav-1 binding occurs via three hydrophobic amino acid residues within NSP4 (*96*), while fluorescence binding assays reveal that cholesterol binding likely occurs via an interaction with the Y131 residue of NSP4 (*Chapter III, this work*).

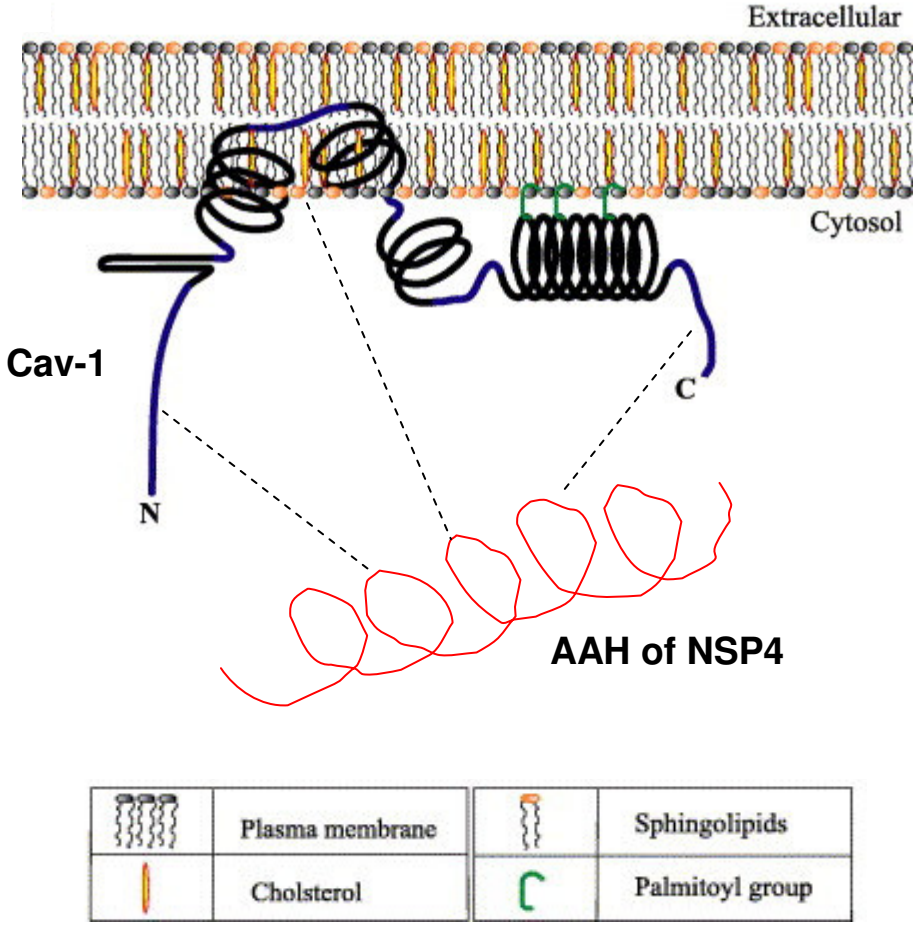

Figure 17: Model for the Interaction of Caveolin-1 and Cholesterol with a Monomeric Form of NSP4. The dotted lines indicate binding of the N- and C-termini of cav-1, as well as cholesterol, to hydrophobic amino acid residues within the AAH of NSP4.

Therefore, it is possible that the N-terminus of cav-1 interacts with one hydrophobic residue within the AAH of NSP4, while the C-terminus of cav-1 interacts with another hydrophobic residue and cholesterol interacts with the Y131 residue.

In the second model (Figure 18), both the N- and C-termini of cav-1, as well as cholesterol, are postulated to interact with separate monomers of an oligomeric form of NSP4.

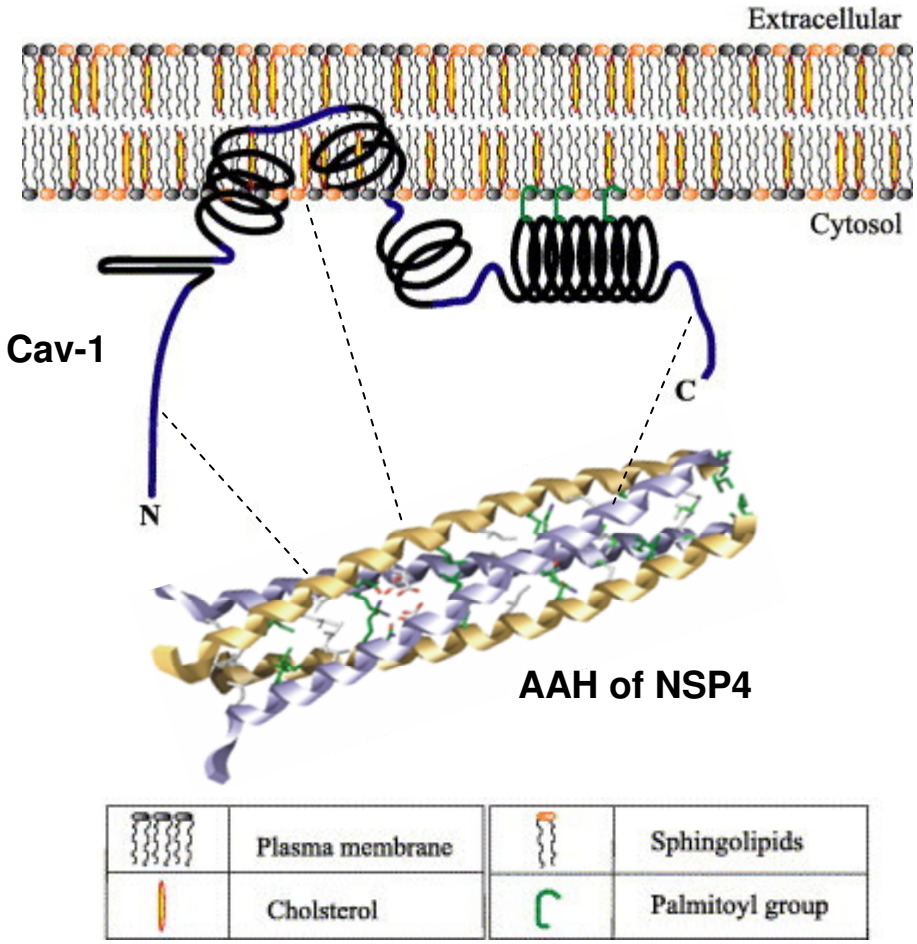

Figure 18: Model for the Interaction of Caveolin-1 and Cholesterol with an Oligomeric Form of NSP4. The dotted lines indicate binding of the N- and C-termini of cav-1, as well as cholesterol, to hydrophobic amino acid residues within the AAH of separate monomers of NSP4.

Since crystallographic data reveals that NSP4 oligomerizes into homotetrameric forms (*39*), each terminus of cav-1, as well as cholesterol, likely interacts with hydrophobic amino acid residues within the AAH of separate NSP4 monomers.

Once at the PM, NSP4 interacts with signaling molecules to initiate signaling processes that result in fluid mobilization (*57, 62*). Recent reports reveal that NSP4 also crosses the PM of RV infected cells whereupon it is hypothesized to initiate signaling pathways in neighboring uninfected cells (*59, 60, 61*). The mechanism by which this occurs, however, is currently unknown. The differential binding observed between NSP4 and each of the cav-1 termini may serve to position NSP4 at the PM where it can interact with the proper signaling molecules and/or lipids. Once properly aligned at the membrane, the C-terminus of cav-1 may dissociate from NSP4, allowing the protein to carry out its enterotoxic function(s). This may explain the observed weak interaction between NSP4 and the cav-1 C-terminus.

What currently remains to be resolved is whether NSP4 accomplishes the above mentioned functions through homo-oligomerization with other NSP4 molecules. In regards to this research, it is unknown whether the NSP4 peptides used in these studies were in a monomeric or oligomeric form. Each of the wt- and mtNSP4 peptides utilized corresponded to a portion of the amphipathic α-helix, oligomerization domain of NSP4. An abundance of research shows that this domain is associated with many functions, including cav-1 binding (*45, 61, 67, 95, 96*), enterotoxic function (*3*), integrin binding (*60*), tubulin binding (*43*), cholesterol binding (*Chapter III, this work*) and lipid interactions (*93, 94*). The association of NSP4 into higher oligomeric forms may explain

how one domain is associated with various functions. Additional research is needed to elucidate the role of oligomerization in NSP4 function(s).

In conclusion, NSP4 enterotoxic function is presumably a result of the careful and complex orchestration between oligomerization, caveolin-1 binding, cholesterol binding, receptor/integrin binding and lipid interactions.

Pitfalls

Proteins, Peptides and Structure/Function Studies

Purification of full length NSP4 has proven to be a difficult undertaking. NSP4 is a membrane protein that contains three hydrophobic domains, which consequently make purification of the protein somewhat problematic. Furthermore, secondary structural studies require protein stocks of significant purity (>95%). As anyone familiar with protein purification knows, protein purity usually comes at the expense of protein yield. Due to the difficulties associated with purifying a membrane protein to reasonable purity and yield needed for our studies, the use of synthetic peptides was an acceptable alternative, as sufficient quantities could be synthesized, purified and characterized with relative ease.

This research utilized synthetic peptides of the amphipathic α-helix, enterotoxic peptide, cav-1 binding domain of RV NSP4 to study secondary structural changes as a result of interactions with cav-1 peptides and model membranes (small unilamellar vesicles, SUV). Mutations were then incorporated within these domains and changes in secondary structure were assessed. In addition, each of the NSP4 peptides was evaluated for cholesterol binding and diarrheagenic function. The use of peptides for these studies has obvious drawbacks, most notably the fact that peptides only represent a small portion

of their corresponding protein and may not always display the same structural and functional characteristics as the full length protein. However, several structure-function studies highlight the use of peptides as models for full length proteins (*108, 109, 110, 111*). Therefore, it is reasonable to presume that the results obtained with these peptide studies are relevant and reflective of the full length NSP4 protein.

Circular Dichroism and the Analysis of Peptide-Peptide Interactions

Circular dichroism (CD) has many advantages as a spectroscopic technique for studying peptide and protein secondary and tertiary structure. It is relatively fast and easy, requires low sample concentrations and allows researchers to study the native structure of peptides or proteins in solution. Furthermore, CD is a reliable method for studying protein-protein or peptide-peptide interactions, as the interaction of a protein/peptide with another protein/peptide can result in changes in the overall structure following interaction (*137*). However, one disadvantage of this technique is that these interactions sometimes result in relatively small, if any, changes in the overall structure. Therefore, when studying protein-protein or peptide-peptide interactions, CD should be only one of several techniques used to indicate or verify an interaction.

Another disadvantage of CD is that it is a low resolution technique that only provides an overall picture of the secondary structure. While the percentage of α-helix, β-sheet, turns and random coil can be determined, the exact location and arrangement of these structures cannot. Furthermore, when using this technique to study protein-protein or peptide-peptide interactions, one cannot determine the contribution of each individual protein/peptide to the overall structure. To obtain more detailed structural information, a

high resolution technique, such as nuclear magnetic resonance (NMR) or X-ray crystallography should be utilized.

Currently, there is limited structural data available on NSP4 due to the difficulties associated with purifying the full length protein. Nevertheless, there have been a few X-ray crystallographic studies, as well as secondary structural studies, performed on the AAH domain (aa95-137) (*39, 46, 93, 94*). These studies have provided initial insight into aspects of NSP4 structure and how it contributes to the function of the viral protein. Future research should focus on developing an improved method for NSP4 protein purification, such that a sufficient quantity of full length protein can be purified for use in additional structural studies.

The Interaction between NSP4 and the N- and C-termini of Caveolin-1

While this research revealed differential binding between the $NSP4_{112-140}$ peptide and N- and C-terminal peptides of cav-1, it did not determine how both termini of cav-1 bind to NSP4. Through the use of a fluorescence binding assay, we determined that the N- and C-termini of cav-1 do not bind to each other. Therefore, the interaction of both termini with NSP4 must occur via different amino acid residues, or possibly via different molecules of NSP4.

Oligomerization of NSP4

The peptides used in this research included a portion of the oligomerization domain of NSP4; however, whether these peptides oligomerized or aggregated in the functional assays was undetermined. Previous studies on an $NSP4_{114-135}$ peptide reveal that the peptide does not aggregate when used at concentrations between 2-20μM (*93*). Since the wt- and $mtNSP4_{112-140}$ peptides utilized in this research contained the same

sequence as the $NSP4_{114-135}$ peptide, and were used at concentrations below 20μM, it is likely that the peptides were not oligomerizing or aggregating. However, whether the introduction of mutations affected the concentration at which oligomerization occurs for the $mtNSP4_{112-140}$ peptides is unknown.

Future Research

Purify wt- and mtNSP4 and Caveolin-1 Proteins for Structural and Functional Studies

This research investigated the structure and functions of NSP4, including cav-1 binding, cholesterol binding and diarrhea induction, using wt- and mt-peptides corresponding to the relevant functional domain (aa112-140). While we postulate that the results of our peptide studies are relevant and predictive of what would be observed with full length proteins, the structural and functional studies should be verified using purified proteins. Site-directed mutagenesis would allow for the introduction of the appropriate mutations within the NSP4 sequence. Each of the NSP4 proteins would be expressed in a yeast expression system, so that large quantities of protein are available for purification. Caveolin-1 would be purified from a cav-1 expressing cell line, such as MDCK cells. A purification method using a combination of techniques, such as HPLC and affinity chromatography, would have to be optimized so that the highest possible purity is obtained for each of the proteins. Once purified, the proteins would be utilized in structural and functional studies to verify the results observed with the peptide studies.

Verify and Characterize the NSP4-Cholesterol Interaction

While our initial research indicates that RV NSP4 binds cholesterol, additional studies are needed to verify and further define this interaction. There are currently a

number of different *in vitro* assays available to demonstrate cholesterol binding, including thin layer chromatography (TLC) and enzyme-linked immunosorbent assays (ELISA) (*138, 139, 140*). To test for an NSP4-cholesterol interaction via a TLC assay, standard lipid samples or lipids extracted from cells would be applied to a TLC plate and run in a solvent mixture for lipid separation. The remainder of the assay would be performed similar to a western blot, where the plate is blocked for non-specific binding, incubated with NSP4 (either full length protein or a peptide) followed by an anti-NSP4 primary antibody and a conjugated secondary antibody. The plate would then be developed to determine if NSP4 bound cholesterol. Performing an ELISA using cholesterol coated plates and incubating with either NSP4 protein or peptide would be another option for ascertaining cholesterol binding.

To further define the amino acid residues involved in the interaction of NSP4 with cholesterol, NSP4-specific peptides corresponding to only the CRAC motif (aa126/127-133) could be synthesized and examined for cholesterol binding via TLC or ELISA. Mutations could be introduced at different positions within the CRAC motif to definitively determine which residues are important for cholesterol interaction.

To validate an NSP4-cholesterol interaction *in vivo*, [H^3]photocholesterol, a photoactivatable cholesterol analogue, could be utilized to photoaffinity label cholesterol-interacting proteins in RV-infected cells (*133, 141*). Following ultraviolet irradiation, which activates photocholesterol crosslinking and labels cholesterol interacting proteins, NSP4 would be immunoprecipitated from the cells and evaluated for cholesterol binding by SDS-PAGE and fluorography.

Determine Whether the Lack of Diarrheagenic Function by the $NSP4_{Hydro112-140}$ and $NSP4_{AlaBasic112-140}$ Peptides is due to a Lack of Integrin Signaling

Functional data on the wt- and $mtNSP4_{112-140}$ peptides revealed that mutation of hydrophobic and basic amino acid residues within the AAH of NSP4 eliminates diarrheagenic function in mouse pups (*Chapter IV this work*). Since both of these mutants contain mutations within the integrin signaling domain (*60*), it is postulated that both mutants lack diarrheagenic function as a result of an inability to induce integrin-mediated signaling. Therefore, these mutants should be tested for integrin signaling. Seo *et al*. utilized a C2C12-α2 mouse myoblast cell line, which is a model for collagen-integrin I signaling, to demonstrate that full length NSP4 induces signaling through an interaction with an integrin domain (*60*). This cell line expresses the α2β1 integrin. Ligand attachment to the integrin induces signaling, which is demonstrated via cell spreading (*142*). By investigating the attachment of the $NSP4_{Hydro112-140}$ and $NSP4_{AlaBasic112-140}$ peptides to C2C12-α2 cells and examining for cell spreading, we can determine if the lack of diarrhea induction by these peptides was a result of an inability to induce integrin-mediated signaling. The $NSP4_{112-140}$ peptide contains the integrin signaling domain and therefore would serve as a positive control. Bovine serum albumin would serve as a negative control.

Determine the Stoiciometry of the NSP4-Caveolin-1 Interaction

Cross-linking and crystallography experiments revealed that RV NSP4 has an oligomerization domain that mediates the formation of dimers and tetramers (*38, 39, 48*). The ability of NSP4 to oligomerize is likely important for its function(s), however, studies have yet to examine whether the interaction(s) of NSP4 with other molecules

occurs via an oligomeric state. In regards to the interaction with cav-1, the formation of NSP4 oligomers may explain how both termini of cav-1 bind the hydrophobic face of the viral protein.

There are several techniques available for investigating the stoichiometry of peptide or protein complexes, including size-exclusion chromatography (SEC), analytical ultracentrifugation, laser light scattering (LS) and mass spectroscopy. While each of these methods allows the estimation of the molecular weight of a sample, which can be used to determine the stoichiometry of a complex, the best method for absolute determination of molecular weight is a combination of SEC and laser light scattering (*143, 144, 145, 146, 147, 148*). Using SEC and laser light scattering, in combination with interferometric refractometry, the stoichiometry of the NSP4-cav-1 complex could be determined. In the case of the NSP4-cav-1 peptide-peptide interaction, the $NSP4_{112\text{-}140}$ peptide could be mixed with the N- and C-terminal cav-1 peptides (aa19-40 and aa161-178, respectively) and examined by SEC/LS. The NSP4-cav-1 complex would first be separated from unbound NSP4 and cav-1 peptides by SEC. Eluted fractions would be monitored by both light scattering and refractive index detectors. The amount of light scattered by the samples in the eluted fractions is directly proportional to the product of the concentration and molecular mass (*147*). While the light scatter would be measured by the light scattering detector, the concentration would be measured by the refractive index detector. The data gathered from these two detectors would then be used to calculate the absolute molecular weight. From this calculated value, the stoichiometry of the NSP4-cav-1 complex can be determined. This should reveal whether NSP4 interacts with both termini of cav-1 via a monomeric or an oligomeric state. However, to

definitively determine how the NSP4 interacts with both the N- and C-termini of cav-1, the structure of the complex should be resolved using x-ray crystallography. Ideally, this experiment should be completed using purified full length NSP4 and cav-1 proteins.

REFERENCES

1. Parashar, U.D., Alexander, J.P., and Glass, R.I. (2006) Prevention of rotavirus gastroenteritis among infants and children. *CDC MMWR*, *55(No. RR-12)*, 1-13.
2. Parashar, U.D., Hummelman, E.G., Bresee, J.S., Miller, M.A., and Glass, R.I. (2003) Global illness and deaths caused by rotavirus disease in children. *Emerg. Infect. Dis. 9(5)*, 565-572.
3. Ball, J.M., Tian, P., Zeng, C.Q-Y., Morris, A.P., and Estes, M.K. (1996) Age-dependent diarrhea induced by a rotavirus non-structural glycoprotein. *Science*, *272*, 455-458.
4. Kapikian, A.Z., and Chanock, R.M., 1996, Rotaviruses, pp. 1657-1708, In *Fields Virology*, Third Edition, B.N. Fields, D.M. Knipe and P.M. Howley (eds.), Lippincott-Raven Publishers, Philadelphia, Pa.
5. Fang, Z. Y., Ye, Q., Ho, M. S., Dong, H., Qing, S., Penaranda, M. E., Hung, T., Wen, L., and Glass, R. I. (1989) Investigation of an outbreak of adult diarrhea rotavirus in China. *J. Infect. Dis. 160(6)*, 948-953.
6. Krishnan, T., Sen, A., Choudhury, J. S., Das, S., Naik, T. N., and Bhattacharya, S. K., (1999) Emergence of adult diarrhoea rotavirus in Calcutta, India. *Lancet 353(9150)*, 380-381.
7. Ramig, R.F. (2004) Pathogenesis of intestinal and systemic rotavirus infection. *J. Virol. 78(19)*, 10213-10220.

8. Blutt, S.E., Kirkwood, C.D., Parreno, V., Warfield, K.L., Ciarlet, M., Estes, M.K., Bok, K., Bishop, R.F., and Conner, M.E. (2003) Rotavirus antigenaemia and viraemia: A common event? *Lancet 362*, 1445-1449.
9. Chiappini, E., Azzari, C., Moriondo, M., Galli, L., and de Martino, M. (2005) Viraemia is a common finding in immunocompetent children with rotavirus infection. *J. Med. Virol. 76*, 265-267.
10. Fisher, T.K., Ashely, D., Kerin, K., Reynolds-Hedmann, E., Gentsch, J., Widdowson, M.A., Westerman, L., Ruhr, N., Turcios, R.M., and Glass, R.I. (2005) Rotavirus antigenemia in patients with acute gastroenteritis. *J. Infect. Dis. 192*, 913-919.
11. Crawford, S.E., Patel, D.G., Cheng, E., Berkova, Z., Hyser, J.M., Ciarlet, M., Finegold, M.J., Conner, M.E., and Estes, M.K. (2006) Rotavirus viremia and extraintestinal viral infection in the neonatal rat model. *J. Virol. 80(10)*, 4820-4832.
12. Estes, M.K. (1996) Rotaviruses and their replication, pp. 1625-1655, In *Fields Virology*, Third Edition, B.N. Fields, D.M. Knipe and P.M. Howley (eds.), Lippincott-Raven Publishers, Philadelphia, PA.
13. Prasad, B.V., Burns, J.W., Marietta, E., Estes, M.K., and Chui, W. (1990) Localization of VP4 neutralization sites in rotavirus by three-dimensional cryo-electron microscopy. *Nature 343*, 476-479.
14. Jayaram, H., Estes, M. K., and Prasad, B. V. (2004) Emerging themes in rotavirus cell entry, genome organization, transcription and replication. *Virus Res. 101(1)*, 67-81.

15. Fiore, L., Greenberg, H.B., and Mackow, E.R. (1991) The VP8 fragment of VP4 is the rhesus rotavirus hemagglutinin. *Virology 181*, 553-563.

16. Lopez, S. and Arias, C.F. (2006) Early steps in rotavirus cell entry. *Curr. Top. Microbiol. Immunol. 309*, 39-66.

17. Isa, P., Realpe, M., Romero, P., Lopez, S., and Arias, C.F. (2004) Rotavirus RRV associates with lipid membrane microdomains during cell entry. *Virol. 322(2)*, 370-381.

18. Ruiz, M.C., Cohen, J., and Michelangeli, F. (2000) Role of Ca^{2+} in the replication and pathogenesis of rotavirus and other viral infections. *Cell Calcium 28(3)*, 137-149.

19. Patton, J.T., Silvestri, L.S., Tortorici, M.A., Vasquez-Del Carpio, R., and Taraporewala, Z.F. (2006) Rotavirus genome replication and morphogenesis: Role of the viroplasm. *Curr. Top. Microbiol. Immunol. 309*, 170-187.

20. Pesavento, J.B., Crawford, S.E., Estes, M.K., and Venkataram Prasad, B.V. (2006) Rotavirus proteins: Structure and assembly. *Curr. Top. Microbiol. Immunol. 309*, 190-219.

21. Afrikanova, I., Fabbretti, E., Miozzo, M.C., and Burrone, O.R. (1998) Rotavirus NSP5 phosphorylation is up-regulated by interaction with NSP2. *J. Gen. Virol. 79*, 2679-2686.

22. Aponte, C., Poncet, D., and Cohen, J. (1996) Recovery and characterization of a replicase complex in rotavirus-infected cells by using a monoclonal antibody against NSP2. *J. Virol. 70*, 985-991.

23. Campagna, M., Eichwald, C., Vascotto, F., and Burrone, O.R. (2005) RNA interference of rotavirus segment 11 mRNA reveals the essential role of NSP5 in the virus replicative cycle. *J. Gen. Virol. 86*, 1481-1487.

24. Fabbretti, E., Afrikanova, I., Vascotto, F., and Burrone, O.R. (1999) Two non-structural rotavirus proteins, NSP2 and NSP5, form viroplasm-like structures in vivo. *J. Gen. Virol. 80*, 333-339.

25. Gallegos, C.O., and Patton J.T. (1989) Characterization of rotavirus replication intermediates: a model for the assembly of single-shelled particles. *Virology 172*, 616-627.

26. Kattoura, M., Chen, X., and Patton, J. (1994) The rotavirus RNA-binding protein NS35 (NSP2) forms 10S multimers and interacts with the viral RNA polymerase. *Virology 202*, 803-813.

27. Silvestri, L.S., Taraporewala, Z.F., and Patton, J.T. (2004) Rotavirus replication: Plus-sense templates for double-stranded RNA synthesis are made in viroplasms. *J. Virol. 78*, 7763-7774.

28. Taraporewala, Z., Chen, D., and Patton, J.T. (1999) Multimers formed by the rotavirus nonstructural protein NSP2 bind to RNA and have nucleoside triphosphatase activity. *J. Virol. 73*, 9934-9943.

29. Berois, M., Sapin, C., Erk, I., Poncet, D., and Cohen, J. (2003) Rotavirus nonstructural protein NSP5 interacts with major core protein VP2. *J. Virol. 77*, 1757-1763.

30. Vende, P., Taraporewala, Z.F., and Patton, J.T. (2002) RNA-binding activity of the rotavirus phosphoprotein NSP5 includes affinity for double-stranded RNA. *J. Virol. 76*, 5291-5299.

31. Nejmeddine, M., Trugnan, G., Sapin, C., Kohli, E., Svensson, L., Lopez, S., and Cohen, J. (2000) Rotavirus spike protein VP4 is present at the plasma membrane and is associated with microtubules in infected cells. *J. Virol. 74*, 3313-3320.

32. Sapin, C., Colard, O., Delmas, O., Tessier, C., Breton, M., Enouf, V., Chwetzoff, S., Ouanich, J., Cohen, J., Wolf, C., and Trugnan, G. (2002) Rafts promote assembly and atypical targeting of a nonenveloped virus, rotavirus, in Caco-2 cells. *J. Virol. 76*, 4591-4602.

33. Jourdan, N., Maurice, M., Delautier, D., Quero, A.M., Servin, A.L., and Trugnan, G. (1997) Rotavirus is released from the apical surface of cultured human intestinal cells through nonconventional vesicular transport that bypasses the Golgi apparatus. *J. Virol. 71(11)*, 8268-8278.

34. Delmas, O., Gardet, A., Chwetzoff, S., Breton, M., Cohen, J., Colard, O., Sapin, C., and Trugnan, G. (2004) Different ways to reach the top of a cell. Analysis of rotavirus assembly and targeting in human intestinal cells reveals an original raft-dependent, Golgi-independent apical targeting pathway. *Virol*ogy *327*, 157-161.

35. Cuadras, M.A., Bordier, B.B., Zambrano, J.L., Ludert, J.E., and Greenberg, H.B. (2006) Dissecting rotavirus particle-raft interaction with small interfering RNAs: Insights into rotavirus transit through the secretory pathway. *J. Virol. 80(8)*, 3935-3946.

36. Ericson, B.L., Graham, D.Y., Mason, B.B., Hanssen, H.H., and Estes, M.K.

(1983) Two types of glycoprotein precursors are produced by the simian rotavirus SA11. *Virology 127*, 320-332.

37. Bergman, C.C., Maass, D., Poruchynsky, M.S., Atkinson, P.H., and Bellamy, A.R. (1989) Topology of the non-structural rotavirus receptor glycoprotein NS28 in the rough endoplasmic reticulum. *EMBO 8(6)*, 1695-1703.
38. Taylor, J.A., O'Brien, J.A., and Yeager, M. (1996) The cytoplasmic tail of NSP4, the endoplasmic reticulum-localized non-structural glycoprotein of rotavirus, contains distinct virus binding and coiled coil domains. *EMBO 15(17)*, 4469-4476.
39. Bowman, G.D., Nodelman, I.M., Levy, O., Lin, S.L., Tian, P., Zamb, T.J., Udem, S.A., Venkataraghavan, B., and Schutt, C.E. (2000) Crystal structure of the oligomerization domain of NSP4 from rotavirus reveals a core metal-binding site. *J. Mol. Biol*. *304*, 861-871.
40. Au, K.S., Mattion, N.M., and Estes, M.K. (1993) A subviral particle binding domain on the rotavirus nonstructural glycoprotein NS28. *Virology 194*, 665-673.
41. Au, K.S., Chan, W.K., Burns, J.W., and Estes, M.K. (1989) Receptor activity of rotavirus nonstructural glycoprotein NS28. *J. Virol*. *63*, 4553-4562.
42. O'Brien, J. A., Taylor, J. A., and Bellamy, A. R. (2000) Probing the structure of rotavirus NSP4: A short sequence at the extreme C terminus mediates binding to the inner capsid particle. *J. Virol. 74*, 5388-5394.
43. Xu, A., Bellamy, A.R., and Taylor, J.A. (2000) Immobilization of the early secretory pathway by a virus glycoprotein that binds to microtubules, *EMBO*, *19(23)*, 6465-6474.

44. Horie, Y., Masamune, O., and Nakagomi, O. (1997) Three major alleles of rotavirus NSP4 proteins identified by sequence analysis. *J. Gen. Virol*. *78*, 2341-2346.

45. Parr, R.D., Storey, S.M., Mitchell, D.M., McIntosh, A.L., Zhou, M., Mir, K.M., and Ball, J.M. (2006) The rotavirus enterotoxin NSP4 directly interacts with the caveolar structural protein caveolin-1. *J. Virol*. *80(6)*, 2842-2854.

46. Deepa, R., Durga Rao, C., and Suguna, K. (2007) Structure of the extended diarrhea-inducing domain of rotavirus enterotoxigenic protein NSP4. *Arch. Virol*. *152*, 847-859.

47. Mirazimi, A., Magnusson, K.E., and Svensson, L. (2003) A cytoplasmic region of the NSP4 enterotoxin of rotavirus is involved in retention in the endoplasmic reticulum. *J. Gen. Virol*. *84*, 875-883.

48. Maass, D., and Atkinson, P.H. (1990) Rotavirus proteins VP7, NS28 and VP4 form oligomeric structures. *J. Virol*. *64(6)*, 2632-2641.

49. Maruri-Avidal, L., Lopez, S., and Arias, C.F. (2008) Endoplasmic reticulum chaperones are involved in the morphogenesis of rotavirus infectious particles. *J. Virol*. *82(11)*, 5368-5380.

50. Zambrano, J.L., Diaz, Y, Pena, F., Vizzi, E., Ruiz, M.C., Michelangeli, F. Liprandi, F., and Ludert, J.E. (2008) Silencing of rotavirus NSP4 or VP7 expression reduces alterations in Ca^{2+} homeostasis induced by infection of cultured cells. *J. Virol*. *82(12)*, 5815-5824.

51. Silvestri, L.S., Tortorici, M.A., Vasquez-Del Carpio, R., and Patton, J.T. (2005) Rotavirus glycoprotein NSP4 is a modulator of viral transcription in the infected cell. *J. Virol. 79(24)*, 15165-15174.

52. Lopez, T., Camacho, M., Zayas, R., Najera, R., Sanchez, R., Arias, C.F., and Lopez, S. (2005) Silencing the morphogenesis of rotavirus. *J. Virol. 79*, 184-192.

53. Berkova, Z., Crawford, S.E., Trugnan, G., Yoshimori, T., Morris, A.P., and Estes, M.K. (2006) Rotavirus NSP4 induces a novel vesicular compartment regulated by calcium and associated with viroplasms. *J. Virol. 80(12)*, 6061-6071.

54. Lundgren, O., Peregrin, A.T., Persson, K., Kordasti, S., Uhnoo, I., and Svensson, L. (2000) Role of the enteric nervous system in the fluid and electrolyte secretion of rotavirus diarrhea. *Science 287(5452)*, 491-495.

55. Dong, Y., Zeng, C. Q., Ball, J.M., Estes, M.K., and Morris, A.P. (1997) The rotavirus enterotoxin NSP4 mobilizes intracellular calcium in human intestinal cells by stimulating phospholipase C-mediated inositol 1,4,5-trisphosphate production. *Proc. Natl. Acad. Sci. U.S.A. 94*, 3960-3965.

56. Tian, P., Hu, Y., Schilling, W.P., Lindsay, D.A., Eiden, J., and Estes, M.K. (1994) The nonstructural glycoprotein of rotavirus affects intracellular calcium levels. *J. Virol.. 68*, 251-257.

57. Tian, P., Estes, M.K., Hu, W.P., Ball, J.M., Zeng, C.Q-Y., and Schilling, W.P. (1995) The rotavirus nonstructural glycoprotein NSP4 mobilizes Ca^{2+} from the endoplasmic reticulum. *J. Virol. 69*, 5763-5772.

58. Tafazoli, F., Zeng, C.Q., Estes, M.K., Magnusson, K.E., and Svensson, L. (2001) NSP4 enterotoxin of rotavirus induces paracellular leakage in polarized epithelial cells. *J. Virol. 75*, 1540-1546.

59. Boshuizen, J.A., Rossen, J.W., Sitaram, C.K., Kimenai, F.F., Simons-Oosterhuis, Y., Laffeber, C., Büller, H.A., and Einerhand, A.W. (2004) Rotavirus enterotoxin NSP4 binds to the extracellular matrix proteins laminin-β3 and fibronectin. *J. Virol. 78(18)*, 10045-10053.

60. Seo, N.S., Zeng, C.Q., Hyser, J.M., Utama, B., Crawford, S.E., Kim, K.J., Höök, M., and Estes, M.K. (2008) Integrins α1β1 and α2β1 are receptors for the rotavirus enterotoxin. *PNAS 105(26)*, 8811-8818.

61. Gibbons, T. F. (2007) Rotavirus NSP4 in extrareticular sites: Support for its pathogenic role as an enterotoxin. Unpublished doctoral dissertation, Texas A&M University, College Station.

62. Berkova, Z., Morris, A.P., and Estes, M.K. (2003) Cytoplasmic calcium measurement in rotavirus enterotoxin-enhanced green fluorescent protein (NSP4-EGFP) expressing cells loaded with Fura-2. *Cell Calcium 34(1)*, 55-68.

63. Beaulieu, J.F. (1999) Integrins and human intestinal cell functions. *Front Biosci. 4*, D310-D321.

64. Berkova, Z., Crawford, S.E., Blutt, S.E., Morris, A.P., and Estes, M.K. (2007) Expression of rotavirus NSP4 alters the actin network organization through the actin remodeling protein cofilin. *J. Virol. 81(7)*, 3545-3553.

65. Gardet, A., Breton, M., Fontages, P., Trugnan, G., and Chwetzoff, S. (2006) Rotavirus spike protein VP4 binds to and remodels actin bundles of the epithelial brush border into actin bodies. *J. Virol*. *80*, 3947-3956.

66. Taylor, J.A., O'Brien, J.A., Lord, V.J., Meyer, J.C., and Bellamy, A.R. (1993) The RER-localized rotavirus intracellular receptor: A truncated purified soluble form is multivalent and binds virus particles. *Virol*ogy *194*, 807-814.

67. Storey, S.M., Gibbons, T.F., Williams, C.V., Parr, R.D., Schroeder, F., and Ball, J.M. (2007) Full-length, glycosylated NSP4 is localized to plasma membrane caveolae by a novel raft isolation technique. *J. Virol*. *81(11)*, 5472-5483.

68. Zhang, M., Zeng, C.Q., Morris, A.P., and Estes, M.K. (2000) A Functional NSP4 Enterotoxin Peptide Secreted from Rotavirus-Infected Cells. *J. Virol. 74(24)*, 11663-11670.

69. Anderson, R. G. (1998) The caveolae membrane system. *Annu. Rev. Biochem*. *67*, 199-225.

70. Krajewska, W.M., and Maslowska, I. (2004) Caveolins: Structure and function in signal transduction. *Cell. Mol. Biol. Lett*. *9*, 195-220.

71. Gumbleton, M., Abulrob, A.G., and Campbell, L. (2000) Caveolae: An alternate membrane transport compartment. *Pharm. Res*. *17(9)*, 1035-1048.

72. Couet, J., Belanger, M.M., Roussel, E., and Drolet, M.C. (2001) Cell biology of caveolae and caveolin. *Advanced Drug Delivery Reviews 49*, 223-235.

73. Hill, M.M., Bastiani, M., Luetterforst, R., Kirkham, M., Kirkham, A., Nixon, S.J., Walser, P., Abankwa, D., Oorschot, V.M., Martin, S., Hancock, J.F., and Parton,

R.G. (2008) PTRF-Cavin, a conserved cytoplasmic protein required for caveola formation and function. *Cell 132*, 113-124.

74. Nelson, D.L., and Cox, M.M., In: Lehninger's Principles of Biochemistry, 4th Edition, Chapter 11, Biological Membranes and Transport, pp. 385-386, 2005.
75. Fernandez, I., Ying, Y., Albnesi, J., and Anderson, R.G. (2002) Mechanism of caveolin filament assembly. *Proc. Natl. Acad. Sci U.S.A. 92*, 9407-9411.
76. Spisni, E., Tomasi, V., Cestaro, A., and Tosatto, S.C. (2005) Structural insights into the function of human caveolin 1. *Biochem. Biophys. Res. Commun. 338(3)*, 1383-1390.
77. Epand, R.M., Sayer, B.G., and Epand, R.F. (2005) Caveolin scaffolding region and cholesterol-rich domains in membranes. *J. Mol. Biol. 345*, 339-350.
78. Dietzen, D.J., Hastings, W.R., and Lublin, D.M. (1995) Caveolin is palmitoylated on multiple cysteine residues. *J. Biol. Chem. 270*, 6838-6842.
79. Murata, M., Peranen, J., Schreiner, R., Wieland, F., Kurzchalia, T.V., and Simons, K. (1995) VIP21/caveolin is a cholesterol-binding protein. *Proc. Natl. Acad. Sci. U.S.A. 92*, 10339-10343.
80. Uittenbogaard, A., and Smart, E.J. (2000) Palmitoylation of caveolin-1 is required for cholesterol binding, chaperone complex formation, and rapid transport of cholesterol to caveolae. *J. Biol. Chem. 275*, 25595-25599.
81. Monier, S., Parton, R.G., Vogel, F., Behlke, J., Henske, A., and Kurzchalia, T.V. (1995) VIP21-caveolin, a membrane protein constituent of the caveolar coat, oligomerizes in vivo and in vitro. *Mol. Biol. Cell 6*, 911-927.
82. Pol, A., Martin, S., Fernandez, M.A., Ingelmo-Torres, M., Ferguson, C., Enrich,

C., and Parton, R.G. (2005) Cholesterol and fatty acids regulate dynamic caveolin trafficking through the Golgi complex and between the cell surface and lipid bodies. *Mol. Biol. Cell 16*, 2091-2105.

83. Parton, R.G., Hanzal-Bayer, M., and Hancock, J.F. (2006) Biogenesis of caveolae: A structural model for caveolin-induced domain formation. *J. Cell Sci. 119*, 787-796.
84. Parat, M.O. (2009) The biology of caveolae: achievements and perspectives. *Int. Rev. Cell Mol. Biol. 273*, 117-162.
85. Song, K.S., Tang, Z., Li, S., and Lisanti, M.P. (1997) Mutational analysis of the properties of caveolin-1: A novel role for the C-terminal domain in mediating homo-typic caveolin-caveolin interactions. *J. Biol. Chem. 272(7)*, 4398-4403.
86. Li, H., and Papadopoulos, V. (1998) Peripheral-type benzodiazepine receptor function in cholesterol transport. Identification of a putative cholesterol recognition/interaction amino acid sequence and consensus pattern. *Endocrinology 139(12)*, 4991-4997.
87. Ikonen, E. and Parton, R.G. (2000) Caveolins and Cellular Cholesterol Balance. *Traffic 1*, 212-217.
88. Rothberg, K.G., Heuser, J.E., Donzell, W.C., Ying, Y.S., Glenney, J.R., and Anderson, R.G. (1992) Caveolin, a protein component of caveolae membrane coats. *Cell 68*, 673-682.
89. Smart, E.J., Ying, Y., Donzell, W.C., and Anderson, R.G. (1996) A role for caveolin in transport of cholesterol from endoplasmic reticulum to plasma membrane. *J. Biol. Chem. 271(46)*, 29427-29435.

90. Isshiki, M., and Anderson, R.G. (2003) Function of caveolae in Ca^{2+} entry and Ca^{2+}-dependent signal transduction. *Traffic 4(11)*, 717-723.

91. Fujimoto, T. (1993) Calcium pump of the plasma membrane is localized in caveolae. *J. Cell Biol. 120(5)*, 1147-1157.

92. Fujimoto, T., Nakade, S., Miyawaki, A., Mikoshiba, K., and Ogawa, K. (1992) Localization of inositol 1,4,5-trisphosphate receptor-like protein in plasmalemmal caveolae. *J. Cell Biol. 119*, 1507-1513.

93. Huang, H., Schroeder, F., Zeng, C., Estes, M.K., Schoer, J.K., and Ball, J.M. (2001) Membrane interactions of a novel viral enterotoxin: Rotavirus nonstructural glycoprotein NSP4. *Biochemistry 40*, 4169-4180.

94. Huang, H., Schroeder, F., Estes, M.K., McPherson, T., and Ball, J.M. (2004) Interaction(s) of rotavirus non-structural protein 4 (NSP4) C-terminal peptides with model membranes. *Biochem. J. 380*, 723-733.

95. Mir, K.D., Parr, R.D., Schroeder, F., and Ball, J.M. (2007) Rotavirus NSP4 interacts with both the amino- and carboxyl-termini of caveolin-1. *Virus Res. 126(1-2)*, 106-115.

96. Williams, C.V. (2008) Mapping of the rotavirus non-structural protein 4-caveolin-1 binding site to three hydrophobic residues within the extended, C-terminal amphipathic alpha-helix. Unpublished doctoral dissertation, Texas A&M University, College Station.

97. Segrest, J.P., De Loof, H., Dohlman, J.G., Brouillette, C.G., and Anantharamaiah, G.M. (1990) Amphipathic helix motif: Classes and properties. *PROTEINS: Struc., Func., Gen. 8*, 103-117.

98. Baxevanis, A.D., and Vinson, C.R. (1993) Interactions of coiled coils in transcription factors: where is the specificity? *Curr. Opin. Genet. Dev. 3(2)*, 278-285.

99. Segrest, J.P., Jackson, R.L., Morrisett, J.D., and Gotto, A.M. (1973) A molecular theory of lipid-protein interactions in the plasma lipoproteins. *FEBS Lett. 38(3)*, 247-253.

100. Ben-Tal, N., Honig, B., Miller, C., and McLaughlin, S. (1997) Electrostatic binding to proteins to membranes: Theoretical predictions and experimental results with charybdotoxin and phospholipids vesicles. *Biophys. J. 73*, 1717-1727.

101. Gazzara, J.A., Phillips, M.C., Lund-Katz, S., Palgunachari, M.N., Segrest, J.P., Anantharamaiah, G.M., and Snow, J.W. (1997) Interaction of class A amphipathic helical peptides with phospholipids unilamellar vesicles. *J. Lipid Res. 38*, 2134-2146.

102. Mangavel, C., Maget-Dana, R., Tauc, P., Brochon, J.C., Sy, D., and Reynaud, J.A. (1998) Structural investigations of basic amphipathic model peptides in the presence of lipid vesicles studied by circular dichroism, fluorescence, monolayer and modeling. *Biochem. Biophys. Acta 1371*, 265-283.

103. Denisov, G., Wanaski, S., Luan, P., Glaser, M., and McLaughlin, S. (1998) Binding of basic peptides to membranes produces lateral domains enriched in the acidic lipids phosphatidylserine and phosphatidylinositol 4,5-bisphosphate: An electrostatic model and experimental results. *Biophys. J. 74*, 731-744.

104. Couet, J., Li, S., Oka, T., Ikezu, T., and Lisanti, M.P. (1997) Identification

of peptide and protein ligands for the caveolin-scaffolding domain. *J. Biol. Chem. 272*, 6525-6533.

105. Okamoto, T., Schlegel, A., Scherer, P.E., and Lisanti, M.P. (1998) Caveolins, a family of scaffolding proteins for organizing "preassembled signaling complexes" at the plasma membrane. *J. Biol. Chem. 273*, 5419-5422.

106. Smart, E. J., Graf, G.A., McNiven, M.A., Sessa, W.C., Engelman, J.A., Scherer, P.E., Okamoto, T., and Lisanti, M.P. (1999) Caveolins, liquid-ordered domains, and signal transduction. *Mol. Cell Biol. 19*, 7289-7304.

107. Ostrom, R. S., and Insel, P.A. (2004) The evolving role of lipid rafts and caveolae in G protein-coupled receptor signaling: Implications for molecular pharmacology. *Br J Pharmacol. 143*, 235-245.

108. Lawless, M.K., Barney, S., Guthrie, K.I., Bucy, T.B., Petteway, S.R., and Merutka, G. (1996) HIV-1 membrane fusion mechanism: Structural studies of the interactions between biologically-active peptides from gp41. *Biochem. 35*, 13697-13708.

109. Mucha, P., Rekowski, P., Szyk, A., Kupryszewski, G., Giel-Pietraszuk, M., and Barciszewski, J. (1998) Circular dichroism studies of the interaction of Tat analogues substituted in the Arg52 position with TAR RNA HIV-1. *Lett. Pep. Sci. 5*, 345-348.

110. Greenfield, N.J., Kotlyanskaya, L., and Hitchcock-DeGregori, S.E. (2009) Structure of the N terminus of a nonmuscle α-tropomyosin in complex with the C terminus: implications for actin binding. *Biochem. 48*, 1272-1283.

111. Herrera, E., Gomara, M.J., Mazzini, S., Ragg, E., and Haro, I. (2009) Synthetic peptides of hepatitis G virus (GBV-C/HGV) in the selection of putative peptide inhibitors of the HIV-1 fusion peptide. *J. Phys. Chem. B. 113*, 7383-7391.

112. White, P.D., and Chan, W.C. (2000), Basic Principles, pp.2-40, In *Fmoc Solid Phase Peptide Synthesis: A Practical Approach*, W.C. Chan and P.D. White (eds.), Oxford University Press, New York, NY.

113. Johnson, W.C. (1990) Protein secondary structure and circular dichroism: a practical guide. *PROTEINS: Struc. Func. Gen. 7*, 205-214.

114. Mulkerrin, M.G. (1996) Protein Structure Analysis Using Circular Dichroism, Chap. 2, pp5-27, In *Spectroscopic Methods for Determining Protein Structure in Solution*, H.A. Howel (ed.), VCH Publishers, Inc., New York, NY.

115. Sreerama, N., and Woody, R.W. (2000) Circular Dichroism of Peptides and Proteins, Chap. 21, pp601-620, In *Circular Dichroism: Principles and Applications*, Second Ed, N. Berova, K. Nakanishi, R.W. Woody (eds.), John Wiley and Sons, Oxford, NY.

116. Drake, A.F. (2001) Circular Dichroism, Chap. 3, pp123-167, In *Protein-Ligand Interactions: Structure and Spectroscopy, a Practical Approach*, S.E. Harding (ed.), Oxford University Press, Oxford, NY.

117. Kelly, S.M., Jess, T.J., and Price, N.C. (2005) How to study proteins by circular dichroism. *Biochem. Biophys. Acta. 1751*, 119-139.

118. Greenfield, N.J. (1996) Methods to estimate the conformation of proteins and polypeptides from circular dichroism data. *Analy. Biochem. 235*, 1-10.

119. Sreerama, N., and Woody, R.W. (2000) Estimation of protein secondary structure from circular dichroism spectra: comparison of CONTIN, SELCON, and CDSSTR methods with an extended reference set. *Analy. Biochem. 287*, 252-260.

120. Ribeiro, M.M., Franquelim, H.G., Castanho, M.A., and Veiga, A.S. (2007) Molecular interaction studies of peptides using steady-state fluorescence intensity. Static (de)quenching revisited. *J. Pept. Sci. 14(4)*, 401-406.

121. Mateo, C.R., De Almeida, R.F., Loura, L.M., and Prieto, M. (2006) From Lipid Phases to Membrane Protein Organization: Fluorescence Methodologies in the Study of Lipid-Protein Interactions, Chap.1, pp. 1-33, In *Protein-Lipid Interactions*, C.R. Mateo, J. Gomez, J. Villalain, J.M. Gonzalez Ros (eds.), Springer, New York, NY.

122. Williams, T.M., and Lisanti, M.P. (2004) The caveolin genes: From cell biology to medicine. *Ann Med. 36(8)*, 584-595.

123. Isshiki, M., and Anderson, R.G. (1999) Calcium signal transduction from caveolae. *Cell Calcium 26(5)*, 201-208.

124. Liu, P., Rudick, M., and Anderson, R.G. (2002) Multiple functions of caveolin-1. *J. Biol. Chem. 277(44)*, 41295-41298.

125. Chen, Y.H., Yang, J.T., and Chau, K.H. (1974) Determination of the helix and β form of proteins in aqueous solution by circular dichroism. *Biochemistry 13*, 3350-3359.

126. Hostetler, H.A., Petrescu, A.D., Kier, A.B., and Schroeder, F. (2005) Peroxisome proliferator-activated receptor α interacts with high affinity and is conformationally responsive to endogenous ligands. *J. Biol. Chem. 280(19)*,

18667-18682.

127. Ames, B.N. (1966) Assay of inorganic phosphate, total phosphate and phosphatases. *Methods Enzymol*., *8*, 115-118.

128. Li, S., Okamoto, T., Chun, M., Sargiacomo, M., Casanova, J.E., Hansen, S.H., Nishimoto, I., and Lisanti, M.P. (1995) Evidence for a regulated interaction between heterotrimeric g proteins and caveolin. *J. Biol. Chem. 270(26)*, 15693-15701.

129. Li, S., Couet, J., and Lisanti, M.P. (1996) Src tyrosine kinases, g alpha subunits, and h-ras share a common membrane-anchored scaffolding protein, caveolin. *J. Biol. Chem. 271(46)*, 29182-29190.

130. Garcia-Cardena, G., Martasek, P., Masters, B.S., Skidd, P.M., Couet, J., Li, S., Lisanti, M.P., and Sessa, W.C. (1997) Dissecting the interaction between nitric oxide synthase (nos) and caveolin. *J. Biol. Chem. 272(10)*, 25437-25440.

131. Epand, R.F. (2006) Cholesterol and the interaction of proteins with membrane domains. *Prog. Lipid Res. 45(4)*, 279-294.

132. Schroeder, C., Heider, H., Möncke-Buchner, E., and Lin, T.I. (2005) The influenza virus ion channel and maturation cofactor M2 is a cholesterol-binding protein. *Eur. Biophys. J. 34(1)*, 52-66.

133. Umashankar, M., Sanchez-San Martin, C., Liao, M., Reilly, B., Guo, A., Taylor, G., and Kielian, M. (2008) Differential cholesterol binding by class II fusion proteins determines membrane fusion properties. *J. Virol. 82(18)*, 9245-9253.

134. Vincent, N., Genin, C., and Malvoisin, E., (2002) Identification of a conserved domain of the HIV-1 transmembrane protein gp41 which interacts with cholesteryl groups. *Biochim. Biophys. Acta. 1567(1-2)*, 157-164.

135. Uittenbogaard, A., Ying, Y., and Smart, E.J. (1998) Characterization of a cytosolic heat-shock protein-caveolin chaperone complex. Involvement in cholesterol trafficking. *J. Biol. Chem. 273*, 6525-6532.

136. Jamin, N., Neumann, J.M., Ostuni, M.A., Vu, T.K., Yao, Z.X., Murail, S., Robert, J.C., Giatzakis, C., Papadopoulos, V., and Lacapere, J.J. (2005) Characterization of the cholesterol recognition amino acid consensus sequence of the peripheral-type benzodiazepine receptor. *Mol. Endocrinol. 19(3)*, 588-594.

137. Kelly, S.M., and Price, N.C. (2006) Circular dichroism to study protein interactions. *Curr. Protoc. Protein Sci*. Chapter 20, Unit 20.10.

138. Iwamoto, M., Ohno-Iwashita, Y., and Ando, S. (1990) Effect of isolated C-terminal fragment of θ-toxin (perfringolysin O) on toxin assembly and membrane lysis. *Eur. J. Biochem. 194(1)*, 25-31.

139. Aniagolu, J., Swartz, G.M., Dijkstra, J., Madsen, J.W., Raney, J.J., and Green, S.J. (1995) Analysis of anticholesterol antibodies using hydrophobic membranes. *J. Immunol. Methods 182(1)*, 85-92.

140. Shimada, Y., Nakanura, M., Naito, Y., Nomura, K., and Ohno-Iwashita, Y. (1999) C-terminal amino acid residues are required for the folding and cholesterol binding property of perfringolysin O, a pore-forming cytolysin. *J. Biol. Chem. 274(26)*, 18536-18542.

141. Thiele, C., Hannah, M.J., Fahrenholz, F., and Huttner, W.B. (2000) Cholesterol binds to synaptophysin and is required for biogenesis of synaptic vesicles. *Nat. Cell. Biol. 2(1)*, 42-49.

142. Giancotti, F.G., and Ruoslahti, E. (1999) Integrin signaling. *Science 285*, 1028-1032.

143. Wen, J., Arakawa, T., and Philo, J.S. (1996) Size-exclusion chromatography with on-line light-scattering, absorbance, and refractive index detectors for studying proteins and their interactions. *Analy. Biochem. 240*, 155-166.

144. Arakawa, T., and Wen, J. (2001) Size-exclusion chromatography with on-line light scattering. *Curr. Protoc. Protein Sci*. Chap. 20, Unit 20.6, 20.6.1-20.6.21.

145. Modridge, J., Cunningham, K., and Collier, R.J. (2002) Stoichiometry of anthrax toxin complexes. *Biochemistr 41*, 1079-1082.

146. Wang, T., and Lucey, J.A. (2003) Use of multi-angle laser light scattering and size-exclusion chromatography to characterize the molecular weight and types of aggregates present in commercial whey protein products. *J. Dairy Sci. 86*, 3090-3101.

147. Modridge, J. (2004) Using light scattering to determine the stoichiometry of protein complexes. *Methods Mol. Biol. 261*, 113-118.

148. van Dieck, J., Fernandez-Fernandez, M.R., Veprintsev, D.B., and Fersht, A.R. (2009) Modulation of the oligomerization state of p53 by differential

binding of proteins of the S100 family to p53 monomers and tetramers. *J. Biol. Chem*. *284(20)*, 13804-13811.

VITA

Name: Megan Elizabeth Schroeder

Address: Texas A&M University, VTPB, MS4467, College Station, TX 77843

Email Address: mschroeder@cvm.tamu.edu

Education: B.A., Biology and Chemistry, Bellarmine University, 2003
Ph.D., Veterinary Microbiology, Texas A&M University, 2009

Publications: Kang, H., Feng, M., **Schroeder**, **M.E.**, Giedroc, D.P., Leibowitz, J.L. (2006) Putative *cis*-Acting Stem-Loops in the 5' Untranslated Region of the Severe Acute Respiratory Syndrome Coronavirus Can Substitute for Their Mouse Hepatitis Virus Counterparts, *J. Virol.*, 80(21), 10600-10614.

Parr, D.R., Martin, G.G., Hostetler, H.A., **Schroeder**, **M.E.**, Mir, K.D., Kier, A.B., Ball, J.M., Schroeder, F. (2007) A New N-Terminal Recognition Domain in Caveolin-1 Interacts with Sterol Carrier Protein-2 (SCP-2), *Biochemistry*, 46, 8301-8314.